Towards Sustainable Textiles: Microplastics, Coffee, and Closing the Loop

by

Julie M. Rieland

A dissertation submitted in partial fulfillment
of the requirements for the degree of
Doctor of Philosophy
(Macromolecular Science and Engineering)
in the University of Michigan
2023

Doctoral Committee:

Professor Brian J. Love, Chair
Professor Mihaela Banu
Associate Professor Mojgan Nejad
Professor Alan Taub

Julie M. Rieland
jmriel@umich.edu
ORCID iD: 0000-0003-0796-792X

ACKNOWLEDGEMENTS

I am grateful to all my friends and family, and my advisor, Brian Love for keeping me going and supporting me on this journey.

I have so much appreciation for the Beakes Crew; The University of Michigan Kendo Club members, past and present, and Joe Sensei, Watanabe Sensei; also my past roommates, Sophia Mehdizadeh and Elizabeth Stanley who saw me though the first year of grad school and the depths of Covid; and my DnD group who continue to be a source of escape and imagination.

I also couldn't have made it through this last month without the emotional support of Hayao Miyazaki and Angela Lansbury keeping me company during the long hours of writing.

And finally, I am especially grateful to the support of my fiancé. Thank you Thomas for putting up with me for the last months of writing and keeping me grounded.

TABLE OF CONTENTS

ACKNOWLEDGEMENTS ii

LIST OF FIGURES vi

LIST OF TABLES ix

ABSTRACT x

1 Introduction 1

1.1 The Big Picture 1
1.2 Microplastic Pollution 5
1.2.1 Microplastics 5
1.2.2 Microplastic sources and sinks in the environment 6
1.2.3 Microplastic solutions 10
1.2.4 Microplastics outlooks 12
1.3 Ionic Liquid Dissolution of Cellulose 14
1.3.1 Ionic liquids 14
1.3.2 Dissolution of cellulose by ionic liquids 14
1.3.3 Coffee Fruit 16
1.4 Summary of work 17
1.4.1 Quantification and capture of microplastics via pressure sensitive adhesives 17
1.4.2 Ionic liquid processing of untreated coffee fruit residues 18
1.4.3 Influence of pretreatments on the ionic liquid processing of coffee fruit residues 18
1.5 References 19

2 Quantification and Capture of Microplastics Via Pressure Sensitive Adhesives 35

2.1 Introduction 35
2.1.1 State of microplastic capture at bench scale and in real-world scenarios 35
2.1.2 Microplastic quantification and harmonization 37
2.1.3 Pressure sensitive adhesives applied towards microplastic capture 38
2.2 Materials and Methods 39
2.2.1 Materials 39
2.2.2 Synthesis of 950k poly(2-ethylhexyl acrylate) 40

2.2.3 Preparing glass slide substrates . . . 41
2.2.4 Shake tests – Calibration curves . . . 42
2.2.5 Shake tests – Environmental interferents . . . 43
2.2.6 Shake tests – Microplastic survey and mixed assays . . . 44
2.2.7 Observational assessment . . . 44
2.2.8 Environmental interferent characterization . . . 45
2.2.9 Rheology . . . 45
2.3 Limitations . . . 46
2.3.1 Fighting buoyancy (and losing) . . . 46
2.3.2 Optical microscopy artifacts and adhesive degradation . . . 47
2.3.3 ImageJ® boundary conditions . . . 49
2.3.4 Glass slide edge effects . . . 51
2.4 Results and Discussion . . . 52
2.4.1 Resin variations: impact on binding . . . 53
2.4.2 Impact of interferents and more realistic dispersions found in the built environment . . . 56
2.4.3 Binding assessments using mixed particulates . . . 61
2.5 Conclusion . . . 64
2.6 References . . . 66

3 Ionic Liquid Processing of Untreated Coffee Fruit Residues . . . 73

3.1 Introduction . . . 73
3.1.1 Impact of residual lignin and hemicellulose on ionic liquid processing of biomass . . . 74
3.1.2 Utilization of untreated biomass residues in engineering applications . . . 75
3.2 Materials and Methods . . . 76
3.2.1 Materials . . . 76
3.2.2 Synthesis of ionic liquid [DBUH][OAc] . . . 76
3.2.3 Cascara preparation . . . 76
3.2.4 Biomass Solubility . . . 77
3.2.5 Biomass solutions . . . 78
3.2.6 Cascara characterization . . . 78
3.2.7 Rheology . . . 79
3.2.8 Fiber formation and drawing studies . . . 80
3.2.9 X-ray diffraction and Fourier Transform Infrared analysis . . . 81
3.3 Limitations . . . 81
3.4 Results and Discussion . . . 82
3.4.1 Biomass compositional assessments . . . 82
3.4.2 Biomass solubility assessments . . . 84
3.4.3 Rheological analysis . . . 85
3.4.4 Coagulated product formation . . . 88
3.5 Conclusion . . . 92
3.6 References . . . 93

4 Influence of Pretreatments on the Ionic Liquid Processing of Coffee Fruit Residues . . . 100

4.1 Introduction . . . 100
4.1.1 Biomass pretreatments and impacts . . . 100
4.1.2 Utilization of the whole biomass . . . 101
4.1.3 Behavior of cellulosic materials precipitated from ionic liquids . . . 102
4.2 Materials and Methods . . . 103
4.2.1 Materials . . . 103
4.2.2 Ethanol pretreatment . . . 103
4.2.3 Dilute ionic liquid pretreatment . . . 103
4.2.4 Acid chlorite pretreatment . . . 104
4.2.5 Cascara characterization . . . 105
4.2.6 Solubility assessment . . . 105
4.2.7 Preparation of ionic liquid solutions . . . 106
4.2.8 Rheological assessment . . . 106
4.2.9 Arrhenius calculations . . . 106
4.2.10 Extruded fibers . . . 107
4.3 Limitations . . . 108
4.4 Results and Discussion . . . 108
4.4.1 Assessment of pretreated biomasses . . . 108
4.4.2 Rheological assessment . . . 112
4.4.3 Fibers . . . 117
4.5 Conclusion . . . 119
4.6 References . . . 121

5 Conclusion . . . 127

5.1 Summary . . . 127
5.2 Future Work – Microplastics . . . 129
5.2.1 Improving image based analysis . . . 130
5.2.2 Exploring substrate geometries . . . 130
5.3 Future Work - Cascara . . . 131
5.3.1 Expanding assessment of green pretreatments . . . 131
5.3.2 Assessing intermediary extraction of value-added components . . . 132
5.3.3 Recycling of ionic liquid . . . 132
5.4 References . . . 133

APPENDIX . . . 134

LIST OF FIGURES

FIGURE

1.1 Estimates of MP mass flows into the environment from key point sources based on the work of Boucher & Froit.[31] The asterisks "*" indicate modified measurements based on the distribution of MPs in WWTP biosolids.[35] 7

2.1 SEM micrograph demonstrating an edge-on view of the 92k Poly (2-ethylhexyl acrylate) coating on a glass slide. 41

2.2 a) Change in %SAC versus concentration of Nylon30 in room temperature DI-water/ethanol solutions using 92k PEHA adhesive, 1 minute shaking. b) Change in %SAC coverage of Nylon30 (5 mg mL^{-1}) on 92k PEHA after 1 minute shaking in varying concentrations of ethanol. 46

2.3 Examples of optical microscope images that complicate analysis. A) 0.1 mg mL^{-1} PS captured on 950k after 5 min, b) mixed assay of 50:50 PE50:PE200 on 950k after 5 min, and 5 mg mL^{-1} on 92k after 3 min. 48

2.4 A) Microscope image from PET Fiber shake test, b) image converted to grey-scale and tuned for better contrast, c) the thresholded image, d) the ImageJ output of what is calculated with the "Analyze Particles" feature, a poor representation of the aggregated fibers. 49

2.5 Microscope images demonstrating the edge effect a) 950k PEHA with 1 mg mL^{-1} Nylon30 after 5 min shaking, b) 50:50 BD 2 mg mL^{-1} Nylon30 after 5 min shaking, c) 50:50 BD 2 mg mL^{-1} Nylon30 5 min shaking. The arrow points to the edge showing higher accumulation along the edge of the slide. d) 950k 0.1 mg mL^{-1} Nylon30 after 5 min shaking. 52

2.6 Time based capture of nylon30 from DI water on adhesive-coated glass slides. 92k tests were performed with 5 mg mL^{-1} of nylon30. 950k and the 50:50 bimodal distribution (BD) tests were performed with 1 mg mL^{-1} nylon30. In the 92k sample at the 5 and 10 minute marks, cavities represent the absence of adhesive due to adhesive migration and coalescence. The 950k at 10 minutes also shows some adhesive migration. 54

2.7 a) Plot of time-based assessment versus %SAC for 950k and 50:50 BD of PEHA each with 1 mg mL^{-1} of nylon30 from DI water. b) Plot of %SAC versus concentration of nylon30 for 950k at 5 min shaking and 92k at 1 min shaking in DI water. Adhesives demonstrate rapid particle binding, as indicated by the non-zero intercept of the time-based assessment. 55

2.8 Plot of complex viscosity, storage modulus, and loss modulus for 92k PEHA (left), and 950k (right) PEHA 56

2.9 Optical microscope images showing nylon adsorption in the presence of varying environmental interferants. Results for 5 mg mL^{-1} of nylon and 1 minute of shaking are shown for 92k PEHA (a-f) and 950k PEHA (g-i). Results for 1 mg mL^{-1} of nylon and 5 minutes of shaking with a 50:50 bimodal distribution are depicted in (j-l). 58
2.10 Assessment of interferent properties a) with respect to interferent solution pH, and b) interferent solution density normalized to the density of nylon-12. 60
2.11 Comparison of %SAC for nylon30 and PS10 on 950k PEHA adhesive testing both parametrically and in mixed assay. A) 0.1 mg mL^{-1} nylon30 (nylon30 alone), b) mixed assay of 0.1 mg mL^{-1} of each nylon30/PS10 in DI water, c) 0.1 mg mL^{-1} PS10 (PS10 alone). 62
2.12 Plot of %SAC and particle count with respect to the particle average diameter for 0.1 mg mL^{-1} dispersions with 950k adhesive, 5 min shaking in DI water. . . 64

3.1 Analysis of native biomass and precipitated biomass films using a) FTIR and b) XRD. Dashed lines indicate expected peak positions of Cellulose I (black) and Cellulose II (red). 83
3.2 Solubility of dry cascara biomass in [DBUH][OAc] IL (% w/w) after 4h of heating at 80° C. 85
3.3 Concentration dependent rheology data, complex viscosities of cotton (a) and cascara (b), and storage (G') and loss moduli (G'') for cotton (c) and cascara (d) where closed symbols are G'' and open symbols are G'. 86
3.4 Comparison of concentration dependent η_0 values for a range of biomasses, ionic liquids, and temperatures including our data on cascara and cotton. Data IDs are presented as IL, biomass, molecular weight, temperature.[54,57,58] 88
3.5 Optical image depicting hand drawn fibers. A) cotton derived fiber (top) and a cascara fiber (bottom) both from 10% w/w solutions. B) a cascara fiber swelled with water. Speckles are indicative of undissolved material. 89
3.6 Images of films produced from 10% cascara solutions. A) full sized films, b) optical microscope image of a film showing embedded particulates, c) SEM image of a film, d) SEM image of an unprocessed cascara fruit 91

4.1 Optical and SEM images of the inner wall of cascara fruits before and after treatments. In order, the images show untreated cascara (a,e,i), ethanol treated cascara (b,f,j), dilute IL treated cascara (c,g,k), and acid chlorite treated cascara (d,h,l). Images a, b, c, and d are optical microscope images and have the same scaling. Images e-l are SEM micrographs of the cascara. . 110
4.2 Solubility of treated cascara samples in the ionic liquid, Diazabicyclo[5.4.0]undec-7-inium acetate ([DBUH][OAc]) heated for 4 hr at 100°C. 111
4.3 Temperature dependent complex viscosities of hot ethanol, dilute IL, and acid chlorite treated cascara. Data is presented as an average of 3 replicates, and error bars indicate 1 standard deviation 114
4.4 Arrhenius plot comparing hot ethanol, dilute IL, and acid chlorite pretreatments of cascara including activation energy calculations 115

4.5 Plot of 10% loaded biomass at 60°C. Data is presented as an average of 3 replicates, and error bars indicate 1 standard deviation. 116
4.6 Optical microscope images of ethanol treated fibers as extruded. A) long fiber in methanol during second washing soak, b) cross section of swelled fiber after first washing soak in methanol 117
4.7 Optical microscope images of fibers (a,b,c) and fiber cross-sections (d,e,f) for ethanol treated (a,d), dilute IL treatment (b,e), and acid chlorite treatment (c,f). 118

A.1 Images from PE50/PE200 shake test. a) Images of glass slides including the full adhesive region. b and c) Show the high level of aggregation between the PE50 spheres and PE200 flakes which make it difficult for ImageJ® to identify counts for the respective particle types. 134
A.2 Microscope image from PS10/nylon30 shake test showing moderate degradation of the 950k adhesive after 5 minutes. Red arrows indicate regions of adhesive migration where holes have opened up 135
A.3 ^{1}HNMR spectra of [DBUH][OAc] 136
A.4 DSC scan for [DBUH][OAc] demonstrating induced cold crystallization and onset melting. 137
A.5 Matlab curve fitting output for both Cross and Carreau models on cascara (a,c) and cotton (b,d) 138

LIST OF TABLES

TABLE

1.1 Engineering and behavioral controls for MP remediation[97,98,99,100,101,102,103,104,105] 11

2.1 Surface area coverage of nylon30 particles under different environmental interferants 57

3.1 Compositional assessment of biomass 82
3.2 Zero shear values (μ_0) and Carreau parameters for cotton and cascara at 60°C determined by Carreau model and Newtonian plateau calculations 87

4.1 Characterization of treated and untreated cascara 108
4.2 Cross and Carreau Model values for hot ethanol, ionic liquid, and acid chlorite pretreated cascara 113

A.1 %SAC and number count data for parametric and mixed assay experiments on 950k PEHA at 0.1 mg mL^{-1} under 5 min shaking 135
A.2 Gravimetric data for parametric and mixed assay experiments in percent total capture 135
A.3 Cross and Carreau model parameters for [DBUH][OAc]/cotton 137

ABSTRACT

It is increasingly becoming clear that the way textiles are currently produced and consumed can be unsustainable and negatively impact human and environmental health. In this study both textile production, sourcing, and use-phase related pollution were considered. In the first section of this dissertation, microplastic (MP) pollution is investigated using pressure-sensitive adhesive (PSA)-coated substrates as adsorbents. In the following two sections, coffee fruit (cascara) waste is assessed as a raw material for human-made cellulosic-fibers using ionic liquid (IL) solvents.

PSAs were identified as an effective adsorbent for MPs under aqueous conditions.To better explore PSA-MP interactions, simple glass-slide substrates were made to allow rapid optical quantification. Three formulations of poly(2-ethylhexyl acrylate) PSA were considered including 92k molecular weight (MW), 950k MW, and a 50:50 wt% bimodal distribution (BD) of the 92k and 950k. The BD yielded the most robust adhesive films after 30 min under aqueous shaking conditions while 92k and 950k films degraded after 1 and 5 min respectively. The BD samples captured 50% more nylon particles than the 950k, with maximum slide coverage achieving 25% after 30 min shaking. The broad effectiveness of PSA-based capture was demonstrated through an assessment of 10 aqueous conditions including solid, chemical, and temperature modifications. Although capture was suppressed under all non-deionized water conditions, capture remained viable except at 0.1% w/v surfactant loadings. Finally, a comparison of five MP species of different size revealed an inherent bias to MP quantification. It was found that number counts of particles bias towards smaller particles and size based assessment biases towards larger particles. I propose that future MP reporting should present both count and size based quantification to control for this bias.

ILs are expected to be greener and safer biomass solvents than more conventional fiber-making systems like the viscose and lyocell processes. In conventional fiber processes and most current IL research, purified cellulose is the primary feedstock, which requires caustic alkaline or acidic treatments for isolation. Herein, the IL, Diazabicyclo[5.4.0]undec-7-inium acetate ([DBUH][OAc]) was assessed for the dissolution and shaping of unrefined lignocellulosic biomass.

Unrefined cascara waste was investigated as a feedstock for dissolution in [DBUH][OAc] compared to cotton. Cascara is a high-volume agriculture waste that has heavy economic, environmental, and health burdens associated with disposal in producer countries. Unrefined cascara was partially soluble in [DBUH][OAc] (65% w/w), yielding a high viscosity, cellulose-rich solution that can be shaped and re-coagulated into fibers and films. Following, three pretreatments were assessed including ethanol extraction, dilute IL treatment (10% water), and an acid chlorite treatment. All pretreatments increased cascara solubility in [DBUH][OAc] ($>$ 75% w/w). 10% solutions of treated cascara were extruded into long fibers ($>$ 40 cm) with irregular, lobed cross-sections. Treated cascara fibers were qualitatively more robust than untreated cascara fibers. Ethanol treated fibers performed similarly to those treated with acid chlorite, showing promise that less harsh pretreatments of biomass may be sufficient for some applications. Overall, the cascara work suggests that complex biomass sources from agriculture waste may be viable for synthetic cellulose fibers.

CHAPTER 1

Introduction

1.1 The Big Picture

The global textile industry represents a more than one trillion-dollar (USD) industry accounting for fiber production, processing, dyeing, textile production, garment/product construction, distribution, and commercial sale.[1,2] The textile industry employs an estimated 35 million people worldwide,[3] with much of the production labor situated in the developing world under often dangerous and exploitative conditions.[1] Globally and historically, the textile industry is notorious for poor treatment of workers and human rights violations, including child labor, forced labor, poverty wages, and harmful working conditions.[4,5,6] It is estimated that the apparel industry is the world's largest employer of women, but only 2% of them earn a living wage.[7] Further, it has been calculated that the global textile industry generates 8% of the world's greenhouse gas emissions.[8]

The textile industry is built on fibers made from natural and synthetic materials which are themselves generated through agriculture, animal husbandry, forestry, and petroleum feedstocks. Natural fibers include fibers such as cotton, linen, ramie, wool, and silk. These are directly acquired from the natural world with minimal modification and are generally

considered biodegradable[a] Natural fibers that are plant-derived are rich in cellulose, the most abundant biopolymer. Synthetic fibers include polyester, nylon, acrylic, polyethylene, spandex, viscose rayon, and Tencel. They are generally produced from petroleum products (e.g., polyester, nylon, acrylic, etc.) and are generally non-biodegradable, although some synthetic fibers are produced from natural materials (e.g., viscose rayon and Tencel). Most textile fibers, whether natural or synthetic, are made of polymers. They are generally flexible and resilient, with properties depending on their orientation. In addition to textiles, polymers can be found in almost every part of modern society, including all plastics. Their properties make them ideal for textiles, as they can produce a range of stretch, durability, softness, and fabric feel.

Natural fibers were of course the first textiles, derived from what was at hand and mark an industry older than pottery and agriculture.[10] Natural fibers such as linen, wool, hemp, agave, silk, and cotton represent culturally significant fibers that have been and still are cultivated around the world. Historically, textiles were made by hand, from the cultivation and processing of raw fiber, to dyeing, spinning, weaving, and the construction of garments. This made textiles expensive and highly valued in peoples' lives.[10,11,12] Even kings and nobility were known to wear garments that were "pieced" together, meaning that single panels of clothing were constructed from multiple pieces of fabric to prevent waste and use all possible scraps of the expensive wool and silk brocade fabrics at their disposal.[13] This contrasts dramatically with the present day. Now, the average American owns 136 apparel items[14] and is likely to purchase a new item every 5.5 days.[15] It is worth noting that all garments are still sewn directly by human hands, and many of the handycraft items trendy at this time (i.e., crochet), cannot be recreated by machines and are therefore stitched by human hands. This modern accessibility and affordability to textiles as well as the industrial capacity to meet the current demand, was built up by the industrial revolution, the agricultural green revolution, and modern imperialism.[16,17]

[a]while natural fibers are expected to be biodegradable, other chemical modifications such as dyes and waterproofing may increase time to biodegradation and lead to harmful degradation products[9]

Due to current trends in consumer fashion (often called “fast fashion”) as well as increasing accessibility to high-consumption lifestyles in developing countries, the annual production of textile goods has skyrocketed.[18] Cotton has remained the most popular fiber material due to its look and feel. Cotton is produced intensively, often in areas of poor soil quality where fertilizers are heavily used.[19] It is estimated that under current consumption patterns and the continuing degradation of global soil quality,[17,19] the annual demand for cotton will outpace agricultural capacity by 2030,[17] necessitating the need to identify alternative sources of cellulosic fibers. For over a century, human-made cellulosic fibers such as viscose rayon, Tencel, and modal have been produced to meet this need.[20,21]

The *viscose rayon* process was developed in 1893[20] and is the primary process for making human-made cellulosic fibers (80%), accounting for 5.8 million tonnes in 2021.[21] The production of viscose rayon is a multi-step process that uses sodium hydroxyide (NaOH) and carbon disulfide (CS_2) to convert cellulose pulp into sodium cellulose xanthate, which is then dissolved in more NaOH to produce a ‘spinning dope’, and fibers are precipitated in a bath of dilute sulphuric acid, sodium sulphate, and zinc sulphate.[20] Since its creation, the viscose process has been known to be incredibly dangerous, with workers commonly being blinded, maimed, killed, and driven to suicide by the physical and psychological impacts of the acid coagulation bath and the CS_2 vapors.[22,11] Today most viscose rayon is produced in China, India, and Indonesia, where labor is cheap, and regulations around workers’ safety and environmental protections are weak.[11]

Through the mid to late 20th century, a new fiber process, known as *the lyocell process* was developed to improve the cost/performance profile of human-made fibers as well as produce a more environmentally benign process than used for viscose rayon. The first industrial-scale production of lyocell fibers began in 1984. In the lyocell process, cellulose pulp is directly dissolved in solvent N-Methylmorpholine N-oxide (NMMO) without forming intermediates and spun fibers are coagulated in a water bath.[23] The lyocell process benefits from high recovery rates of the NMMO ($>$ 99%), which is non-toxic and

produces no hazardous effluents. However, the NMMO in solution is prone to exothermic runaway reactions, which is accommodated by bursting pressure release discs that vent volatile amine products to the environment.[23] Both the viscose and lyocell processes require high-purity cellulose for fiber production.[20,23]

In recent years, new forms of cellulose solvents have been investigated at the laboratory and pilot scale. In 2002, Swatloski et al.[24] discovered that ionic liquids (ILs) can dissolve cellulose. Since then, ILs have been investigated as a solvent medium for cellulosic fiber production.[25,26] ILs are bulky organic salts that are proposed to be "greener" solvents due to their negligible vapor pressures, high thermal stability ($>$ 200°C), and low melting points ($<$ 100 °C),[25,26] early scale-up of IL-cellulose fiber production has yielded promising results for industrial adoption.[27,28]

During the life cycle of a textile garment, the constituting fibers wear through abrasion, breakdown, and shed, resulting in threadbare regions, holes, and less visibly laundry lint and microfibers. Particularly in domestic washing machines, estimates of 0.6 to 1.5 million microfibers are released per kg of clothing in a single wash cycle.[29,30] These fibers ultimately convey to wastewater treatment plants (WWTPs), septic tanks, landfills, and direct emissions to the environment depending on the existing waste infrastructure.[30,31] Studies of WWTPs have demonstrated fairly effective microplastic (MP) capture from liquid effluent ($>$ 90%) without infrastructure improvements.[32,33] However, the small uncaptured fraction still represents a staggering volume of MP emission to water– greater than 60 million MPs per day assuming 2 MPs L^{-1} [32,34]–and the solid fraction of WWTP effluent is often deposited in farmlands as fertilizer.[35,36] As with other synthetic polymers, the microfibers generated from the laundering of synthetic fiber clothing do not biodegrade, instead accumulating as persistent pollution in the environment.[37] Microfibers are the most common form of MPs found in many environmental field studies.[38,39]

Overall, more sustainable paths forward would reduce total textile production and consumption, which would ultimately reduce the environmental, social, and human health

impacts of the textile industry.[1] In the meantime, a transition to “greener” and lower impact fiber materials with considerations towards the full textile life-cycle would offer key benefits.[40]

1.2 Microplastic Pollution

1.2.1 Microplastics

There is a range of terminologies for plastic pollution in the environment. At the larger scale, all plastics greater than 5 mm– from automotive fragments to home appliances, bottles, and abandoned fishing nets– are called macroplastics. Microplastics (MPs) are particles between 1-5000 µm. Smaller than MPs are nanoplastics which are all plastic particles smaller than 1 µm. Within the smallest fractions of plastic pollution, micro- and nano- plastics are divided into primary and secondary plastics. *Primary microplastics* are small plastics that are manufactured within the micro and nano size range including commercial plastic pellets, sand-blasting particles, cosmetic microbeads and microfibers.

Secondary microplastics are particles derived from the degradation of larger plastic structures, generally consisting of flakes and fragments. MPs represent a chemically diverse category of pollutants broadly consisting of small polymeric fragments that span the range of common synthetic polymers used in industrial and consumer products (e.g., polyolefins, polyacrylates, urethanes, condensation polymers, etc.).[41] Notably, MPs do not behave like chemical pollutants, and cannot be appropriately considered under the conventional threshold pollution models.[42,43] Secondary MPs are generated through a range of degradation mechanisms dependent on the specific plastic source and ambient condition. The bulk of current literature is focused on marine environments where the majority of plastic by mass consists of macro- and meso-plastics.[44,45] In marine and soil environments, the dominant degradation mechanism is through UV-induced oxidation, which

embrittles surface-bound plastic, allowing for fragmentation by turbulent water, abrasion against rocks and land, and animal interactions.[37,46] In other less-studied environments such as industrial plants, indoor living spaces, and roadways, the primary degradation pathway appears to be abrasion.[47,48]

Popular science media and activism often claim that the final resting place of MPs is in the ocean.[b] However, recent theories suggest that the fate of MPs is much more dynamic. Bank & Hansson proposed "the plastic cycle" like the carbon- and nitrogen-cycles, likening the fate of plastics to the cyclical transport of matter from one environmental compartment to another.[41,49] For example, plastic particles deposited on riverbeds can be recirculated downstream by animal consumption or storm conditions, and sea spray has been observed to convey ocean particles into the atmosphere.[49,50]

Currently it is estimated that 1.5 million tons of MPs enter the ocean each year.[31] Since MPs do not biodegrade, their numbers in the environment will continue to compound at a staggering rate. The impacts of MP pollution have received broad attention in the research community regarding human, animal, and environmental health. As of this writing, there has been little consensus on direct, quantifiable harm; however, it is indisputable that MPs are pervasively present in our air, soil, seas, and bodies. Regardless of harm, MPs are likely to represent humanity's thumbprint on the geological timeline.[51,52]

1.2.2 Microplastic sources and sinks in the environment

MPs are small, chemically diverse, and formed through numerous human activities which makes it hard to assess and control their emission and distribution. For these reasons, estimations of MPs in the environment are hard to appraise[53,54,55] and make MPs unique as pollution and difficult to define within conventional regulatory frameworks.[42] Identifying MP sources has largely been accomplished through visual and chemical anal-

[b] While it is often claimed that the ocean is the final resting place for MPs, it is estimated that 4-23 times as many plastic particles are released on land than the sea.[46]

ysis of particles in the environment. The goal of identifying MP sources is to locate responsibility and enact preventative control measures.[56,57] However, unlike industrial chemical spills, there is no single guilty party liable in MPs emissions. The majority of *known* MP emissions are produced through common human activities such as washing clothes and commuting by car (**Figure 1.1**).[31,35] Other common sources of MPs include industrial losses (i.e., runoff, transit losses) and commercial fishing. Illegal dumping and littering, coastal natural disasters, and poor waste management practices make up much of the remaining MP sources.[58,59] Understanding MP sinks and sources is important for developing relevant solutions that can function within specific environments without negative knock-on effects.

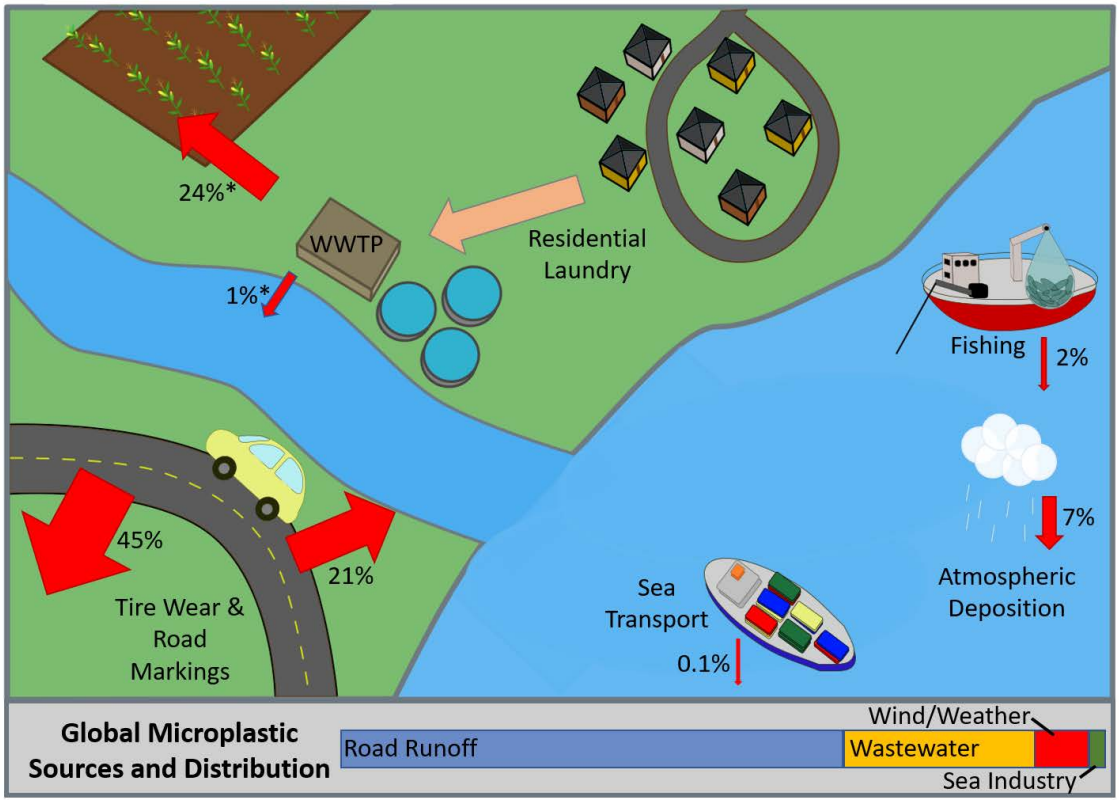

Figure 1.1: Estimates of MP mass flows into the environment from key point sources based on the work of Boucher & Froit.[31] The asterisks "*" indicate modified measurements based on the distribution of MPs in WWTP biosolids.[35]

Textile - wastewater treatment plants

MPs derived from textiles originate from the degradation of clothing and textile goods as they are made, used, and washed. The most common composition of textile derived MPs found in the environment are polyethylene teraphthalate (PET), polypropylene (PP), nylon, and acrylic.[60] These MPs tend to have high aspect ratios and are also commonly called microfibers. The majority of these textile MPs are released during laundering, where they subsequently pass on to wastewater treatment plants (WWTPs) or home septic systems.[60] Several studies have looked at the numerical generation of MPs from home laundry, with emissions measured as high as 640,000 to 1.5 million MPs released per kg of textiles.[29,30] Washing machines have been identified as an important intervention point for capturing MPs.[61,62] Numerous technologies currently exist on the market, generally relying solely on forms of physical filtration and entrapment to remove MPs from the laundry effluent.[62] Laundry effluent is a complicated medium to work in due to the wide range of laundry detergent compositions that can interrupt surface binding.[63,64]

Tire wear

Many microplastics originate from the abrasion of tires during driving and the tensile liberation of particles as tires decouple from the road. Subsequently, these numerous and mobile particles are dispersed via wind and water run-off.[47,65] Tires are typically made from formulations of styrene-butadiene rubber (which is among the most toxic polymers[65,66]) and carbon black. Tire wear debris has been identified near roadways, in urban atmospheric fallout, and in sea water.[31,67,68] In 2015, it was estimated that 60,000 to 111,000 tonnes of MPs could be generated from tire abrasion annually in Germany alone.[68,69,70] While tire particles have been measured in airborne collection,[47,66] the measured specific gravity (1.15-1.18) is higher than the average value of ocean water, and particles are likely to have less retention in the upper water column.[47] The high density of tire wear particles as well as their dark color, will also complicate the ability to isolate

them from soil samples using common density-float methods.

Research on solutions towards the proliferation of tire wear debris has been limited.[71] These particles are particularly complicated to contain because they have a continuous emission directly into the environment, and the sheer volume of roadways would make it economically and logistically prohibitive to retrofit engineering-based solutions. Furthermore, car tire compositions are regulated for friction and weather performance, which makes updating the chemical composition an unlikely avenue for MP control.[72]

Fishing and marine debris

Plastic debris and MPs were recorded in the North Atlantic Ocean as early as the 1970s,[73,74] and have since become a highly visible aspect of global pollution in the public consciousness. The bulk of marine MPs have been identified as secondary MPs highlighting the influence of littering and ocean dumping, among other human activities.[75,76] Other primary MPs are identified as industrial feedstocks sourced at manufacturing facilities[77,78] or introduced during sea transport.[31] These feedstocks are typically in the form of plastic resin powders and pellets.[79] There are also non-negligible contributions from marine-based sources such as fishing, shipping, and aquaculture.[31,80,81] Another major source of marine debris is tied to natural disasters such as hurricanes,[82] tsunamis,[83] and flash flooding.[84]

Marine MPs overall are particularly diverse due to the tendency of land runoff to convey litter and pollution into bodies of water.[59,85] There are significant, positive correlations of MP concentration with proximity to population density.[86] Marine sampling and clean-up activities are complicated by the presence of biological matter that is collected along with the intended MPs, which can clog filters and inflate particle counts.[42,87] There are also a myriad of water conditions that will affect local buoyancy and surface-binding based MP capture such as salinity, temperature, pH, and industrial pollution.[63]

Food

An increasing number of studies have shown the prevalence of MP contamination in packaged consumables. Largely attributed to water sourcing, MPs have been widely identified in bottled water,[88] beer,[89,90] salt,[91] seafood,[92] packaged meat,[93] pet foods,[94] honey,[90] milk,[90] soft drinks,[90] and restaurant take-out.[95] In a study designed to examine the global reach of MP contaminated products, Kosuth et al.[91] identified MPs in all samples of globally sourced sea salts and in 81% of 159 tap water samples from 14 countries. Further, food packaging accounts for a major fraction of single-use plastic items, which shed particles on opening,[48,93] and commonly end up as litter.[46,88]

1.2.3 Microplastic solutions

Within the space of technological research, the study of wastewater treatment plants (WWTPs) occupies a substantial quantity of grant funding and research hours. As a central focus in the efforts to capture MPs before the environment, many studies have focused on the ability of WWTPs to capture MPs.[32,33,96] Despite being able to capture MPs in excess of 90% from the water fraction (**Table 1.1**), the massive volume of wastewater processed still results in a sizeable quantity of MPs re-introduced into the environment.[33] Further, WWTP solid wastes are often directly distributed back into the environment as a rich fertilizer, thus eliminating the efficacy of the MP capture.[35] Using WWTPs as an example, it quickly becomes clear that a system-scale approach that leverages life-cycle thinking is required to develop leak-proof solutions.

Table 1.1: Engineering and behavioral controls for MP remediation[97,98,99,100,101,102,103,104,105]

Device/ Approach	Details	Capture Size	Efficiency	Scalability	Ref.
WWTP					
activated sludge process	a series of screens, sedimentation, clarifiers, filtration, and disinfection processes to treat sewage	≧20μm	97–99%	●●●	32
biofilter	a stacked column of stone wool and granite gravel, as biofilm substrate	≧150 μm	87.9%	●●●	97
biochar	thermally activated biochar with modest surface area (200–600 m²/g)	10 μm – 3 mm	100%	●●	98
coagulation/ flocculation	study of common WWTP coagulants, ferric chloride and polyaluminum chloride	1,6 μm	99.40%	●●●	99
disk filter	a stack of woven PP, PET, polyamide meshes of 10–40 μm pore size	≧18um	89.70%	●●●	100
anodic oxidation	MPs are electro-oxidatively degraded to gaseous byproducts. degrade 58 ± 21% of MPs in 1h		90%	●	101
magnetic carbon nanotubes	M-CNTs adsorb to MP then are magnetically removed	48 μm	100%	●	102
Tires					
wear resistant tires	tire composition and treatment could be adjusted for greater wear resistance	-	-	●●	47
vacuum vehicles	devices for cleaning tire wear debris and litter from cities and roadways			●●	-
reduction in car weight	tire wear is directly proportional to tire load	-	-	●●●	103
smart roads	a micro-porous road can sequester MPs until appropriately cleaned	-	-	●●	71
driving behavioral change	high speed maneuvering and quick acceleration are associated with elevated MP production,	-	-	●●●	47
Laundry					
washing machine filter	externally mounted devices relying on physical trapping fibers from laundry	-	25–78%	●●●	30
Cora Ball	a ball shaped device to be added into laundry to capture MPs on hooked arms	-	31%	●●	30
washing bags	fine mesh bags designed to trap MPs from clothing washed in bags	-	21–54%	●●	30
fiber development	development of "shed-resistant" fibers and fabrics for clothing/household applications	-	-	●●●	-
fiber choice	change selection towards non-synthetic fibers at industry and consumer levels		-	●●	-
Packaging					
designing waste out of the system	packaging can be strategically designed to omit single use plastic	-	-	●●●	104
degradable polymers	developing new polymers that readily biodegrade into non-harmful components	-	-	●●●	105
refillable packaging	adoption of a refill-based retail model for consumables (i.e., bulk foods, cleaning supplies)	-	-	●●●	-

Qualitative Scalability	●●●	readily implementable	●●	promising development	●	early development/ concerns	already broadly implemented

In a 2016 report by the Dutch National Institute for Public Health and the Environment, Verschoor et al.[71] proposed a sweeping approach to minimize MP emissions associated with car tire wear. This approach would involve actions by many stakeholders, from the governmental level to the individual. Notably, the report demonstrated a need to consider both "engineering controls", and "behavioral controls".[71] The former embodies the physical technology and processes that are directly deployed to control the problem, and the latter involves the social, cultural, and industrial buy-in that would be necessary for the broad, effective implementation of new policy and infrastructure. Verschoor et al., highlighted engineering controls in both the roles of MP prevention and retention in the arena of tire MPs. Examples of such innovations included the development of more resilient tire materials that shed fewer MPs, smoother road surfaces that reduce the wear on tires, and improved sewer systems that would facilitate material recovery. All of which highlighted the need for creative interventions throughout the entire system.[71]

Table 1.1 presents an inexhaustive list of engineering and behavior controls targeted at the commonly identified MP sources. More research is needed to assess both the effectiveness and ease of adoptability of various tools, behaviors, and stop-gaps until more robust infrastructure and industrial practice can be implemented. However, in a broader stroke of consideration, much like the management of chlorofluorocarbon (CFC) pollution, it is envisioned that the most effective remediation to MP pollution would be to design unnecessary plastics out of the system. For instance, to reduce MPs originating from tire wear, a city planning initiative that incentivizes broad participation in public transportation and foot travel in conjunction with other preventative and retentive schemes would have superior performance.

1.2.4 Microplastics outlooks

In the last 70 years, plastics have become indispensable to daily life. Moreover, the use of plastics offers many benefits to society, including enhanced access to affordable

goods, sterile single-use products, weight-saving on vehicles and in product packaging that minimizes transit-related CO_2 emissions, functionalized materials that are facilitating the green-energy revolution, and use in life-saving medical devices, implants, and coatings. Simultaneously, the proliferation of convenience plastics and the thorough integration of plastics into our lives is creating a real pollution problem that seems intractable. To measurably move the dial on MP pollution, there needs to be a multilateral approach that brings together governments, industry, and consumers to reduce our total reliance on plastic materials and implement effective barriers to reduce the further release of MPs into the environment.

Key intervention areas such as plastics regulation and policies like the US Microbead-Free Waters Act (MFWA), plastic bag bans,[106] and single-use plastic bans,[106,107,108] as well as device development,[62] and social initiatives[109,110] are growing in popularity. There are exciting prospects for reducing and eliminating MPs emissions, however, large questions remain. First, interventions must be thoroughly considered to assess for harm, whether that is ecosystem harm from device deployment, or social harm through loss of access and accommodations. For example, a single-use plastic ban in Mexico City targeted plastic tampon applicators, which led to menstrual poverty for many citizens who rely on the cheaper and readily accessible plastic options.[111] Second, while MPs may be collected from the environment, there are still no permanent solutions regarding sequestration, elimination, or reuse. Currently, incineration is thought to be one of the only disposal methods that ensures elimination of MPs,[112,113] but many health and environmental issues have been linked to incineration.[114] Recent research also suggests that incineration may function as another distribution source of MPs.[115] Landfilling is the other primary disposal form, although it does not eliminate the MPs and may not be a very permanent solution.[116] As we become better equipped to capture the MPs that are produced, we must also develop better ways to sequester or destroy the particles to prevent their recirculation in the plastic-cycle.[49]

1.3 Ionic Liquid Dissolution of Cellulose

1.3.1 Ionic liquids

Ionic liquids (ILs) are tunable organic salts that tend to have low melting temperatures (T_m <100°C), negligible vapor pressures and high thermal stability.[26] Because of these qualities, ILs are broadly considered "greener" solvents,[117] although there are growing concerns regarding the toxicity of some species.[118] ILs are composed of a cation and an anion that can each have substituents, which contributes to their modular nature. ILs are grouped into categories based on the cation, with the 3 most common being heterocyclic amines (i.e. imidazolium and pyridinium), quaternary cations (i.e. ammonium and phosphonium), and superbases (i.e. DBUH, TMGH).[26] The structure and properties of ILs are dominated by polar forces, with hydrogen-bonding functioning as the primary driver in protic-systems.[119,120] Due to their tunability and unique polar properties, ILs have been applied in numerous applications[121] such as solvents, lubricants, catalysts, battery electrolytes,[122] and substrates for carbon capture.[117]

1.3.2 Dissolution of cellulose by ionic liquids

Cellulose is the most abundant natural polymer on earth, with an estimated annual production of 1.5×10^{12} tons per year.[123] Cellulose is a linear-chain polymer with a β-D-gluco-pyranose monomer linked through $\beta(1 \rightarrow 4)$ glycosidic bonds. Native cellulose is bound in a monoclinic crystal structure by a strong network of inter- and intramolecular hydrogen bonds.[124] The measured crystallinity of native cellulose typically ranges from 30-80% depending on the type of biomass,[125,126,127] with the capacity to increase to 60-90% when isolated as microcrystalline cellulose or nanofibers.[128,129] In plants, cellulose primarily exists in highly recalcitrant lignocellulosic biomass consisting of cellulose, hemicellulose, and lignin; although, there is a diversity of plant structures, with cotton fibers

consisting almost exclusively of cellulose,[130] and coffee beans containing only 8.6% cellulose with 36.7% hemicellulose.[131] Lignocellulosic biomass is generally conceptualized as bundles of cellulose microfibrils that are surrounded with a layer of covalently bonded hemicellulose and lignin that binds the system together.[132] For most engineering applications (paper, bioethanol, cellulosic fibers, etc.), refined cellulose is desired, often requiring harsh chemical processing to strip away the hemicellulose and lignin.[133] In recent years, there has been interest in valorizing these other waste fractions, including extractives, lignin, hemicellulose, and mixed systems.[133]

The dissolution of cellulose by ILs was first reported in 2002 by Swatloski et al.,[24] who investigated a series of halogenated imidazolium ILs. Since then, dozens of ILs have been identified to dissolve cellulosic biomass.[134] The mechanism of cellulose dissolution in ILs is reliant on both H-bonding and coulombic interactions.[135] The current theory is that both the anion and the cation respectively contribute to the dissolution process. It is proposed that first the anion, which is often smaller and more mobile than the cation, infiltrates the cellulosic matrix and H-bonds to the cellulose hydroxyl groups, swelling the biomass.[136] Subsequently, the bulkier cation is drawn into the matrix through H-bonding and coulombic interaction with the anions, which physico-chemically cleaves the remaining H-bonding between adjacent cellulose molecules and creates solvent cages around individual cellulose chains bringing the cellulose into solution.[137,138] The solvated cellulose yields a highly viscous solution that yields the characteristic shear-thinning behavior of solvated polymers.[139,140] In this state, the dissolved cellulose can be spun into fibers[141] or formed into films[142,135] and precipitated into an anti-solvent bath. Anti-solvents typically consist of polar protic-solvents, including water, hot water, methanol, acetone, and mixtures thereof.[26,143]

1.3.3 Coffee Fruit

Coffee is an important global crop grown over a wide band of equatorial countries spanning across South and Central America, Asia, and Africa. It is often claimed that coffee is the second most traded commodity[c] [131,144,145] with 7.0 million metric tons of beans traded annually.[131] As a commodity, the seed (or bean) of the coffee cherry is the primary source of value of the cultivated product, with the fruit generally discarded.[131] The dried fruit mass represents 45% of the cultivated mass (29% by dry weight),[131] therefore producing 2 to 3 million metric tons of coffee fruit waste annually. The dried fruit has recently been marketed as a tea-like product called cascara, derived from the Spanish word for peel or husk, although a coffee fruit tea has long been drunk in Ethiopia (as *hashara*) and Yemen (as *qishr*).[146] In industrial coffee cultivation, the fruit residue is primarily landfilled, burned, or dumped.[131,147] Furthermore, coffee fruit contains caffeine and tannins, which are toxic in concentrated form.[148] Due to the elevated presence of sugars and water in the cascara, the fruit residue is prone to putrefaction and attraction of pests, which is often controlled with pesticide applications.[131] Therefore, there is a sizeable impact from coffee fruit disposal both in monetary maintenance costs, impacts to human health, and ecological health.

Although challenges exist, various uses of coffee fruit residues have been explored. The primary interest is in the extraction of value-added compounds such as bio-fuels,[149] caffeine, antioxidants, anthocyanin-based dyes, and flavoring agents.[131] However, we identified value in the under-explored cellulose fraction of the coffee fruit, which has been reported to consist of 40-63% of the dried mass.[131,150] Previous studies have assessed the use of ILs to extract lignin from coffee husk[151] and extraction of staple fibers from the bleached coffee pulp.[152,153,154] Herein we explore the dimensions of pretreatment that facilitate the functional processing of coffee fruit for manipulation with ILs.

[c] This is likely untrue, at least in 2023, and there is little evidence to back it up

1.4 Summary of work

This dissertation presents work on two projects that aim to advance sustainability goals around establishing a circular economy. In the first section, research performed on PSA-based MP capture will be discussed. In the following two sections, work performed on the IL dissolution of treated coffee fruits for use in fiber applications will be described.

1.4.1 Quantification and capture of microplastics via pressure sensitive adhesives

In Chapter 2, I will describe a novel MP analysis and quantification method based on deploying PSAs to capture MPs from aqueous environments that was previously published in the manuscript *Pressure sensitive adhesives for quantifying microplastic isolation* in the Journal of Separation and Purification Technology.[134] The contents of this chapter include the incorporation of data from the original manuscripts' supplementary information file (section 2.3 and appendix A) as well as some additional data, including the assessment of aqueous interferent density and pH (secion 2.4.2), that was not presented in the original manuscript.[134] Here I describe the mechanism of PSA-based capture of MP and how that is leveraged in poly(2-ethylhexyl acrylate) based systems. Glass slides are assessed as cheap, simple substrates for airbrushed adhesive films to facilitate the rapid capture and quantification of MPs from a variety of aqueous environments. PSA-based capture of five MP species is assessed using optical microscopy and the free, open-source image analysis tool, ImageJ®. Ten environmental conditions are also assessed for inhibition of MP adsorbance.

1.4.2 Ionic liquid processing of untreated coffee fruit residues

Chapter 3 describes the capacity to process untreated, dried coffee fruit with ILs to make fibers and films. The content of this chapter is currently in review for the journal Macromolecular Materials and Engineering in the manuscript “Ionic liquid-mediated biopolymer extraction from coffee fruit”. The superbase-derived IL Diazabicyclo[5.4.0]undec-7-inium acetate ([DBUH][OAc]) is assessed for dissolving whole cascara biomass. The treatment of cascara with [DBUH][OAc] is probed across solubility, solution properties, compositional characterization before and after dissolution, and capacity to shape solid isolates.

1.4.3 Influence of pretreatments on the ionic liquid processing of coffee fruit residues

In Chapter 4, coffee fruit residues are assessed on a spectrum of pretreatments ranging from hot ethanol treatment, dilute IL pretreatment, and a more conventional acid chlorite bleaching. The interaction between pretreated coffee fruit residues and IL, [DBUH][OAc] are assessed on the basis of solubility, solution properties, chemical characterization, fiber extrusion, and tensile testing of uniaxial fiber-epoxy composites.

1.5 References

[1] UN Environment Programme. Sustainability and Circularity in the Textile Value Chain - Global Stocktaking. Technical report, Nairobi, Kenya, 2020.

[2] Laura Wood. Outlook on the textile global market to 2027 - Investment in manufacturing practices that target sustainable products is driving growth. Technical report, Globe Newswire, Dublin, 2021. URL https://www.globenewswire.com/news-release/2021/12/30/2359133/28124/en/Outlook-on-the-Textile-Global-Market-to-2027-Investment-in-Manufacturing-Practices-That-Target-Sustainable-Products-is-Driving-Growth.html.

[3] Anupriya Desore and Sapna A Narula. An overview on corporate response towards sustainability issues in textile industry. *Environment, Development and Sustainability*, 20(4):1439–1459, 2018. ISSN 1573-2975. doi:10.1007/s10668-017-9949-1.

[4] Rajendra N. Srivastava. Children at Work, Child Labor and Modern Slavery in India: An Overview. *Indian Pediatrics*, 56(8):633–638, 2019. ISSN 09747559. doi:10.1007/s13312-019-1584-5.

[5] ILO. Global estimates of child labour: results and treands, 2012-2016. Technical report, International Labour Organization Geneva, Geneva, 2017.

[6] Ana María Herrera Almanza and Blanca Corona. Using Social Life Cycle Assessment to analyze the contribution of products to the Sustainable Development Goals: a case study in the textile sector. *International Journal of Life Cycle Assessment*, 25(9):1833–1845, 2020. ISSN 16147502. doi:10.1007/s11367-020-01789-7.

[7] Maxine Bédat and Michael Shank. There is a major climate issue hiding in your closet: fast fashion. *Fast Company*, November 2016. URL https://www.fastcompany.com/3065532/there-is-a-major-climate-issue-hiding-in-your-closet-fast-fashion.

[8] UNEP. UN launches drive to highlight environmental cost of staying fashionable, 2019. URL https://news.un.org/en/story/2019/03/1035161.

[9] Marielis C. Zambrano, Joel J. Pawlak, Jesse Daystar, Mary Ankeny, and Richard A. Venditti. Impact of dyes and finishes on the aquatic biodegradability of cotton textile fibers and microfibers released on laundering clothes: Correlations between enzyme adsorption and activity and biodegradation rates. *Marine Pollution Bulletin*, 165(January):112030, 2021. ISSN 18793363. doi:10.1016/j.marpolbul.2021.112030. URL https://doi.org/10.1016/j.marpolbul.2021.112030.

[10] E. J. W Barber. *Prehistoric textiles: the development of cloth in the neolithic and bronze ages with special reference to the Aegean*. 2021.

[11] Kassia St.Clair. *The Golden Thread: How Fabric Changed History*. Liveright Publishing, New York, 2019.

[12] Lena Bjerregaard and Ann H. Peters. PreColumbian textile Conference VIII. 2020.

[13] Lilian Zirpolo. (De)Constructing the Madonna's Cloth of Honor Pieced Cloths in Late Medieval Italian Paintings, Their Origins, and Iconographic Significance. *Explorations in Renaissance Culture*, 47(2):196–232, 2021. ISSN 23526963. doi:10.1163/23526963-04702002.

[14] P. Smith. Average number of apparel items owned by consumers worldwide from 2017-2019, 2022. URL https://www.statista.com/statistics/1008465/average-number-of-apparel-items-owned-by-consumers-worldwide/.

[15] Kirsi Niinimäki, Greg Peters, Helena Dahlbo, Patsy Perry, Timo Rissanen, and Alison Gwilt. The environmental price of fast fashion. *Nature Reviews Earth and Environment*, 1(4):189–200, 2020. ISSN 2662138X. doi:10.1038/s43017-020-0039-9.

[16] Majdouline Elhichou. A New Luxury: Deconstructing Fashion's Colonial Episteme. *Luxury*, 8(2):213–227, 2021. ISSN 2051-1817. doi:10.1080/20511817.2021.2030921. URL https://doi.org/10.1080/20511817.2021.2030921.

[17] Franz M. Haemmerle. The Cellulose Gap (The Future Of Cellulose Fibres). In *2011 Lenzing – Nature Jeju Festival*, pages 99–108, 2011. doi:10.1021/ie50113a034.

[18] Kineta Hung and David K. Tse. Luxury brand consumption in emerging economies: review and implications. In *Research Handbook on Luxury Branding*, pages 93–116. 2020.

[19] D. Blaise and K. R. Kranthi. Cotton Production in India. In *Cotton Production*, pages 193– 215. 2019.

[20] Andrew G. Wilkes. The viscose process. In *Regenerated Cellulose Fibres*, pages 37–61. 2001.

[21] Textile Exchange. Preferred Fiber and Materials: Market Report 2022. Technical Report October, 2022.

[22] Enrico C. Vigliani. Carbon disulphide poisoning in viscose rayon factories. *British Journal of Industrial Medicine*, 11:235–244, 1954.

[23] Patrik White. Lyocell: the production process and market development. In *Regenerated Cellulose Fibres*, pages 62–87. 2001.

[24] Richard P. Swatloski, Scott K. Spear, John D. Holbrey, and Robin D. Rogers. Dissolution of cellose with ionic liquids. *Journal of the American Chemical Society*, 124 (18):4974–4975, 2002. ISSN 00027863. doi:10.1021/ja025790m.

[25] Keith E. Gutowski. Industrial uses and applications of ionic liquids. *Green Chemistry in Industry*, pages 43–58, 2018. doi:10.1515/9783110562781-004.

[26] Julie M. Rieland and Brian J. Love. Ionic liquids: A milestone on the pathway to greener recycling of cellulose from biomass. *Resources, Conservation and Recycling*, 155(September 2019):104678, 2020. ISSN 18790658. doi:10.1016/j.resconrec.2019.104678. URL https://doi.org/10.1016/j.resconrec.2019.104678.

[27] Herbert Sixta, Anne Michud, Lauri Hauru, Shirin Asaadi, Yibo Ma, Alistair W.T. King, Ilkka Kilpeläinen, and Michael Hummel. Ioncell-F: A High-strength regenerated cellulose fibre. *Nordic Pulp and Paper Research Journal*, 30(1):43–57, 2015. ISSN 0283-2631. doi:10.3183/npprj-2015-30-01-p043-057.

[28] Y. Ma, M. Hummel, M. Määttänen, A. Särkilahti, A. Harlin, and H. Sixta. Upcycling of waste paper and cardboard to textiles. *Green Chemistry*, 18(3):858–866, 2016. ISSN 14639270. doi:10.1039/c5gc01679g.

[29] Francesca De Falco, Gennaro Gentile, Emilia Di Pace, Maurizio Avella, and Mariacristina Cocca. Quantification of microfibres released during washing of synthetic clothes in real conditions and at lab scale. *European Physical Journal Plus*, 133(7), 2018. doi:10.1140/epjp/i2018-12123-x.

[30] Imogen E. Napper and Richard C. Thompson. Release of synthetic microplastic plastic fibres from domestic washing machines: Effects of fabric type and washing conditions. *Marine Pollution Bulletin*, 112(1-2):39–45, 2016. ISSN 18793363. doi:10.1016/j.marpolbul.2016.09.025. URL http://dx.doi.org/10.1016/j.marpolbul.2016.09.025.

[31] J. Boucher and D. Friot. Primary microplastics in the oceans: A global evaluation of sources. Technical report, 2017.

[32] Eric A. Ben-David, Maryana Habibi, Elias Haddad, Mahdi Hasanin, Dror L. Angel, Andy M. Booth, and Isam Sabbah. Microplastic distributions in a domestic wastewater treatment plant: Removal efficiency, seasonal variation and influence of sampling technique. *Science of the Total Environment*, 752:141880, 2021. ISSN 18791026. doi:10.1016/j.scitotenv.2020.141880. URL https://doi.org/10.1016/j.scitotenv.2020.141880.

[33] Julia Talvitie, Anna Mikola, Outi Setälä, Mari Heinonen, and Arto Koistinen. How well is microlitter purified from wastewater? – A detailed study on the stepwise removal of microlitter in a tertiary level wastewater treatment plant. *Water Research*, 109:164–172, 2017. ISSN 18792448. doi:10.1016/j.watres.2016.11.046.

[34] H. A. Leslie, S. H. Brandsma, M. J.M. van Velzen, and A. D. Vethaak. Microplastics en route: Field measurements in the Dutch river delta and Amsterdam canals,

wastewater treatment plants, North Sea sediments and biota. *Environment International*, 101:133–142, 2017. ISSN 18736750. doi:10.1016/j.envint.2017.01.018. URL http://dx.doi.org/10.1016/j.envint.2017.01.018.

[35] Luca Nizzetto, Martyn Futter, and Sindre Langaas. Are Agricultural Soils Dumps for Microplastics of Urban Origin? *Environmental Science and Technology*, 50(20): 10777–10779, 2016. ISSN 15205851. doi:10.1021/acs.est.6b04140.

[36] Nicolas Weithmann, Julia N. Möller, Martin G.J. Löder, Sarah Piehl, Christian Laforsch, and Ruth Freitag. Organic fertilizer as a vehicle for the entry of microplastic into the environment. *Science Advances*, 4(4):1–7, 2018. ISSN 23752548. doi:10.1126/sciadv.aap8060.

[37] Ee Ling Ng, Esperanza Huerta Lwanga, Simon M. Eldridge, Priscilla Johnston, Hang Wei Hu, Violette Geissen, and Deli Chen. An overview of microplastic and nanoplastic pollution in agroecosystems. *Science of the Total Environment*, 627: 1377–1388, 2018. ISSN 18791026. doi:10.1016/j.scitotenv.2018.01.341. URL https://doi.org/10.1016/j.scitotenv.2018.01.341.

[38] Juan A. Conesa and Nuria Ortuño. Reuse of Water Contaminated by Microplastics, the Effectiveness of Filtration Processes: A Review. *Energies*, 15(7):2432, 2022. ISSN 19961073. doi:10.3390/en15072432.

[39] Ryan Helcoski, Lance T. Yonkos, Alterra Sanchez, and Andrew H. Baldwin. Wetland soil microplastics are negatively related to vegetation cover and stem density. *Environmental Pollution*, 256:113391, 2020. ISSN 18736424. doi:10.1016/j.envpol.2019.113391. URL https://doi.org/10.1016/j.envpol.2019.113391.

[40] Maarit Aakko and Ritva Koskennurmi-Sivonen. Designing Sustainable Fashion: Possibilities and Challenges. *Research Journal of Textile and Apparel*, 17(1):13–22, 2013. ISSN 25158090. doi:10.1108/RJTA-17-01-2013-B002.

[41] Penghui Li, Xiaodan Wang, Min Su, Xiaoyan Zou, Linlin Duan, and Hongwu Zhang. Characteristics of Plastic Pollution in the Environment: A Review. *Bulletin of Environmental Contamination and Toxicology*, 107(4):577–584, 2021. ISSN 14320800. doi:10.1007/s00128-020-02820-1. URL https://doi.org/10.1007/s00128-020-02820-1.

[42] Max Liboiron. *Pollution is Colonialism*. Duke University Press, 2021.

[43] Albert A. Koelmans, Paula E. Redondo-Hasselerharm, Nur Hazimah Mohamed Nor, Vera N. de Ruijter, Svenja M. Mintenig, and Merel Kooi. Risk assessment of microplastic particles. *Nature Reviews Materials*, 7(2):138–152, 2022. ISSN 20588437. doi:10.1038/s41578-021-00411-y.

[44] Atsuhiko Isobe and Shinsuke Iwasaki. The fate of missing ocean plastics: Are they just a marine environmental problem? *Science of the Total Environment*,

825:153935, 2022. ISSN 18791026. doi:10.1016/j.scitotenv.2022.153935. URL https://doi.org/10.1016/j.scitotenv.2022.153935.

[45] L. Lebreton, B. Slat, F. Ferrari, B. Sainte-Rose, J. Aitken, R. Marthouse, S. Hajbane, S. Cunsolo, A. Schwarz, A. Levivier, K. Noble, P. Debeljak, H. Maral, R. Schoeneich-Argent, R. Brambini, and J. Reisser. Evidence that the Great Pacific Garbage Patch is rapidly accumulating plastic. *Scientific Reports*, 8(1):1–15, 2018. ISSN 20452322. doi:10.1038/s41598-018-22939-w. URL http://dx.doi.org/10.1038/s41598-018-22939-w.

[46] Alice A. Horton, Alexander Walton, David J. Spurgeon, Elma Lahive, and Claus Svendsen. Microplastics in freshwater and terrestrial environments: Evaluating the current understanding to identify the knowledge gaps and future research priorities. *Science of the Total Environment*, 586:127–141, 2017. ISSN 18791026. doi:10.1016/j.scitotenv.2017.01.190. URL http://dx.doi.org/10.1016/j.scitotenv.2017.01.190.

[47] Pieter Jan Kole, Ansje J. Löhr, Frank G.A.J. Van Belleghem, and Ad M.J. Ragas. Wear and tear of tyres: A stealthy source of microplastics in the environment. *International Journal of Environmental Research and Public Health*, 14(10), 2017. ISSN 16604601. doi:10.3390/ijerph14101265.

[48] Zahra Sobhani, Yongjia Lei, Youhong Tang, Liwei Wu, Xian Zhang, Ravi Naidu, Mallavarapu Megharaj, and Cheng Fang. Microplastics generated when opening plastic packaging. *Scientific Reports*, 10(1):1–7, 2020. ISSN 20452322. doi:10.1038/s41598-020-61146-4. URL http://dx.doi.org/10.1038/s41598-020-61146-4.

[49] Michael S. Bank and Sophia V. Hansson. The Plastic Cycle: A Novel and Holistic Paradigm for the Anthropocene. *Environmental Science and Technology*, 53(13): 7177–7179, 2019. ISSN 15205851. doi:10.1021/acs.est.9b02942.

[50] Steve Allen, Deonie Allen, Kerry Moss, Gaël Le Roux, Vernon R. Phoenix, and Jeroen E. Sonke. Examination of the ocean as a source for atmospheric microplastics. *PLoS ONE*, 15(5):1–14, 2020. ISSN 19326203. doi:10.1371/journal.pone.0232746.

[51] Jan Zalasiewicz, Colin N. Waters, Juliana A. Ivar do Sul, Patricia L. Corcoran, Anthony D. Barnosky, Alejandro Cearreta, Matt Edgeworth, Agnieszka Gałuszka, Catherine Jeandel, Reinhold Leinfelder, J. R. McNeill, Will Steffen, Colin Summerhayes, Michael Wagreich, Mark Williams, Alexander P. Wolfe, and Yasmin Yonan. The geological cycle of plastics and their use as a stratigraphic indicator of the Anthropocene. *Anthropocene*, 13:4–17, 2016. ISSN 22133054. doi:10.1016/j.ancene.2016.01.002.

[52] Jake Martin, Amy L. Lusher, and Francis Chantel Nixon. A review of the use of microplastics in reconstructing dated sedimentary archives. *Science of the Total Environment*, 806(7491):150818, 2022. ISSN 18791026.

doi:10.1016/j.scitotenv.2021.150818. URL https://doi.org/10.1016/j.scitotenv.2021.150818.

[53] L. M. van Mourik, S. Crum, E. Martinez-Frances, B. van Bavel, H. A. Leslie, J. de Boer, and W. P. Cofino. Results of WEPAL-QUASIMEME/NORMANs first global interlaboratory study on microplastics reveal urgent need for harmonization. *Science of the Total Environment*, 772, 2021. ISSN 18791026. doi:10.1016/j.scitotenv.2021.145071.

[54] Atsuhiko Isobe, Nina T. Buenaventura, Stephen Chastain, Suchana Chavanich, Andrés Cózar, Marie DeLorenzo, Pascal Hagmann, Hirofumi Hinata, Nikolai Kozlovskii, Amy L. Lusher, Elisa Martí, Yutaka Michida, Jingli Mu, Motomichi Ohno, Gael Potter, Peter S. Ross, Nao Sagawa, Won Joon Shim, Young Kyoung Song, Hideshige Takada, Tadashi Tokai, Takaaki Torii, Keiichi Uchida, Katerina Vassillenko, Voranop Viyakarn, and Weiwei Zhang. An interlaboratory comparison exercise for the determination of microplastics in standard sample bottles. *Marine Pollution Bulletin*, 146(July):831–837, 2019. ISSN 18793363. doi:10.1016/j.marpolbul.2019.07.033. URL https://doi.org/10.1016/j.marpolbul.2019.07.033.

[55] Yanina K. Müller, Theo Wernicke, Marco Pittroff, Cordula S. Witzig, Florian R. Storck, Josef Klinger, and Nicole Zumbülte. Microplastic analysis—are we measuring the same? Results on the first global comparative study for microplastic analysis in a water sample. *Analytical and Bioanalytical Chemistry*, 412(3):555–560, 2020. ISSN 16182650. doi:10.1007/s00216-019-02311-1.

[56] Denise M. Mitrano and Wendel Wohlleben. Microplastic regulation should be more precise to incentivize both innovation and environmental safety. *Nature Communications*, 11(1):1–12, 2020. ISSN 20411723. doi:10.1038/s41467-020-19069-1. URL http://dx.doi.org/10.1038/s41467-020-19069-1.

[57] Chelsea M Rochman, Keenan Munno, Carolynn Box, Anna Cummins, Xia Zhu, and Rebecca Sutton. Think Global, Act Local: Local Knowledge Is Critical to Inform Positive Change When It Comes to Microplastics. *environmental science and Technology*, 55:4–6, 2021. doi:10.1021/acs.est.0c05746.

[58] Riaz Ahmed, Ansley K. Hamid, Samuel A. Krebsbach, Jianzhou He, and Dengjun Wang. Critical review of microplastics removal from the environment. *Chemosphere*, 293(January):133557, 2022. ISSN 18791298. doi:10.1016/j.chemosphere.2022.133557. URL https://doi.org/10.1016/j.chemosphere.2022.133557.

[59] Karen Duis and Anja Coors. Microplastics in the aquatic and terrestrial environment: sources (with a specific focus on personal care products), fate and effects. *Environmental Sciences Europe*, 28(1):1–25, 2016. ISSN 21904715. doi:10.1186/s12302-015-0069-y.

[60] Aravin Prince Periyasamy and Ali Tehrani-Bagha. A review on microplastic emission from textile materials and its reduction techniques. *Polymer Degradation and Stability*, 199:109901, 2022. ISSN 01413910. doi:10.1016/j.polymdegradstab.2022.109901. URL https://doi.org/10.1016/j.polymdegradstab.2022.109901.

[61] Markus Sillanpää and Pirjo Sainio. Release of polyester and cotton fibers from textiles in machine washings. *Environmental Science and Pollution Research*, 24 (23):19313–19321, 2017. ISSN 16147499. doi:10.1007/s11356-017-9621-1.

[62] Melania Fiore, Silvia F. Garofalo, Alessandro Migliavacca, Alessandro Mansutti, Debora Fino, and Tonia Tommasi. Tackling Marine Microplastics Pollution : an Overview of Existing Solutions. *Water, Air, and Soil Pollution*, 233:276, 2022. ISSN 1573-2932. doi:10.1007/s11270-022-05715-5. URL https://doi.org/10.1007/s11270-022-05715-5.

[63] Imran Ali, Xiao Tan, Juying Li, Changsheng Peng, Peng Wan, Iffat Naz, Zhipeng Duan, and Yinlan Ruan. Innovations in the Development of Promising Adsorbents for the Remediation of Microplastics and Nanoplastics – A Critical Review. *Water Research*, 230(September 2022):119526, 2023. ISSN 18792448. doi:10.1016/j.watres.2022.119526. URL https://doi.org/10.1016/j.watres.2022.119526.

[64] Ilona Leppänen, Timo Lappalainen, Tia Lohtander, Christopher Jonkergouw, Suvi Arola, and Tekla Tammelin. Capturing colloidal nano- and microplastics with plant-based nanocellulose networks. *Nature Communications*, 13(1):1–12, 2022. ISSN 20411723. doi:10.1038/s41467-022-29446-7.

[65] Alistair Thorpe and Roy M. Harrison. Sources and properties of non-exhaust particulate matter from road traffic: A review. *Science of the Total Environment*, 400 (1-3):270–282, 2008. ISSN 00489697. doi:10.1016/j.scitotenv.2008.06.007. URL http://dx.doi.org/10.1016/j.scitotenv.2008.06.007.

[66] Delilah Lithner, Å. Larsson, and G. Dave. Environmental and health hazard ranking and assessment of plastic polymers based on chemical composition. *Science of the total environment*, 409:3309–3324, 2011.

[67] M. Ketzel, G. Omstedt, C. Johansson, I. Düring, M. Pohjola, D. Oettl, L. Gidhagen, P. Wåhlin, A. Lohmeyer, M. Haakana, and R. Berkowicz. Estimation and validation of PM2. 5/PM10 exhaust and non-exhaust emission factors for practical street pollution modelling. *Atmospheric Environment*, 41:9370–9385, 2007.

[68] R. Essel, L. Engel, M. Carus, and R. H. Ahrens. Sources of Microplastics Relevant to Marine Protection in Germany Texte. Technical report, 2015.

[69] T. Hillenbrand, D. Toussaint, E. Böhm, S. Fuchs, U. Scherer, A. Rudolphi, and Hoffmann F. Einträge von Kupfer, Blei und Zink in Gewässer und Böden. In *UBA-Texte*. 2005.

[70] S. Fuchs, U. Scherer, R. Wander, H.M. Behrendt, D. Venohr, T. Opitz, T. Hillenbrand, F. Marscheider-Weidemann, and T. Götz. Berechnung von Stoffeinträgen in die Fließgewässer Deutschlands mit dem Modell Moneris. In *UBA-Texte*. Umweltbundesamt, Dessau-Roßlau, bd. 45/201 edition, 2010.

[71] A. Verschoor, L. De Poorter, R. Dröge, J. Kuenen, and E. de Valk. Emission of microplastics and potential mitigation measures: Abrasive cleaning agents, paints and tyre wear. Technical report, 2016.

[72] NHTSA. Tires, 2023. URL https://www.nhtsa.gov/equipment/tires.

[73] E. J. Carpenter and K. L. Jr Smith. Plastics on the Sargasso Sea Surface. *Science*, 175:1240–1241, 1972.

[74] J. B. Jr Colton, B. R. Burns, and F. D. Knapp. Plastic Particles in Surface Waters of the Northwestern Atlantic: The abundance, distribution, source, and significance of various types of plastics are discussed. *Science*, 185:491–497, 1974.

[75] V. Hidalgo-Ruz, L. Gutow, R. C. Thompson, and M. Thiel. Microplastics in the marine environment: a review of the methods used for identification and quantification. *Environmental science and Technology*, 46:3060–3075, 2012.

[76] Atsuhiko Isobe, Kaori Uchiyama-Matsumoto, Keiichi Uchida, and Tadashi Tokai. Microplastics in the Southern Ocean. *Marine Pollution Bulletin*, 114(1):623–626, 2017. ISSN 18793363. doi:10.1016/j.marpolbul.2016.09.037. URL http://dx.doi.org/10.1016/j.marpolbul.2016.09.037.

[77] D. P. Redford, W. R. Trulli, and H. K. Trulli. Composition of floating debris in harbours of the United States. *Chemistry and Ecology*, 7:75–92, 1992.

[78] Thomas Mani, Armin Hauk, Ulrich Walter, and Patricia Burkhardt-Holm. Microplastics profile along the Rhine River. *Scientific Reports*, 5(December):1–7, 2015. ISSN 20452322. doi:10.1038/srep17988.

[79] Dafne Eerkes-Medrano, Richard C. Thompson, and David C. Aldridge. Microplastics in freshwater systems: A review of the emerging threats, identification of knowledge gaps and prioritisation of research needs. *Water Research*, 75:63–82, 2015. ISSN 18792448. doi:10.1016/j.watres.2015.02.012. URL http://dx.doi.org/10.1016/j.watres.2015.02.012.

[80] Amy L. Lusher, Valentina Tirelli, Ian O'Connor, and Rick Officer. Microplastics in Arctic polar waters: The first reported values of particles in surface and sub-surface samples. *Scientific Reports*, 5(June):1–9, 2015. ISSN 20452322. doi:10.1038/srep14947.

[81] Ostin Garcés-Ordóñez, Victoria A. Castillo-Olaya, Andrés F. Granados-Briceño, Lina M. Blandón García, and Luisa F. Espinosa Díaz. Marine litter and microplastic pollution on mangrove soils of the Ciénaga Grande de Santa Marta,

Colombian Caribbean. *Marine Pollution Bulletin*, 145(2):455–462, 2019. ISSN 18793363. doi:10.1016/j.marpolbul.2019.06.058. URL https://doi.org/10.1016/j.marpolbul.2019.06.058.

[82] N. Culligan, K. B. Liu, K. Ribble, J. Ryu, and M Dietz. Sedimentary records of microplastic pollution from coastal Louisiana and their environmental implications. *Journal of Coastal Conservation*, 26:1–14, 2022.

[83] Jean Pierre W. Desforges, Moira Galbraith, Neil Dangerfield, and Peter S. Ross. Widespread distribution of microplastics in subsurface seawater in the NE Pacific Ocean. *Marine Pollution Bulletin*, 79(1-2):94–99, 2014. ISSN 0025326X. doi:10.1016/j.marpolbul.2013.12.035. URL http://dx.doi.org/10.1016/j.marpolbul.2013.12.035.

[84] Rachel Hurley, Jamie Woodward, and James J. Rothwell. Microplastic contamination of river beds significantly reduced by catchment-wide flooding. *Nature Geoscience*, 11:251–257, 2018.

[85] K. M. Unice, M. P. Weeber, M. M. Abramson, R. C.D. Reid, J. A.G. van Gils, A. A. Markus, A. D. Vethaak, and J. M. Panko. Characterizing export of land-based microplastics to the estuary - Part I: Application of integrated geospatial microplastic transport models to assess tire and road wear particles in the Seine watershed. *Science of the Total Environment*, 646:1639–1649, 2019. ISSN 18791026. doi:10.1016/j.scitotenv.2018.07.368. URL https://doi.org/10.1016/j.scitotenv.2018.07.368.

[86] Lance T. Yonkos, Elizabeth A. Friedel, Ana C. Perez-Reyes, Sutapa Ghosal, and Courtney D. Arthur. Microplastics in four estuarine rivers in the chesapeake bay, U.S.A. *Environmental Science and Technology*, 48(24):14195–14202, 2014. ISSN 15205851. doi:10.1021/es5036317.

[87] Philip J. Anderson, Sarah Warrack, Victoria Langen, Jonathan K. Challis, Mark L. Hanson, and Michael D. Rennie. Microplastic contamination in Lake Winnipeg, Canada. *Environmental Pollution*, 225:223–231, 2017. ISSN 18736424. doi:10.1016/j.envpol.2017.02.072. URL http://dx.doi.org/10.1016/j.envpol.2017.02.072.

[88] Barbara E. Oßmann, George Sarau, Heinrich Holtmannspötter, Monika Pischetsrieder, Silke H. Christiansen, and Wilhelm Dicke. Small-sized microplastics and pigmented particles in bottled mineral water. *Water Research*, 141:307–316, 2018. ISSN 18792448. doi:10.1016/j.watres.2018.05.027.

[89] G. Liebezeit and E. Liebezeit. Synthetic particles as contaminants in German beers. *Food Additives and Contaminants: Part A*, 31:1574–1578, 2014.

[90] Milene F Diaz-basantes and Juan A Conesa. Microplastics in Honey , Beer , Milk and Refreshments in Ecuador as Emerging Contaminants. 2020.

[91] Mary Kosuth, Sherri A. Mason, and Elizabeth V. Wattenberg. Anthropogenic contamination of tap water, beer, and sea salt. *PLoS ONE*, 13(4):1–19, 2018. ISSN 19326203. doi:10.1371/journal.pone.0194970. URL http://dx.doi.org/10.1371/journal.pone.0194970.

[92] M. Smith, D. C. Love, C. M. Rochman, and R. A. Neff. Microplastics in seafood and the implications for human health. *Current environmental health reports*, 5: 375–386, 2018.

[93] M. Kedzierski, B. Lechat, O. Sire, G. Le Maguer, V. Le Tilly, and S. Bruzaud. Microplastic contamination of packaged meat: Occurrence and associated risks. *Food Packaging and Shelf Life*, 24:100489, 2020.

[94] Xin Zhang, Yimin Mao, Madhusudan Tyagi, Feng Jiang, Doug Henderson, Bo Jiang, Zhiwei Lin, Ronald L. Jones, Liangbing Hu, Robert M. Briber, and Howard Wang. Molecular partitioning in ternary solutions of cellulose. *Carbohydrate Polymers*, 220 (February):157–162, 2019. ISSN 01448617. doi:10.1016/j.carbpol.2019.05.054. URL https://doi.org/10.1016/j.carbpol.2019.05.054.

[95] Fangni Du, Huiwen Cai, Qun Zhang, Qiqing Chen, and Huahong Shi. Microplastics in take-out food containers. *Journal of Hazardous Materials*, 399(February): 122969, 2020. ISSN 18733336. doi:10.1016/j.jhazmat.2020.122969. URL https://doi.org/10.1016/j.jhazmat.2020.122969.

[96] Radhakrishnan Yedhu Krishnan, Sivasubramanian Manikandan, Ramasamy Subbaiya, Natchimuthu Karmegam, Woong Kim, and Muthusamy Govarthanan. Recent approaches and advanced wastewater treatment technologies for mitigating emerging microplastics contamination – A critical review. *Science of the Total Environment*, 858(September 2022):159681, 2023. ISSN 18791026. doi:10.1016/j.scitotenv.2022.159681. URL https://doi.org/10.1016/j.scitotenv.2022.159681.

[97] Fan Liu, Nadia B. Nord, Kai Bester, and Jes Vollertsen. Microplastics Removal from Treated Wastewater by a Biofilter. *Water*, 12(4):1085, 2020.

[98] Virpi Siipola, Stephan Pflugmacher, Henrik Romar, Laura Wendling, and Pertti Koukkari. Low-Cost Biochar Adsorbents for Water Purification Including Microplastics Removal. *Applied Science*, 10(3):788, 2020.

[99] Katriina Rajala, Outi Grönfors, Mehrdad Hesampour, and Anna Mikola. Removal of microplastics from secondary wastewater treatment plant effluent by coagulation/flocculation with iron, aluminum and polyamine-based chemicals. *Water Research*, 15:116045, 2020.

[100] Márta Simon, Alvise Vianello, and Jes Vollertsen. Removal of >10 µm Microplastic Particles from Treated Wastewater by a Disc Filter. *Water*, 11(9):1935, 2019.

[101] Marthe Kiendrebeogo, M. R. Karimi Estahbanati, Ali Khosravanipour Mostafazadeh, Patrick Drogui, and R. D. Tyagi. Treatment of microplastics in water by anodic oxidation: A case study for polystyrene. *Environmental Pollution*, 269:116168, 2021.

[102] Ye Tang, Suhua Zhang, Yinglong Su, Dong Wu, Yaping Zhao, and Bing Xie. Removal of microplastics from aqueous solutions by magnetic carbon nanotubes. *Chemical Engineering Journal*, 406(August 2020):126804, 2021. ISSN 13858947. doi:10.1016/j.cej.2020.126804. URL https://doi.org/10.1016/j.cej.2020.126804.

[103] Kaul DS Aatmeeyata and Sharma M. Traffic generated non-exhaust particulate emissions from concrete pavement: A mass and particle size study for two-wheelers and small cars. *Atmospheric Environment*, 43:5691–5697, 2009.

[104] E. Foschi, S. Zanni, and A. Bonoli. Combining Eco-Design and LCA as Decision-Making Process to Prevent Plastics in Packaging Application. *Sustainability*, 12: 1–13, 2020.

[105] Ge Xia Wang, Dan Huang, Jun Hui Ji, Carolin Völker, and Frederik. R. Wurm. Seawater-Degradable Polymers—Fighting the Marine Plastic Pollution. *Advanced Science*, 8(1):2001121, 2020.

[106] Carole Excell, Salcedo-La Viña, Jesse Worker, and Elizabeth Moses. Legal Limits on Single-Use Plastics and Microplastics: A Global Review of National Laws and Regulations. Technical report, UNEP, 2018.

[107] CMS. Plastics and Packaging Laws in Mexico, 2023. URL https://cms.law/en/int/expert-guides/plastics-and-packaging-laws/mexico.

[108] Stuart Braun. 5 things to know about the EU plastics ban, 2021. URL https://www.dw.com/en/5-things-to-know-about-the-eu-single-use-plastics-ban/a-58109909.

[109] Carbon Neutrality - A2ZERO, 2023. URL https://www.a2gov.org/departments/sustainability/Carbon-Neutrality/Pages/default.aspx.

[110] Maja van der Velden. Fixing the World One Thing at a Time': Community repair and a sustainable circular economy. *Journal of cleaner production*, 304:127151, 2021.

[111] Cassandra Garrison. Mexico City plastic ban causes tampon concerns for women, 2021. URL https://www.reuters.com/article/us-mexico-environment-tampons-idUSKBN2AI1KL.

[112] Junliang Chen, Jing Wu, Peter C. Sherrell, Jun Chen, Huaping Wang, Wei xian Zhang, and Jianping Yang. How to Build a Microplastics-Free Environment: Strategies for Microplastics Degradation and Plastics Recycling. *Advanced Science*, 9 (6):1–36, 2022. ISSN 21983844. doi:10.1002/advs.202103764.

[113] Mario Urso and Martin Pumera. Nano/Microplastics Capture and Degradation by Autonomous Nano/Microrobots: A Perspective. *Advanced Functional Materials*, 32 (20), 2022. ISSN 16163028. doi:10.1002/adfm.202112120.

[114] Alba Maceira, Francesc Borrull, and Rosa Maria Marcé. Occurrence of plastic additives in outdoor air particulate matters from two industrial parks of Tarragona, Spain: Human inhalation intake risk assessment. *Journal of Hazardous Materials*, 373(March):649–659, 2019. ISSN 18733336. doi:10.1016/j.jhazmat.2019.04.014. URL https://doi.org/10.1016/j.jhazmat.2019.04.014.

[115] Z. Yang, F. Lü, H. Zhang, W. Wang, J. Shao, L., Ye, and P. He. Is incineration the terminator of plastics and microplastics? *Journal of Hazardous Materials*, 401: 123429, 2021.

[116] Maocai Shen, Weiping Xiong, Biao Song, Chengyun Zhou, Eydhah Almatrafi, Guangming Zeng, and Yaxin Zhang. Microplastics in landfill and leachate: Occurrence, environmental behavior and removal strategies. *Chemosphere*, 305(December 2021):135325, 2022. ISSN 18791298. doi:10.1016/j.chemosphere.2022.135325. URL https://doi.org/10.1016/j.chemosphere.2022.135325.

[117] Abhishek Krishnan, Kannappan Panchamoorthy Gopinath, Dai Viet N. Vo, Rajagopal Malolan, Vikas Madhav Nagarajan, and Jayaseelan Arun. Ionic liquids, deep eutectic solvents and liquid polymers as green solvents in carbon capture technologies: a review. *Environmental Chemistry Letters*, 18(6):2031–2054, 2020. ISSN 16103661. doi:10.1007/s10311-020-01057-y. URL https://doi.org/10.1007/s10311-020-01057-y.

[118] C.W. Cho, T.P.T. Pham, Y. Zhao, S. Stolte, and Y.S. Yun. Review of the toxic effects of ionic liquids. *Science of The Total Environment*, 786:147309, 2021.

[119] John D. Holbrey, W. Matthew Reichert, Mark Nieuwenhuyzen, Suzanne Johnson, Kenneth R. Seddon, and Robin D. Rogers. Crystal polymorphism in 1-butyl-3-methylimidazolium halides: supporting ionic liquid formation by inhibition of crystallizationElectronic supplementary information (ESI) available: packing diagrams for I and II; table of closest contacts for I, I-Br and I. *Chemical Communications*, (14):1636, 2003. ISSN 1359-7345. doi:10.1039/b304543a.

[120] Angshuman R. Choudhury, Neil Winterton, Alexander Steiner, Andrew I. Cooper, and Kathleen A. Johnson. In situ crystallization of low-melting ionic liquids. *Journal of the American Chemical Society*, 127(48):16792–16793, 2005. ISSN 00027863. doi:10.1021/ja055956u.

[121] Natalia V. Plechkova and Kenneth R. Seddon. Applications of ionic liquids in the chemical industry. *Chemical Society Reviews*, 37(1):123–150, 2008. ISSN 03060012. doi:10.1039/b006677j.

[122] Candice F.J. Francis, Ilias L. Kyratzis, and Adam S. Best. Lithium-Ion Battery Separators for Ionic-Liquid Electrolytes: A Review. *Advanced Materials*, 32(18):1–22, 2020. ISSN 15214095. doi:10.1002/adma.201904205.

[123] Dieter Klemm, Brigitte Heublein, Hans Peter Fink, and Andreas Bohn. Cellulose: Fascinating biopolymer and sustainable raw material. *Angewandte Chemie - International Edition*, 44(22):3358–3393, 2005. ISSN 14337851. doi:10.1002/anie.200460587.

[124] Zugenmaier Peter. Order in cellulosics: Historical review of crystal structure research on cellulose. *Carbohydrate Polymers*, 254(August 2020):117417, 2021. ISSN 01448617. doi:10.1016/j.carbpol.2020.117417. URL https://doi.org/10.1016/j.carbpol.2020.117417.

[125] Yehia Elmogahzy and Ramsis Farag. *Tensile properties of cotton fibers*. Elsevier Ltd, 2018. ISBN 9780081012727. doi:10.1016/B978-0-08-101272-7.00007-9. URL http://dx.doi.org/10.1016/B978-0-08-101272-7.00007-9.

[126] Guomin Zhao, Jun Du, Weimin Chen, Mingzhu Pan, and Dengyu Chen. Preparation and thermostability of cellulose nanocrystals and nanofibrils from two sources of biomass: rice straw and poplar wood. *Cellulose*, 26:8625–8643, 2019.

[127] Hanping Chen, Zihao Liu, Xu Chen, Yingquan Chen, Zhiguo Dong, Xianhua Wang, and Haiping Yang. Comparative pyrolysis behaviors of stalk, wood and shell biomass: Correlation of cellulose crystallinity and reaction kinetics. *Bioresource Technology*, 310:123498, 2020.

[128] Moufida Beroual, Djalal Trache, Oussama Mehelli, Lokmane Boumaza, Ahmed F. Tarchoun, Mehdi Derradji, and Kamel Khimeche. Effect of the Delignification Process on the Physicochemical Properties and Thermal Stability of Microcrystalline Cellulose Extracted from Date Palm Fronds. *Waste and Biomass Valorization*, 12: 2779–2793, 2021.

[129] Chuanwei Miao and Wadood Y. Hamad. Cellulose reinforced polymer composites and nanocomposites: A critical review. *Cellulose*, 20(5):2221–2262, 2013. ISSN 09690239. doi:10.1007/s10570-013-0007-3.

[130] Elizabeth R. McCall and Julian F. Jurgens. Chemical Composition of Cotton. *Textile Research Journal*, 21(1):19–21, 1951. ISSN 00405175. doi:10.1177/004051755102100105.

[131] Pushpa S Murthy and M Madhava Naidu. Resources , Conservation and Recycling Sustainable management of coffee industry by-products and value addition — A review. *"Resources, Conservation and Recycling"*, 66:45–58, 2012. ISSN 0921-3449. doi:10.1016/j.resconrec.2012.06.005. URL http://dx.doi.org/10.1016/j.resconrec.2012.06.005.

[132] Aliakbar Gholampour and Togay Ozbakkaloglu. *A review of natural fiber composites: properties, modification and processing techniques, characterization, applications*, volume 55. Springer US, 2020. ISBN 1085301903990. doi:10.1007/s10853-019-03990-y. URL https://doi.org/10.1007/s10853-019-03990-y.

[133] Yanrong Liu, Yi Nie, Xingmei Lu, Xiangping Zhang, Hongyan He, Fengjiao Pan, Le Zhou, Xue Liu, Xiaoyan Ji, and Suojiang Zhang. Cascade utilization of lignocellulosic biomass to high-value products. *Green Chemistry*, 21(13):3499–3535, 2019. ISSN 14639270. doi:10.1039/c9gc00473d.

[134] Julie M. Rieland, Zeyuan Hu, Julian S. Deese, and Brian J. Love. Pressure sensitive adhesives for quantifying microplastic isolation. *Separation and Purification Technology*, 307(November 2022):122819, 2023. ISSN 18733794. doi:10.1016/j.seppur.2022.122819. URL https://doi.org/10.1016/j.seppur.2022.122819.

[135] Hanbin Liu, Kenneth L. Sale, Blake A. Simmons, and Seema Singh. Molecular dynamics study of polysaccharides in binary solvent mixtures of an ionic liquid and water. *Journal of Physical Chemistry B*, 115(34):10251–10258, 2011. ISSN 15205207. doi:10.1021/jp111738q.

[136] Seema Singh, Blake A. Simmons, and Kenneth P. Vogel. Visualization of biomass solubilization and cellulose regeneration during ionic liquid pretreatment of switchgrass. *Biotechnology and Bioengineering*, 104(1):68–75, 2009. ISSN 00063592. doi:10.1002/bit.22386.

[137] Kirtikumar C. Badgujar and Bhalchandra M. Bhanage. Factors governing dissolution process of lignocellulosic biomass in ionic liquid: Current status, overview and challenges. *Bioresource Technology*, 178(2015):2–18, 2015. ISSN 18732976. doi:10.1016/j.biortech.2014.09.138. URL http://dx.doi.org/10.1016/j.biortech.2014.09.138.

[138] Marc Kostag, Kerstin Jedvert, Christian Achtel, Thomas Heinze, and Omar A. El Seoud. Recent advances in solvents for the dissolution, shaping and derivatization of cellulose: Quaternary ammonium electrolytes and their solutions in water and molecular solvents. *Molecules*, 23(3), 2018. ISSN 14203049. doi:10.3390/molecules23030511.

[139] R J Sammons, J R Collier, T G Rials, and S Petrovan. Rheology of 1-Butyl-3-Methylimidazolium Chloride Cellulose Solutions . I . Shear Rheology. *Journal of Applied Polymer Science*, 110:1175–1181, 2008. doi:10.1002/app.

[140] Xun Chen, Siwei Liang, Shih-Wa Wang, and Ralph H. Colby. Linear viscoelastic response and steady shear viscosity of native cellulose in 1-ethyl-3-methylimidazolium methylphosphonate. *Journal of Rheology*, 62(1):81–87, 2017. ISSN 0148-6055. doi:10.1122/1.4990049.

[141] Anne Michud, Marjaana Tanttu, Shirin Asaadi, Yibo Ma, Eveliina Netti, Pirjo Kääriainen, Anders Persson, Anders Berntsson, Michael Hummel, and Herbert Sixta. Ioncell-F: ionic liquid-based cellulosic textile fibers as an alternative to viscose and Lyocell. *Textile Research Journal*, 86(5):543–552, 2016. ISSN 00405175. doi:10.1177/0040517515591774.

[142] Jinhui Pang, Miao Wu, Qiaohui Zhang, Xin Tan, Feng Xu, Xueming Zhang, and Runcang Sun. Comparison of physical properties of regenerated cellulose films fabricated with different cellulose feedstocks in ionic liquid. *Carbohydrate Polymers*, 121:71–78, 2015. ISSN 01448617. doi:10.1016/j.carbpol.2014.11.067. URL http://dx.doi.org/10.1016/j.carbpol.2014.11.067.

[143] María C. Castro, Alberto Arce, Ana Soto, and Héctor Rodríguez. Influence of Methanol on the Dissolution of Lignocellulose Biopolymers with the Ionic Liquid 1-Ethyl-3-methylimidazolium Acetate. *Industrial and Engineering Chemistry Research*, 54(39):9605–9614, 2015. ISSN 15205045. doi:10.1021/acs.iecr.5b02604.

[144] João M. Valente Nabais, Pedro Nunes, Peter J. M. Carrott, M. Manuela L. Ribeiro Carrott, A. Macías García, and M.A. Díaz-Díez. Production of activated carbons from coffee endocarp by CO2 and steam activation. *Fuel Processing Technology*, 89(3):262–268, 2008.

[145] Solange I. Mussatto, Machado Ercília M. S., Silvia Martins, and José A. Teixeira. Production, Composition, and Application of Coffee and Its Industrial Residues. *Food and Bioproducts Processing*, 4:661–672, 2011.

[146] Sara Eckhardt, Heike Franke, Steffen Schwarz, and Dirk W. Lachenmeier. Risk Assessment of Coffee Cherry (Cascara) Fruit Products for Flour Replacement and Other Alternative Food Uses. *Molecules*, 27(23):8435, 2022.

[147] Abebe Beyene, Yared Kassahun, Taffere Addis, Fassil Assefa, Aklilu Amsalu, Worku Legesse, Helmut Kloos, and Ludwig Triest. The impact of traditional coffee processing on river water quality in Ethiopia and the urgency of adopting sound environmental practices. *Environmental Monitoring and Assessment*, 184:7053–7063, 2012.

[148] L Fan, A. T Soccol, A Pandey, and C. R Soccol. Cultivation of Pleurotus Mushrooms on Brazilian Coffee Husk and Effects of Caffeine and Tannic Acid. *Micologia Aplicada International*, 15(1):15–21, 2003.

[149] Verónica Alejandra Bonilla-hermosa, Whasley Ferreira Duarte, and Rosane Freitas Schwan. Utilization of coffee by-products obtained from semi-washed process for production of value-added compounds. *Bioresource Technology*, 166:142–150, 2014. doi:10.1016/j.biortech.2014.05.031.

[150] R. Gurram, M. Al-Shannag, S. Knapp, T. Das, E. Singsaas, and M. Alkasrawi. Technical possibilities of bioethanol production from coffee pulp: a renewable feedstock. *Clean Technologies and Environmental Policy*, 18:269–278, 2016.

[151] Leta Deressa Tolesa, Bhupender S. Gupta, and Ming Jer Lee. Treatment of Coffee Husk with Ammonium-Based Ionic Liquids: Lignin Extraction, Degradation, and Characterization. *ACS Omega*, 3(9):10866–10876, 2018. ISSN 24701343. doi:10.1021/acsomega.8b01447.

[152] Sofía Collazo-Bigliardi, Rodrigo Ortega-Toro, and Amparo Chiralt Boix. Isolation and characterisation of microcrystalline cellulose and cellulose nanocrystals from coffee husk and comparative study with rice husk. *Carbohydrate Polymers*, 191(October 2017):205–215, 2018. ISSN 01448617. doi:10.1016/j.carbpol.2018.03.022. URL https://doi.org/10.1016/j.carbpol.2018.03.022.

[153] Mounir El Achaby, Mariana Uesgas-Ramon, Nour-E Houda Fayoud, Maria Cruz Figueroa-Espinoza, Vera Trabadelo, Khalid Draoui, and Hicham Ben Youcef. Biosourced porous cellulose microfibrils from coffee pulp for wastewater treatment. *Cellulose*, 26:3873–3889, 2019. doi:10.1007/s10570-019-02344-w.

[154] Geyandraprasath Karunakaran, Aravin Prince Periyasamy, and Ali Tehrani. Extraction of Micro, Nanocrystalline Cellulose and Textile Fibers from Coffee Waste. *Journal of Testing and Evaluation*, 51(5):20220487, 2023. ISSN 00903973. doi:10.1520/jte20220487.

CHAPTER 2

Quantification and Capture of Microplastics Via Pressure Sensitive Adhesives

2.1 Introduction

2.1.1 State of microplastic capture at bench scale and in real-world scenarios

The problem of microplastic (MP) pollution is particularly dynamic and complex because 1) MPs are a broad category of materials spanning diverse chemistries, densities, sizes, and form factors, 2) MPs are generated through many dispersed activities that are critical to modern daily-life, and 3) MPs, and plastic materials in general are persistent in the environment and cannot be easily sequestered or destroyed. Given such a complex problem space, there is a need to develop robust, targeted solutions that can help us both better understand the scope of the problem and move toward measurable solutions. A survey of the MPs literature shows that there is increasing research capacity

being put towards developing MP remediation strategies.[1,2,3] There have been several reviews that discuss the existing infrastructure and scope of commercial products available for MP controls, largely involving wastewater treatment plant infrastructure, home-laundry accessories, and ocean cleanup campaigns. These activities primarily rely on physical filtration,[4,5] which is shown to be fairly effective for MPs of a size compatible with the filter being used. However, methods based exclusively on physical filtration have drawbacks, including the inability to capture particles smaller than the pore size, membrane fouling, and reduced throughput inversely proportional to the pore size.[6] Furthermore, there has still been minimal discussion of what is done with captured MPs, which can reduce the overall efficacy of removal.

In the literature, much of the research-stage science considers other capture mechanisms including active capture with functionalized microbots,[7] in-situ degradation of MPs,[8] and adsorbent materials[9]. Many of these new techniques rely on surface-chemistry-based affinity and binding of MPs on surfaces. Surface binding of MPs has been investigated for a range of mechanisms, including $\pi - \pi$ interactions,[10,6] hydrophobicity,[11,12] electrostatics,[5,6,7,8] coagulation,[13] and van der Waals forces.[14,15] Natural binding and adhesion in mussels and coral has also been identified as a potentially significant sink of ocean MPs[16,17] and has inspired new ideas.[14] Notably, many of these new technologies aim to leverage multiple capture mechanisms, often combining surface effects with physical impingement or multiple surface binding mechanisms.[6,18,19] While these diverse binding systems have proven effective in sterile environments devoid of impurities,[20,21,22,23] there is a need to identify robust systems that can operate under realistic conditions such as in natural waters, laundry surfactants, and wastewater treatment plant (WWTP) conditions.

2.1.2 Microplastic quantification and harmonization

Despite the pressure to develop preventative and remedial MP technologies, there still remain many foundational questions about MPs that we can't yet answer confidently. Namely, identification, quantification, and harmonization of the various quantification methods makes it difficult to measure the efficacy of MP capturing technologies, and overall inhibits our ability to establish the scope of global MP pollution.[24,25] The assessment of MPs is a multistep process that presents unique challenges at each step. First the MPs are collected, whether from ocean water,[26] soil,[27] animal organs,[28] or a Styrofoam takeout box.[29] Then the MPs are isolated (and concentrated if required) to the highest degree possible; often with chemical digestants, and finally the particle remnants are analyzed whether optically, gravimetrically, or chemically. At each step of the process, there can be material losses, contamination introduction, and user bias that reduce the certainty of measurements, especially for the smallest particle fractions. Primpke et al.[30] effectively outlines the primary analytical techniques used to analyze MPs including optical microscopy, Fourier transform infrared (FTIR) and Raman spectroscopy, and flow-cytometry, elaborating on the costs, analytical throughput, and any limitations. The large range of instrumentation commonly used for MP analysis and a lack of standardized procedures and reporting conventions has led to a muddy landscape of data with units that can't be reconciled (#/kg media, #/km^2, #/km^3, g/kg media, g/m^3, etc.),[31] and a known blind spot regarding the smallest particles.[32]

Efforts are being made to standardize procedures[33] and international cross-laboratory studies have been undertaken to assess the extent of variation between instrumentation and user processes.[25,31,34] However, variation between laboratories continues to be high, and there remains a need to build up analytical throughput, and reduce cost of analysis.[25,31,34] Implementation of computational methods such as AI assisted optical analysis,[35,36] large-scale data processing methods such as principal component analysis (PCA),[37] and integration of MPs into predictive large scale planetary models[38,39] introduce

promising new directions for leveraging the data that already exists, improving analytical accuracy, and increasing throughput.

2.1.3 Pressure sensitive adhesives applied towards microplastic capture

In this chapter, we assess the ability of pressure-sensitive adhesives (PSA) to capture MPs. PSA-based MP capture was first reported in a paper by Chazovachii et al.[15] in which we investigated PSA coated ceramic spheres to capture monodisperse 10 µm PS spheres analyzed using flow cytometry. The inciting idea for using PSAs to capture MPs came from a serendipitous observation of PSA-micronized rubber binding in a chemical waste bottle. PSAs are unique among adhesives as they remain tacky over the course of their lifetime until fouled. Unlike glues and epoxies, which have a short window of application in the liquid state before the solvents evaporate or the monomers cure and polymerize, PSAs are designed to have weak van der Waals attractions that are active until fouled.[40] A common application of PSAs is in “sticky notes” which demonstrates the stick, peel, and stick again functionality.

The binding mechanism of PSAs has two components, with adhesion being controlled both by van der Waals surface interactions as well as a physical interlocking enabled by their relatively low viscosities.[40,41] The viscoelastic requirements for a polymer to be considered a PSA are described by the Chu[42] and Dahlquist criteria.[43,44] Both criteria depend on the storage modulus (G') of the polymer measured in Pascals, as well as the frequency (ω) of the rheological analysis, measured in radians per second. The Chu criterion[42] is based on the ability of PSAs to bond rapidly, as well as the ability for PSAs to debond while maintaining cohesion. These criteria can be expressed as

$$G'(\omega = 0.1 \text{ rad s}^{-1}) \sim 24 \times 10^4 \text{ Pa}, \tag{2.1}$$

$$5 < \frac{G'(\omega = 100 \text{ rad s}^{-1})}{G'(\omega = 0.1 \text{ rad s}^{-1})} < 300. \tag{2.2}$$

The Dahlquist criterion,[43,44] by contrast, defines the acceptable limit as

$$G'(\omega = 1 \text{ rad s}^{-1}) < 3 \times 10^5 \text{ Pa}. \tag{2.3}$$

The properties of PSAs are commonly tuned by polymer selection, polymer architecture, molecular weight, cross-linking, and 'tackifying' additives. Prior work in our group has found that both the surface energy and the physical interlocking play important roles in the capture of MPs.[18,45] In application, the common PSA, poly(2-ethylhexyl acrylate) (PEHA) has been found to be effective in the aqueous capture of MPs for a range of polymer compositions and interferent environments.[15] Herein we present our methodology for preparing adhesive-coated substrates, experimental conditions, and the analysis procedures for observing MPs captured from an aqueous dispersion. Adhesive binding is tested with several MP species both independently and in competitive assays demonstrating pathways to assess how MP composition, size, and shape affect binding. Schemes to gauge robustness and effectiveness of this system are also presented.

2.2 Materials and Methods

2.2.1 Materials

Poly(2-ethylhexyl acrylate) (PEHA) in toluene solution reported as 92 kg mol^{-1} (92k) was purchased from Sigma Aldrich then dried on a rotary evaporator and confirmed via gel permeation chromatography (GPC). Tetrahydrofuran (THF), Tergitol® 15-S-9, and

methanol were purchased from Fisher Scientific. The following materials for the synthesis of 950 kg mol^{-1} (950k) PEHA were used as received unless specified. Polyacrylic acid (PAA) was purchased from Scientific Polymer Products and was reported as 1,033 kg mol^{-1}. 2-ethylhexanol and sulfuric acid ($H2SO_4$) were purchased from Millipore Sigma. Borosilicate glass slides (25 $\times$ 75 $\times$ 1 mm) were purchased from Fisher Scientific. A variety of microplastics (MPs) were acquired and used as received unless specified otherwise. Nylon-12 powder (avg size $\sim$ 30µm) (Nylon30) was obtained from Goodfellow Cambridge Ltd. polyethylene (PE) microspheres (#CPMS-0.96 45-53 µm, avg size $\sim$ 50 µm) (PE50) and polystyrene (PS) microspheres (#$PSMs^{-1}$.07 9.5-11.5 µm, avg size $\sim$ 10 µm) (PS10) were obtained from Cospheric. Commercial polyethylene terephthalate (PET) yarn was purchased from Joann Fabrics and cut with a straight razor to $\sim$ 1 mm long fibers, cut yarn was subsequently processed in an electric coffee grinder to break up clumping. Post-Consumer PE was acquired as an empty 1-gallon vinegar bottle which was cryo-ground in a SPEX SamplePrep 6775 Freezer/Mill (avg size $\sim$ 200 µm) (PE200). Silica sand was provided by the Van Vlack Undergraduate Laboratory at the University of Michigan, and bentonite clay was purchased from Adventures in Home Brewing in Ann Arbor, Michigan. Huron River water was collected at the dock of the Argo Park Livery in Ann Arbor, Michigan.

2.2.2 Synthesis of 950k poly(2-ethylhexyl acrylate)

To make 950k PEHA, 2-ethylhexanol (5.0 equiv), H2SO4 (0.25 equiv), and 1033k PAA (1.0 equiv) were added to a 75 mL pressure vessel magnetic stirring. A Teflon screw cap was used to seal the pressure vessel, and it was heated to 20°C for 8 hr. Then a water bath was used to cool the vessel to room temperature. Once cooled, the reaction mixture was poured into methanol ($\sim$50 mL) to precipitate the PEHA. The PEHA was isolated by dissolving in THF ($\sim$10 mL) and reprecipitating in methanol ($\sim$50 mL). The mixture was centrifuged and the PEHA was retrieved by decanting off the supernatant.

This precipitation process was repeated three times to ensure sample purity. After the final reprecipitation step, the polymer was heated at 60°C for 3 hr under high vacuum to dry, providing a 73% yield. The 950k PEHA was confirmed using nuclear magnetic resonance (^{1}HNMR) spectroscopy and GPC.

2.2.3 Preparing glass slide substrates

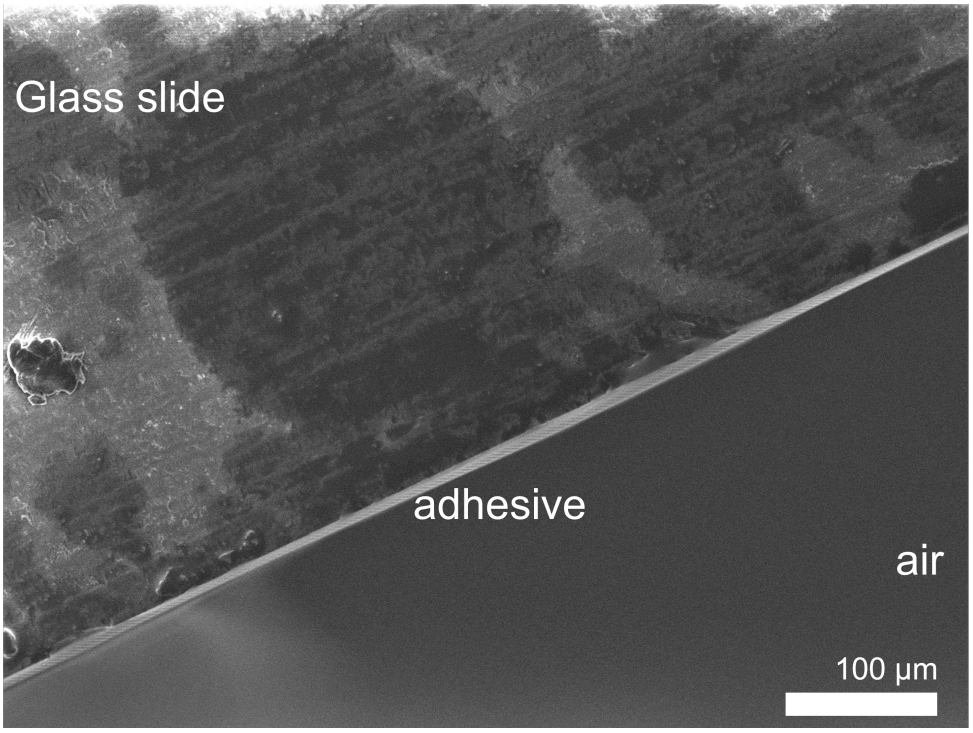

Figure 2.1: SEM micrograph demonstrating an edge-on view of the 92k Poly (2-ethylhexyl acrylate) coating on a glass slide.

Glass slides were prepared by first applying masking tape to the slide for labeling and to mark the upper boundary of a 1 in square adhesive zone. The designated adhesive zone was cleaned with acetone before spray coating. The concentration and temperature of adhesive solutions for spraying were determined through an Edisonian approach to identify the maximum concentration that could be deployed through the airbrush (AGPTEK Mini Airbrush purchased from Amazon) while maintaining an effective spray cone. 92k PEHA was dispensed at 5% w/v at room temperature, 950k PEHA was dispensed

at 2% w/v at 60°C, and 50:50 bimodal distributions (50:50 BD) was dispensed at 2% w/v at 60°C. 92k and 950k PEHA solutions were prepared by dissolving the polymer in THF. 92k could be dissolved at room temperature, while 950k required oven heating. 50:50 BD solution was produced on an equal weight basis of 0.1 g of 92k and 0.1 g of 950k dissolved in 10 mL of THF at 60° C to yield a net 2% w/v solution.

The slides were airbrushed using a circular brushing motion with the airbrush held at a distance 10 cm from the slide. To accommodate similar adhesive deposition, 92k PEHA solutions were dispensed for 3 seconds, and the more dilute 950k and 50:50 BD solutions were dispensed for 5 seconds. Slides were then stored in a ventilated cardboard box with a lid at room temperature for at least 24 hours to allow for solvent evaporation. Adhesive deposition on glass slides was confirmed by both optical microscopy and scanning electron microscope (SEM) (JEOL JSM-IT500HR) imaging. The film thickness was measured by assessing the side profile of the glass slides under SEM identifying 92k films having a thickness of 6 ± 1 µm, 950k films having a thickness of 4 ± 2µm, and 50:50 BD films having a thickness of 6.5 ± 1 µm with relatively smooth surface finishes (**Figure 2.1**).

2.2.4 Shake tests – Calibration curves

Calibration data was collected for all three PEHA formulations (92k, 950k, 50:50 BD) using a 30 µm nylon-12 particle (Nylon30) as the MP species in room temperature deionized (DI) water. Shake tests were performed by immersing adhesive-coated glass slides into Nylon30 dispersions and shaking on a Thermo Scientific multi-purpose rotator table at 200 RPM for a predetermined exposure time. Calibration was performed for MP concentration (0.01, 0.1, 1, 2, and 5 mg mL^{-1} Nylon30) and exposure time (1, 5, 10, and 30 min intervals). For dilute MP dispersions (< 0.5 mg mL^{-1}), stock dispersions were produced and 30 mL were transferred to 50 mL glass vials. For more concentrated dispersions (≥ 0.5 mg mL^{-1}), samples were prepared individually rather than as a stock dispersion to reduce dispensing errors due to poor particle dispersion. In concentrated samples, MPs

were weighed out and added to 50 mL vials and then 30 mL of DI water was measured out and added to the vials. Samples were performed in triplicate and secured to the rotator table in a weighted and padded box. After shaking, glass slides were immediately removed from the vials and rinsed with DI water (20 mL) to wash off weakly bound particles and those collected outside of the defined adhesive region. Before measurement, slides were dried overnight, covered to prevent collection of dust. Particle capture was assessed both gravimetrically and using optical microscopy.

2.2.5 Shake tests – Environmental interferents

Environmental interference shake tests were performed as with the calibration tests to assess the influence of select soluble and insoluble interferents on MP adsorption. Nylon30 was used as the MP species, and all three PEHA formulations were assessed. Varying conditions were used for each adhesive: 92k samples were performed for 1 min with 5 mg mL^{-1} Nylon30, 950k were performed for 1 min with 5 mg mL^{-1} Nylon30, and 50:50 BD samples were performed for 5 min with 1 mg mL^{-1} Nylon30.

Environment stock solutions were prepared ahead. NaCl solutions were prepared at 35% w/v salinity (NaCl in DI water). A reduced temperature stock solution of 3°C DI water was prepared in the refrigerator. Humic acid and surfactant solutions (Sodium dodecyl sulfate (SDS) and Tergitol) were prepared on an individual basis. Surfactants were prepared by measuring out 0.1% v/v surfactant (30 mg) added directly to each sample. Humic acid was added at 200 mg L^{-1} to DI water. Solid interferents were also tested using silica sand and bentonite clay. Water from the Huron River was collected from the Argo Park Livery in a 1 L jar that was rinsed in the river 3 times to ensure no atmospheric contamination. River water had minimal silt or large biomass. Sand was sieved to 200 µm using a McMaster Carr filter. Bentonite clay was sieved to 50 µm. Samples were vigorously shaken by hand before adding a glass slide.

2.2.6 Shake tests – Microplastic survey and mixed assays

The survey of MP species was performed as with the calibration tests to understand how different plastic species interact with PEHA. 950k PEHA in room temperature DI water was used for all tests. The investigated MPs include: Nylon30, 10 µm polystyrene, 50 and 200 µm polyethylene (PE50, PE200), and 1000 µm polyester fibers (PET1000). PS10, nylon30, and PET1000 were assessed individually at 0.1 mg mL^{-1} for 5 min. Mixed assays were performed with equal weight quantities (0.1 mg mL^{-1} each) PS10/nylon30, PE50/PE200, and PET fiber/nylon30/PS10 to assess competitive binding and to test the ability of ImageJ® to differentiate particle types. Microplastic survey and mixed assay samples were measured both gravimetrically and through optical microscopy. Gravimetric blanks were assessed by performing triplicated shake tests in DI water with no adhesives. After 5 min of shaking there was negligible weight change. Gravimetric data was calculated as a function of the captured MP mass ($M_{capture}$) with respect to the initial mass ($M_{initial}$) of MPs in dispersion (Equation 2.4).

$$\%\text{capture} = \frac{M_{capture}}{M_{initial}} \times 100 \tag{2.4}$$

2.2.7 Observational assessment

Optical microscopy images were taken on a Nikon Eclipse LV100ND microscope with a DS-RI2 camera maintained by the Van Vlack undergraduate laboratory. Adhesive regions on dried glass slides were imaged 3 times in a pre-assigned diagonal pattern to control for bias and the influence of MP buoyancy. Glass slides were placed under the optical region of the microscope guided by the light beam, and images were taken as placed with minor adjustments to account for large adhesive defects or contamination (e.g., unexpected fibers) if present. Images were processed with ImageJ® software to collect number count and percent surface area coverage (%SAC) of particles and particle clusters. Objects with

a planar surface area less than 85 µm^2 were omitted as dust and extraneous discoloration. More in-depth discussion of ImageJ® processing is available in our published paper on this work.23 Images from each individual slide were aggregated to determine a more holistic %SAC value for each slide using Equation 2.5.

$$\%\text{SAC} = \frac{\sum SA_{\text{particles and clusters}}}{3\ SA_{\text{image area}}} \times 100 \tag{2.5}$$

2.2.8 Environmental interferent characterization

Environmental interferents were assessed for pH and density. pH measurements were performed using an Apera PH700 pH Meter calibrated using 4, 7, and 10 calibration buffers. pH measurements were taken at an ambient temperature of 16°C except for the reduced temperature condition which was measured at 3.7°C. Density measurements were performed using a 5 mL pycnometer (Thermo Fisher). Density measurements were calculated using Equation 2.6, where ρ_L is the density of the liquid, $M_{P,L}$ is the mass of the pycnometer filled with liquid, M_P, A is the mass of the pycnometer filled with air (i.e. empty and dry), V_P is the volume of the pycnometer to 4 decimal places as reported by the manufacturer, and ρ_A is the density of air at ambient temperature (0.00192 g mL^{-1} at 23°C).

$$\rho_L = \frac{M_{P,L} - M_{P,A}}{V_P} + \rho_A \tag{2.6}$$

2.2.9 Rheology

Rheology was performed on an AR2000ex rheometer (TA Instruments) using a 20mm crosshatched parallel plate attachment under ambient conditions (25°C). Dynamic frequency sweep measurements were performed over a frequency of 0.01 – 100 rads s^{-1} and 0.01 - 600 rads s^{-1} with a gap dimension of 1 mm for 950k and 92k PEHA respec-

tively. Strain values were selected by performing a preliminary stress sweep to identify the linear regime.

2.3 Limitations

There are a number of limitations to this study that must be acknowledged to contextualize the data presented in this chapter. These limitations stem from physical realities of the system (i.e., particle buoyancy and refractive index), defined limits of ImageJ® analytical software, and literal edge cases where the presented analytical methods were found to be inappropriate for measurement.

2.3.1 Fighting buoyancy (and losing)

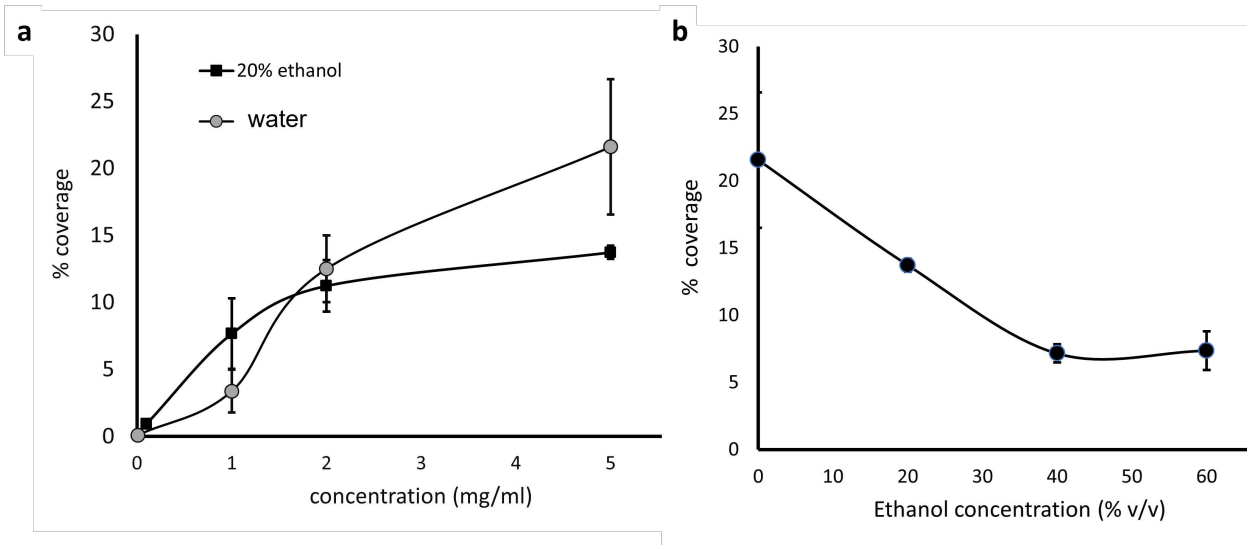

Figure 2.2: a) Change in %SAC versus concentration of Nylon30 in room temperature DI-water/ethanol solutions using 92k PEHA adhesive, 1 minute shaking. b) Change in %SAC coverage of Nylon30 (5 mg mL^{-1}) on 92k PEHA after 1 minute shaking in varying concentrations of ethanol.

A well-established fact of most plastic materials is their low density (0.02 – 1.55 g cm^{-3}) compared to other technical materials.[46] In fact, the low density is a primary reason why

plastic materials are so widely used. This, however, introduces many unique features to MP mobility compared to other commonly tracked particulate matter.[47,48] Namely, MPs tend to float on water, remain suspended in the water column for longer,[49,50] and even have been recorded to travel extended distances through air convection.[51] In the context of the presented work, the buoyancy as well as hydrophobic interactions between particles result in generally poor dispersion of MPs throughout the water volume. In the literature, various additives have been introduced to aqueous MP mixtures to aid in dispersion, including ethanol,[52,15] methanol, and various surfactants like dish soap.[53] I investigated several concentrations of ethanol to assess the influence on dispersion and capture of Nylon30 particles (**Figure 2.2**).

Figure 2.2 demonstrates a clear improvement in the measured standard deviations of the %SAC, which coordinates well with discussions of improved dispersion, however, there is a substantial reduction in MP capture in ethanol solutions. Adsorbents like the PSAs used in this study rely on surface energy interactions to function9, which are clearly inhibited by ethanol solutions. Therefore, DI water and Nylon30 particles (1.01g mL^{-1}), which are negatively buoyant in water, were selected as the neutral baseline for adsorption experiments in this work.

2.3.2 Optical microscopy artifacts and adhesive degradation

The quantification analysis performed using ImageJ® is dependent on inputting clear, unambiguous, high-resolution images for processing by the program. This however can be complicated by particles that approach the resolution limits of the microscope. In **Figure 2.3**, we show some examples of images containing features which complicate our analysis. These include (**2.3a**), larger particles that exceed the focal length of the microscope, (**2.3b**) clear or white particles that camouflage with the clear adhesive (**2.3c**), and adhesive migration that can produce defect zones on the same size scale as the target particles (**2.3b,c**). While the first two features can be corrected by selecting higher

resolution compound microscope lenses, leveraging stereomicroscope or SEM, and vertical image stitching, there remain tradeoffs regarding field of view, image resolution, and throughput speed. For this work, a compound optical 10x lens was selected to maximize the viewing window (2.8 x 1.9 mm). Under these conditions, the smallest MP species (PS10) was observable, and the largest MPs (PE200, PET1000) fit within the viewing window. But the larger particles (PE200, PET1000) were too tall to be completely within the focal range when focus was established at the widest point. Built-in ImageJ® features (i.e. brightness and contrast sliders) and the "include holes" function, were applied to improve the image quality for analysis and to balance tradeoffs to maximize throughput.

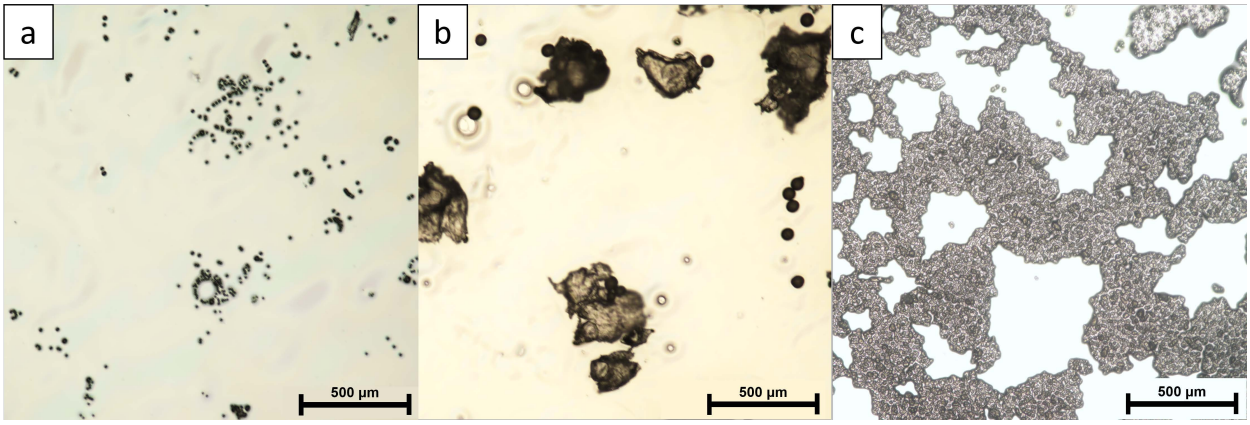

Figure 2.3: Examples of optical microscope images that complicate analysis. A) 0.1 mg mL^{-1} PS captured on 950k after 5 min, b) mixed assay of 50:50 PE50:PE200 on 950k after 5 min, and 5 mg mL^{-1} on 92k after 3 min.

Another feature of the system that complicated analysis was the variable durability of the adhesive films. The 92k adhesive was particularly prone to migration resulting in dense aggregates of particles and areas of bare glass (**Figure 2.3c**). In such cases where there was substantial adhesive migration, it was determined that the present two-dimensional quantification method was inappropriate for analysis, and no measurement was recorded. In other cases, there was less dramatic degradation of the adhesive occurring as round ruptures in the adhesive (**Figure 2.2a,b**). In the cases where the degradation covered a minimal surface area of the adhesive region, MP calculations were carried

out. Here, the thresholding step of the 'analyze particles' function was used strategically to avoid including the perimeter of the ruptured region(s) with the confirmed particles. However, sometimes the pixel contrast between the particles and the adhesive rupture could not be completely distinguished, and therefore thresholding was selected to the best of the user's ability to represent an accurate distribution of capture.

2.3.3 ImageJ® boundary conditions

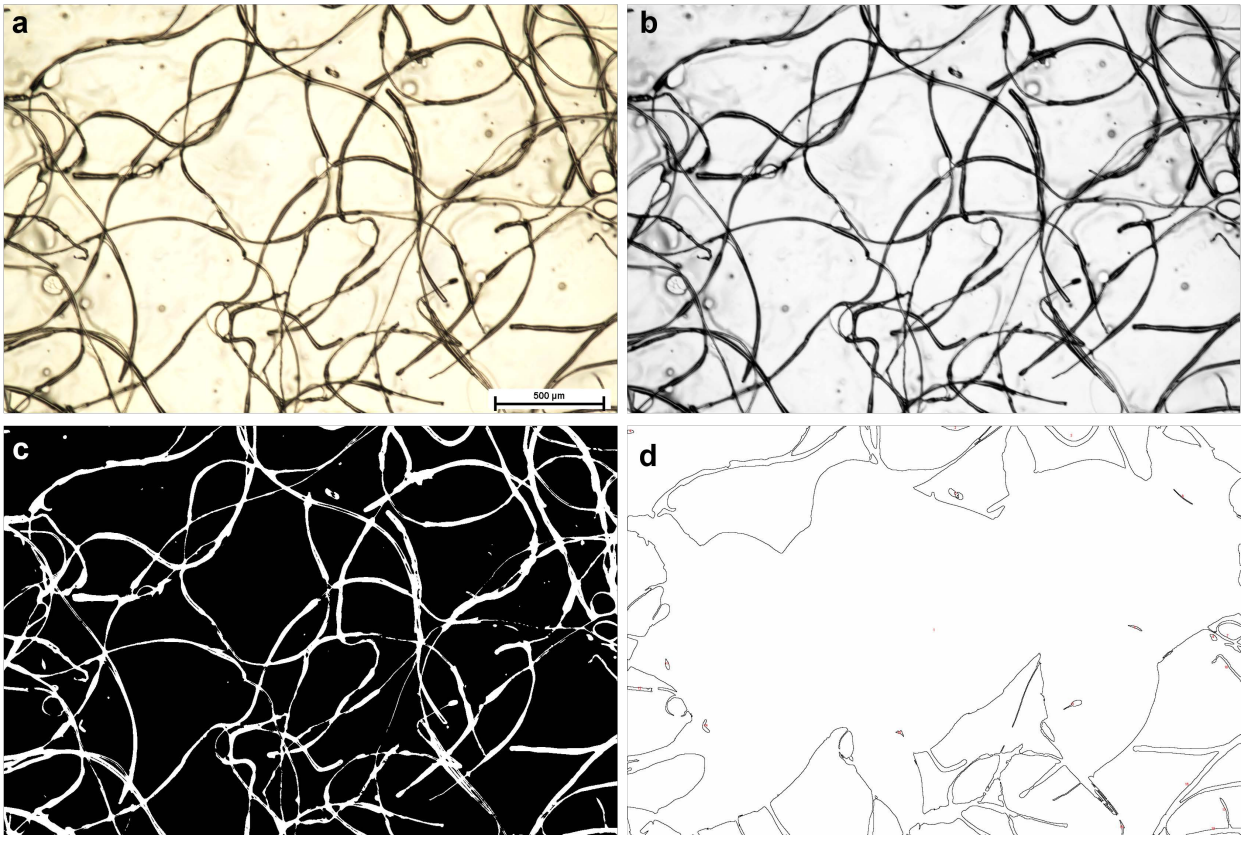

Figure 2.4: A) Microscope image from PET Fiber shake test, b) image converted to grey-scale and tuned for better contrast, c) the thresholded image, d) the ImageJ output of what is calculated with the "Analyze Particles" feature, a poor representation of the aggregated fibers.

ImageJ® is an imperfect tool for the analysis of concentrated particles and fibers. The general functionality of the 'analyze particles' feature, which was used for all optical analysis in this chapter, is a manual fractionation of the image based on greyscale pixel intensi-

ties (0-255) where a range of pixel intensities is designated as the particle phase and the rest is interpreted as background. In this capacity, the software indiscriminately identifies all pixels of a specified intensity range as a 'particle' regardless of if the given pixel is part of a particle, shadow, dust, or image artifact. The software also cannot differentiate particle boundaries, so clusters of several particles are interpreted as single large particles that may also include interstitial regions of uncovered region that are shadowed by the adjacent close-packed particles. To overcome this failing, brightness and contrast controls in the ImageJ® software were used to improve the image quality, however, problems persisted. Overall ImageJ® is prone to over-count the surface area coverage of particles adhered to the adhesive surface. Manual adjustment of thresholding as well as exclusion of particles below 85 μm^2 was performed in this work to control for over-counting as much as possible. It is acknowledged that manual adjustments will make the analysis very subjective to the individual processing the data, however, utilization of of batch processing that applies a consistent thresholding to all images also yields an imperfect interpretation of particle boundaries.

Analysis was also performed on the adsorption of chopped PET fibers on adhesive. Within the microscope view window under 10x magnification, the fibers formed a continuous structure over the background adhesive (**Figure 2.4**). As can be seen in **Figure 2.4d**, ImageJ® struggles to interpret a continuous phase with the 'analyze particles' feature, resulting in a broken outline. While a measurement is provided in the application window, the value may be untrustworthy given the failure of the visual feedback from the outline. In future work, microscope images should be taken to permit the greatest clarity of particle boundaries, and other analysis software should be considered, including machine learning informed software that may better interpret clustered particles and fibers.

2.3.4 Glass slide edge effects

It was observed that during the glass slide shaking experiments, large quantities of particles would agglomerate to the edges of the adhesive region (**Figure 2.5**) resulting in dense clusters of particles that could not be quantified via the presented optical method. In the present study, these particles were not considered in the analysis, however they represent a significant portion of the total captured particles. We believe these particles accumulated as a result of a physical impingement of particles between excess adhesive on the edge of the glass slide and the wall of the vial during shaking. Some particle edge capture may be the result of radial adhesive migration of adhesive captured particles. Overall, this suggests that impingement and other physical forces that can drive MPs into the adhesive would likely improve capture. Within this work, the exclusion of the edge-accumulated particles represents a large under-counting of captured particles and may have affected the real concentration of particles encountered by the adhesive region during the course of the shake test.

Due to the consistent protocol used within this work, the measured percent surface area coverage (%SAC) should be self-consistent and the observed trends should be transferable although the direct measurements under count the total capture. Future work within our group is considering a smaller adhesive region that institutes an uncoated buffer zone ($\sim$ 2 mm) around the physical edge of the glass slide to avoid the accumulation of excessive adhesive in areas that cannot be measured in two-dimensional space. Despite the negative impact on objective measurement, the edge capture observed with the glass slides represents a promising design feature that should be further explored in the context of MP capture devices.

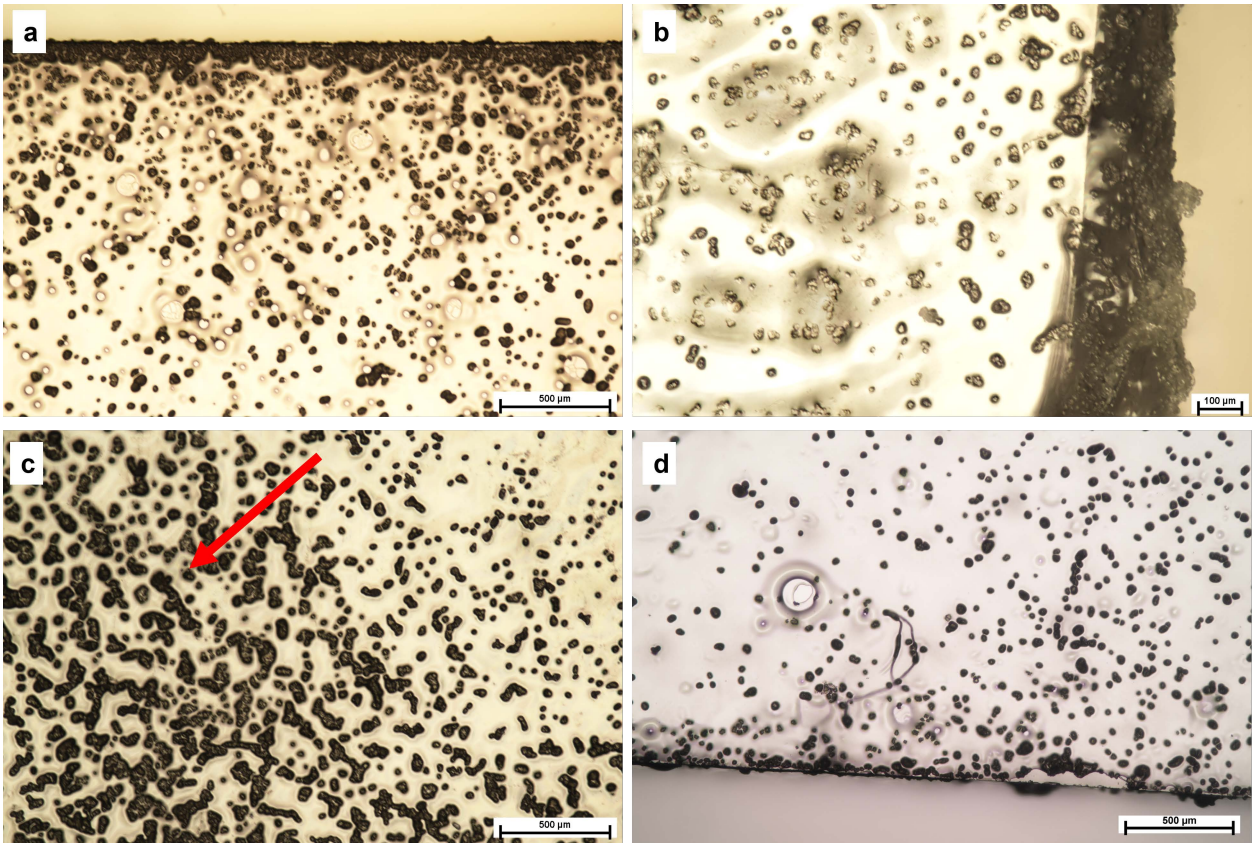

Figure 2.5: Microscope images demonstrating the edge effect a) 950k PEHA with 1 mg mL^{-1} Nylon30 after 5 min shaking, b) 50:50 BD 2 mg mL^{-1} Nylon30 after 5 min shaking, c) 50:50 BD 2 mg mL^{-1} Nylon30 5 min shaking. The arrow points to the edge showing higher accumulation along the edge of the slide. d) 950k 0.1 mg mL^{-1} Nylon30 after 5 min shaking.

2.4 Results and Discussion

Simple glass slide based adhesive substrates were investigated to assess the efficacy of a rapid observation-based quantification method and to further study the deployment of PSAs for MP capture. The system was calibrated using 3 formulations of PEHA to capture 30 µm nylon-12 polydisperse particles in DI water. Further tests were carried out to assess the impact of MP size and chemical composition as well as the impact of different environmental factors including temperature, inorganic particulate matter, and chemical additives. Quantification of MP capture was performed using the open-source software, ImageJ®, to analyze optical microscope images of adhesive capture on flat, adhesive-coated substrates. Built-in ImageJ® features were used to determine the number count of

particles as well as the total surface area coverage of the target MP species which were used to determine %SAC as an aggregate value for the binding affinity of the whole glass slide area.

To make differences in binding more visible, we assessed binding primarily at elevated concentrations (1–5 mg mL^{-1}) compared to most aqueous environmental concentrations, which are highly dependent on time and location.[54] To test for transferability to more dilute conditions we also assessed binding at 0.01 mg mL^{-1} nylon30 with 2 of our 3 adhesives. After 5 min of shaking, the 950k had 0.13 $\pm$ 0.1% surface area coverage (SAC). The experiment was repeated using a mixed, bimodal distribution of 50% 92K and 50% 950K (50:50 BD) and shaken for 30 mins yielding 0.27 $\pm$ 0.1% SAC, showing that binding is measurable at 0.01 mg mL^{-1} and that adhesive formulation and increased time can improve capture.

2.4.1 Resin variations: impact on binding

Figure 2.6 shows select images of the adhesive surfaces with nylon30 binding incidence. Comparison of the MP binding behavior between the two different molecular weight adhesives and the resin mixture demonstrates faster binding for the 92k PEHA compared to 950k at all time points. However, when particle exposure times were longer than 1 minute, the 92k resin migrated on the slide surface and coalesced around dense aggregations of particles. Although the capture with the 92k resin is effective, as demonstrated by the dense packing of particles observed at 5 and 10 minutes (**Figure 2.6**), the loss of a cohesive film made image-based counting inconclusive. The high mobility of the adhesive could also lead to shedding, which may account for unidentified small particles observed in our previous work.[15] The 950k resin deposited on slides also shows binding, with more stable films persisting through 5 minutes of exposure time (**Figure 2.7**).

The viscoelastic quality of the 92k and 950k PEHA are presented in **Figure 2.8**. We expect that the general lower binding of the 950K resin is attributed to its higher adhesive

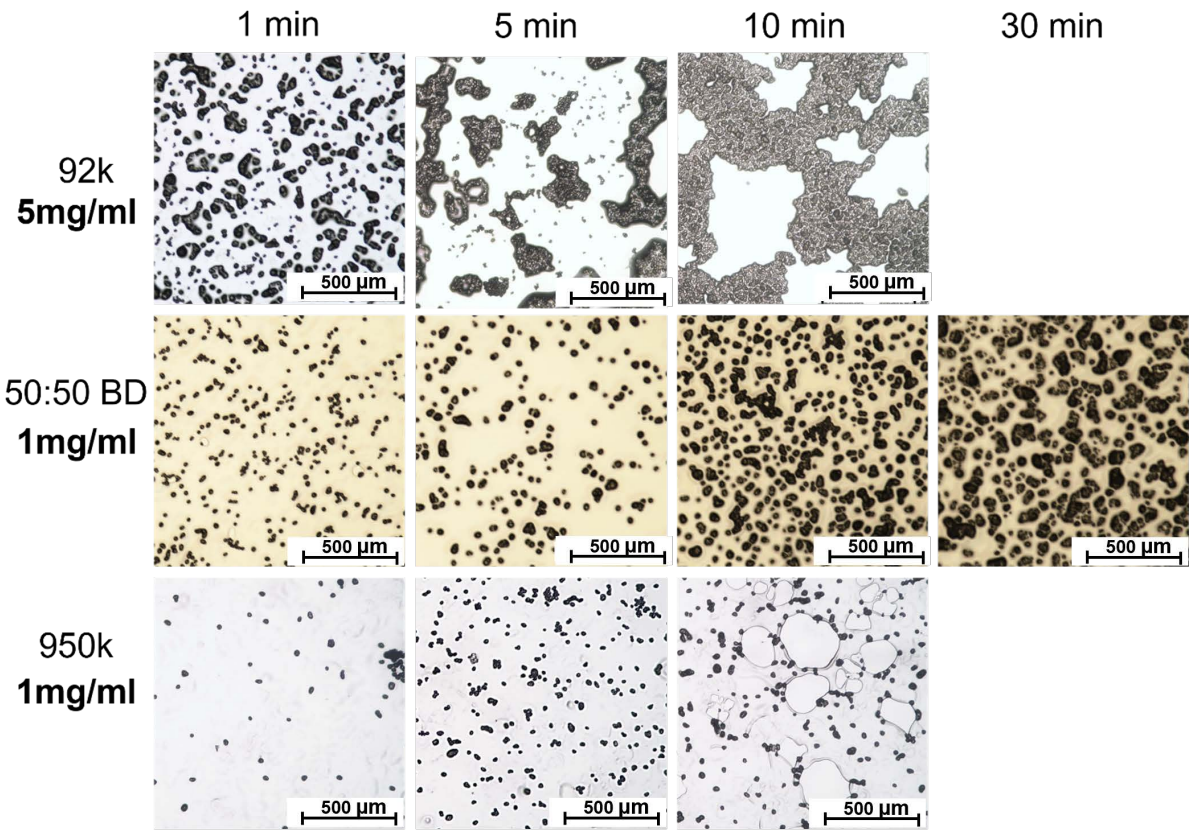

Figure 2.6: Time based capture of nylon30 from DI water on adhesive-coated glass slides. 92k tests were performed with 5 mg mL^{-1} of nylon30. 950k and the 50:50 bimodal distribution (BD) tests were performed with 1 mg mL^{-1} nylon30. In the 92k sample at the 5 and 10 minute marks, cavities represent the absence of adhesive due to adhesive migration and coalescence. The 950k at 10 minutes also shows some adhesive migration.

modulus, which may lead to less binding after particle collision.[41] Higher stiffness could also result in a "catch and release" scheme where captured particles are temporarily bound.[55] Rheological analysis of the 950k PEHA falls well within both the Dahlquist and Chu parameters (**Figure 2.8**) however, it clearly has cohesion issues as demonstrated by **Figure 2.6**. Both the 92k and 950k PSAs fail to produce robust films. While both the Chu and Dahlquist criteria omit the loss modulus (G'') it is worth observing the relationship between G' and G'' through the crossover point (COP). The COP of the 950k is visible in the region shown in **Figure 2.8**, occurring at 13.6 rad s^{-1} with a dynamic modulus of 12.5 MPa. The 92k is largely dominated by the G" in this region, demonstrating its more fluid-like behavior. Paired with its low zero shear viscosity (65 Pa s), and a COP occurring

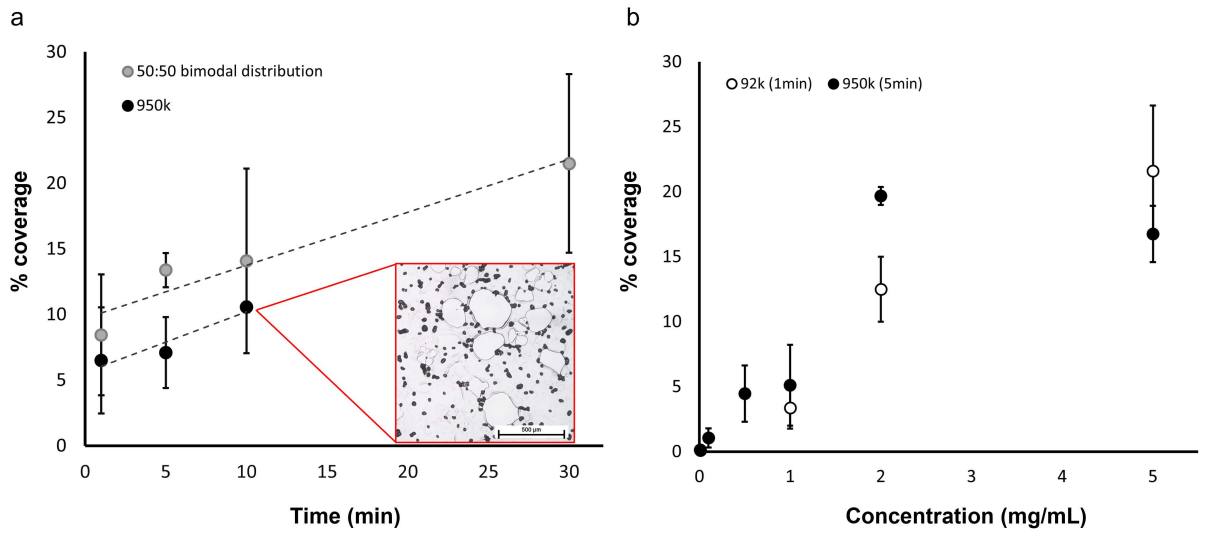

Figure 2.7: a) Plot of time-based assessment versus %SAC for 950k and 50:50 BD of PEHA each with 1 mg mL^{-1} of nylon30 from DI water. b) Plot of %SAC versus concentration of nylon30 for 950k at 5 min shaking and 92k at 1 min shaking in DI water. Adhesives demonstrate rapid particle binding, as indicated by the non-zero intercept of the time-based assessment.

at 483 rad s^{-1} with a dynamic modulus of 10 MPa, the rheological properties point to both the adhesive's high wettability and tendency towards adhesive migration.

We had insufficient material to perform rheological analysis on the 50:50 mixture of 92k and 950k PEHA, however, the improved film robustness and intermediary capture behavior demonstrates promising behavior. These improved properties are attributed to plasticization of the 950k by the 92k resin. 50:50 BD films were generally stable through 30 minutes of aqueous exposure, although some film deterioration was noted. In the literature, bimodal resin distributions have been shown to improve bulk polymer properties such as flow, loop tack, and shear strength in both PSAs[56] and elastomers[57]. The results are instructive, but further exploration into adhesive formulation and compounding is needed to optimize capture.

Glass slide aggregate data shows increasing trends in microplastic binding with both MP concentration and exposure time (**Figure 2.7a,b**). Although not statistically significant, **Figure 2.7a** shows a positive linear trend between MP capture and time, and there

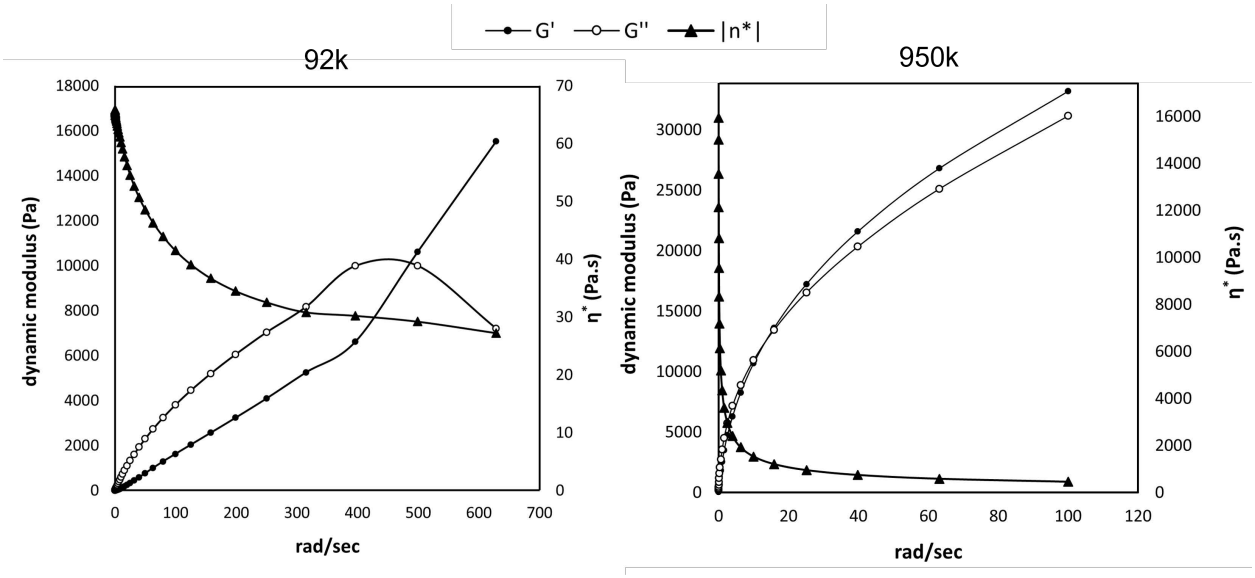

Figure 2.8: Plot of complex viscosity, storage modulus, and loss modulus for 92k PEHA (left), and 950k (right) PEHA

is evidence that adhesive formulation can substantially shift binding affinity. **Figure 2.7a** demonstrates shows a 50% increase in MP capture by the 50:50 BD compared to the 950k. Time-dependent capture was also impacted by film stability as the 950k adhesive degraded after 10 minutes of exposure, and the 92k was unable to be assessed after 1 minute due to resin migration (**Figure 2.6**). This was also highlighted by the similar performance of the 950k at 5 min shaking and the 92k at 1 min shaking. Together, these observations point to the importance of physical entraptment on the effectiveness of MP capture by PSAs. All three adhesive formulations assessed are chemically identical, differing only by their molecular weight. Therefore, the viscoelastic properties of the adhesive play a fundamental role in both the adsorption efficacy and film robustness.

2.4.2 Impact of interferents and more realistic dispersions found in the built environment

Adhesive binding of nylon30 particles was assessed when dispersed in tap water, 35% saline solution, samples of water taken from the Huron River, and aqueous dispersions

Table 2.1: Surface area coverage of nylon30 particles under different environmental interferants

Adhesive	Nylon30 Conc.	Shake time	Interferant^	%SAC
92k PEHA	5 mg mL^{-1}	1 min	DI water	21.6 ± 5.0
			3° C DI water	12 ± 5.2
			35% Saline	11 ± 2.3
			SDS 0.1% w/v	*
			Humic acid 200 mg/L	*
			Tergitol 0.1% w/v	1.0 ± 0.5
950k PEHA	5 mg mL^{-1}	1 min	DI water	19.0 ± 5.8
			Huron River water	15.9 ± 7.4
			Tap water	13.3 ± 6.7
50:50 BD	1 mg mL^{-1}	5 min	DI water	13.4 ± 1.3
			Silica sand 1 mg mL^{-1}	13.8 ± 1.8
			Bentonite clay 1 mg mL^{-1}	2.0 ± 0.8

^All samples are prepared in DI water except Huron River water and Tap water
**These interferents degraded the adhesive too much to assess %SAC*

of surfactants (ionic and non-ionic), humic acid, silica sand, bentonite clay, and DI water samples cooled to 3° C (**Figure 2.9**). Binding data is presented in **Table 2.1**. The microplastic capture was reduced compared to the DI water controls under all conditions except for the 1 mg mL^{-1} silica sand which performed 3% better than the control. Binding in hard tap water and water sampled from the Huron River was also within one standard deviation of the control, however the variance was larger for these tests. Overall, adhesive binding was found to be viable under all conditions tested although the adsorption was severely disrupted by non-ionic surfactants (Tergitol, **2.9**), 3° C DI water (**2.9b**), and bentonite clay (**2.9l**). Several interferents also degraded the adhesive including SDS ionic surfactant (**2.9d**), humic acid (**2.9e**), and silica sand (2.9k), which negatively impacted quantification. The interaction between the environment and the adhesive is the greatest barrier to developing more robust films. In Figure 2.9, all 3 adhesive formulations (92k, 950k, and 50:50 BD) are represented as a result of progressive improvements in understanding of adhesive properties, however they are all composed of the same PEHA functional units and expected to have similar surface energetics.

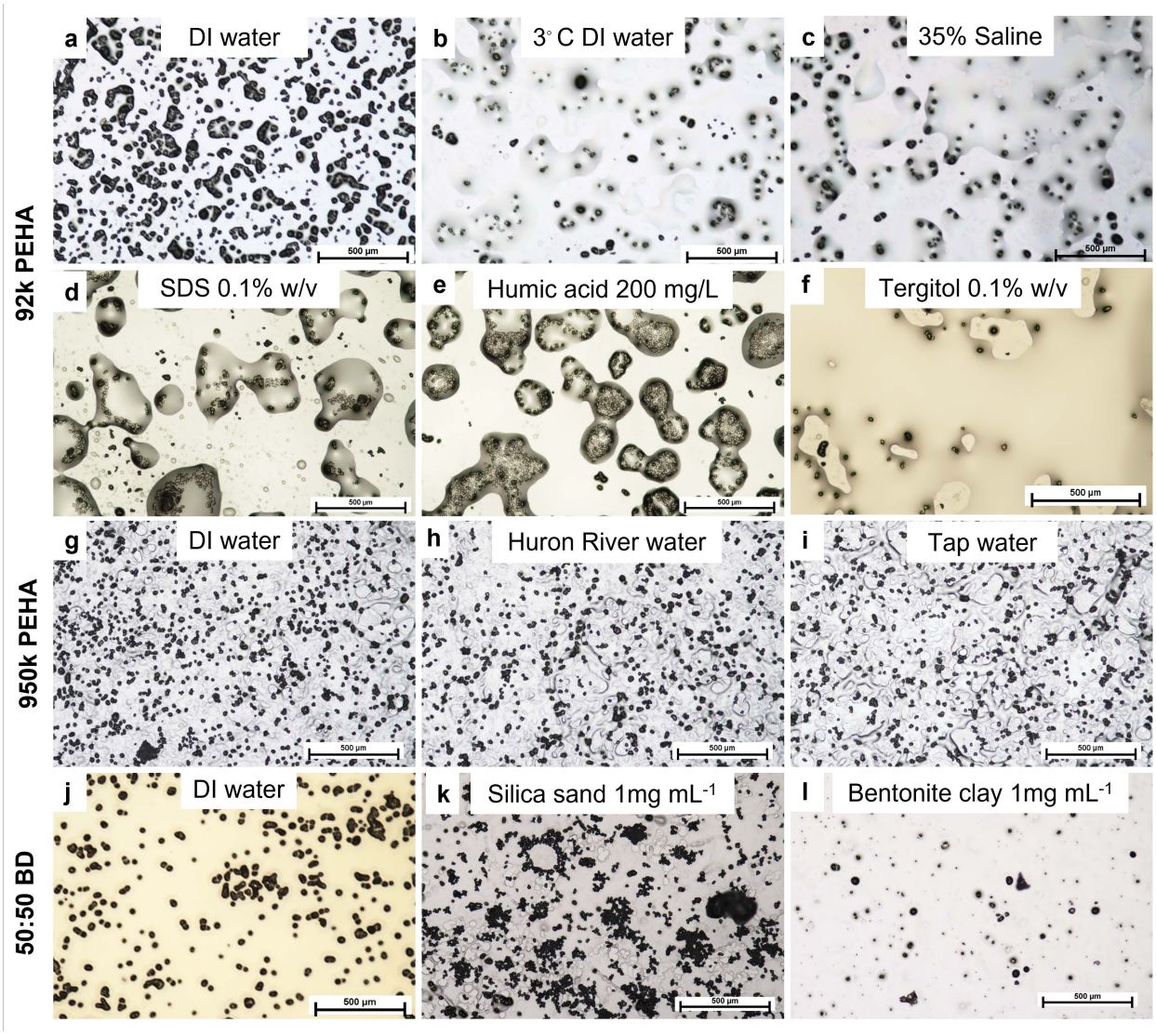

Figure 2.9: Optical microscope images showing nylon adsorption in the presence of varying environmental interferants. Results for 5 mg mL^{-1} of nylon and 1 minute of shaking are shown for 92k PEHA (a-f) and 950k PEHA (g-i). Results for 1 mg mL^{-1} of nylon and 5 minutes of shaking with a 50:50 bimodal distribution are depicted in (j-l).

The 92k was the softest and most unstable of the 3 formulations tested, and it was substantially compromised by the SDS (**2.9d**) and humic acid (**2.9e**), which appear to have plasticized the 92k, leaving islands of adhesive with embedded clusters of nylon particles. However, because it is so soft, the low glass transition temperature likely positions it to function better in low temperature conditions where it's tack would be higher than more glassy resins. The insoluble silica (100 µm) was also destructive to the adhesive. We did not see substantial adhesion of sand to the adhesive (**2.9k**), but there was noticeable abrading of the 50:50 BD suggesting that the plasticized thermoplastic film is weak to collisions with higher density particles.

The Tergitol (**2.9f**) and bentonite (**2.9l**) exposure assessments are unique cases where each interferent fouls the adhesive surface. Preliminary computational assessment suggests that Tergitol binds to PEHA under aqueous conditions.62 Likewise, the bentonite visibly fouls the adhesive surface with small particulate material. We are currently studying surface energetics of binding/debinding under a range of aqueous interferents and will report on this in future publications.

To better understand the influence of the interferents, %SAC was assessed against the measured relative density and pH of the various solutions (**Figure 2.10**). Adsorbents and other surface-active materials tend to be pH sensitive[9] due to their dependence on relative surface energy for binding. The fluid density also becomes relevant as it determines the buoyancy of the particles and where it will tend to exist within the fluid. Density and pH aren't the only parameters that control the interaction between MPs and the adhesive, although some of the observed differences may be explained by one or both of these features. In Figure **2.10a**, it can be seen that pH and relative density introduce different spread into the distribution of %SAC.

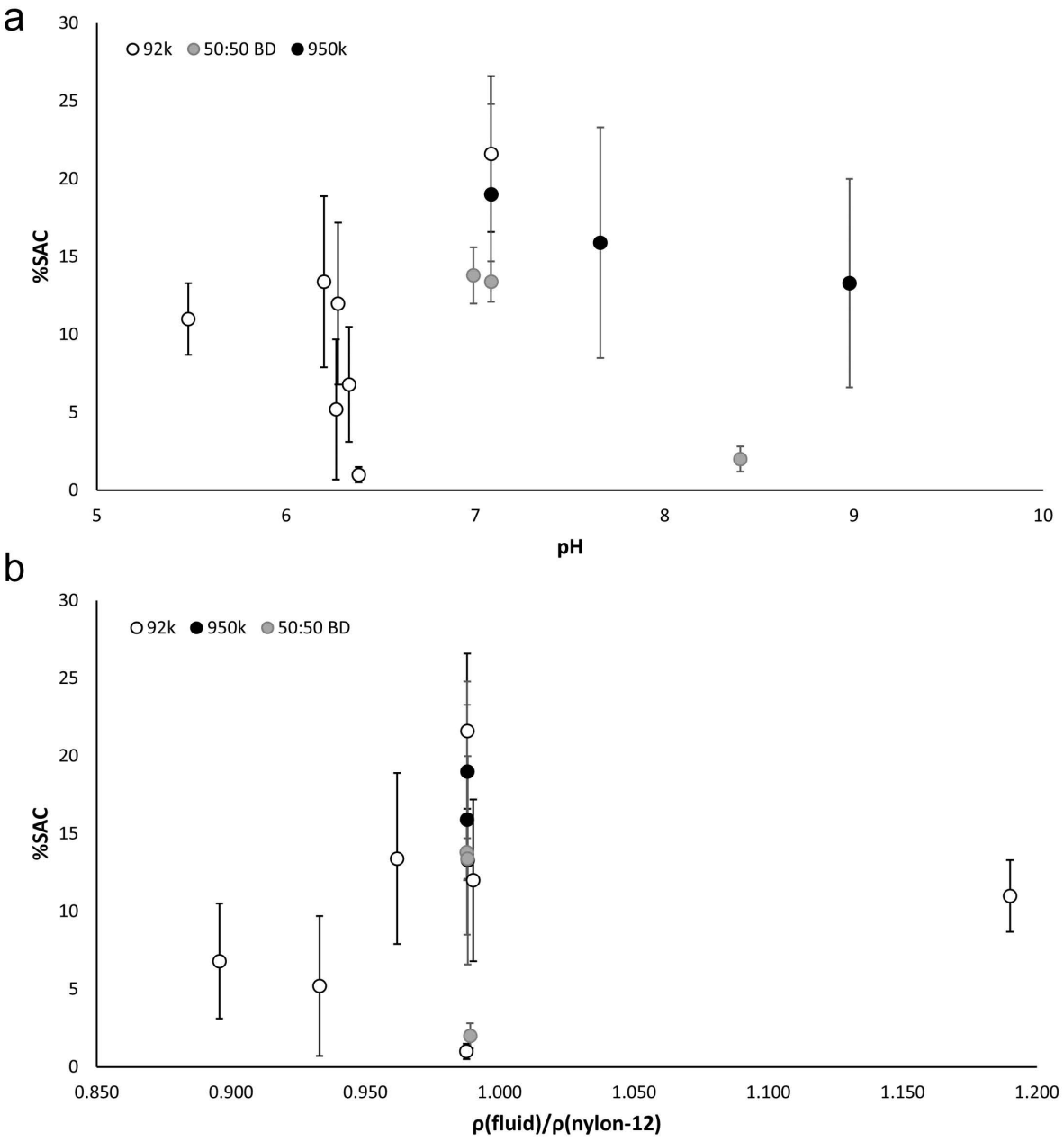

Figure 2.10: Assessment of interferent properties a) with respect to interferent solution pH, and b) interferent solution density normalized to the density of nylon-12.

Overall, pH is more explanatory to the spread, with high R^2 linearity for 950k (0.9275) and 50:50 BD (0.9991) and 0.1508 for 92k. It appears that neutral pH promotes the best binding, with more alkaline and acidic interferents having poorer binding, although more of the sample space should be tested to confirm the relationship. The relationship between binding and relative density didn't show any significant trends, although 70% of the interferents assessed were closely grouped around the density of water (0.997 g mL^{-1} ± 0.08%), and all but one of the interferents were less than the density of the nylon-12 particles.

2.4.3 Binding assessments using mixed particulates

In mixed assays, MPs were specifically selected to be distinct in size and/or shape to distinguish using built-in ImageJ® features. Several representative images were used to calibrate the size range and circularity factor for individual particle types, and those conditions were applied to the rest of the images. When quantifying particles, aggregates of the same particle species were treated as larger individual particles for particle counting and surface area assessments. Individual images were excluded from the analysis when aggregation and/or overlap of different particle types was frequent and when aggregate formation of one species compromised size-based particle identification in ImageJ®.

Combinations of common plastic species were assessed to study the influence of MP composition (PS10/nylon30) and particle size (PE50/PE200). Individual parametric studies were also performed for both PS10 and cut PET fibers at 0.1 mg mL^{-1} respectively which are included in **Appendix A**. Adsorption was assessed on both metrics of %SAC and number count. In the PS10/nylon30 test, the nylon30 particles adsorbed at similar rates as in pure nylon30 tests, while PS10 binding in mixed conditions was lower compared to pure PS10 tests. A 73% reduction in %SAC between pure PS10 tests and PS10/nylon30 mixed conditions was noted based on particle differentiation with ImageJ® (**Figure 2.11**). Figure 5c shows aggregates of PS10 that could be misidentified as larger

nylon30 particles, which may have under counted PS10 in the mixed assay. It's also possible that co-binding between the two particles occurs. The lower PS10 binding could be a result of the more polar nylon30 having greater affinity for PEHA when mixed with PS10.[55] The larger nylon30 particles may also block the access of smaller PS10 particles to the adhesive substrate or dislodge particles that are insufficiently adsorbed. Overall, mixed assay assessment of PS10/nylon30 looks promising for image based assessment to quantify co-binding. Limitations exist with image resolution/analysis that could be improved with integration of other analytical techniques like Fourier transform infrared spectroscopy (FTIR) or Raman microscopy.

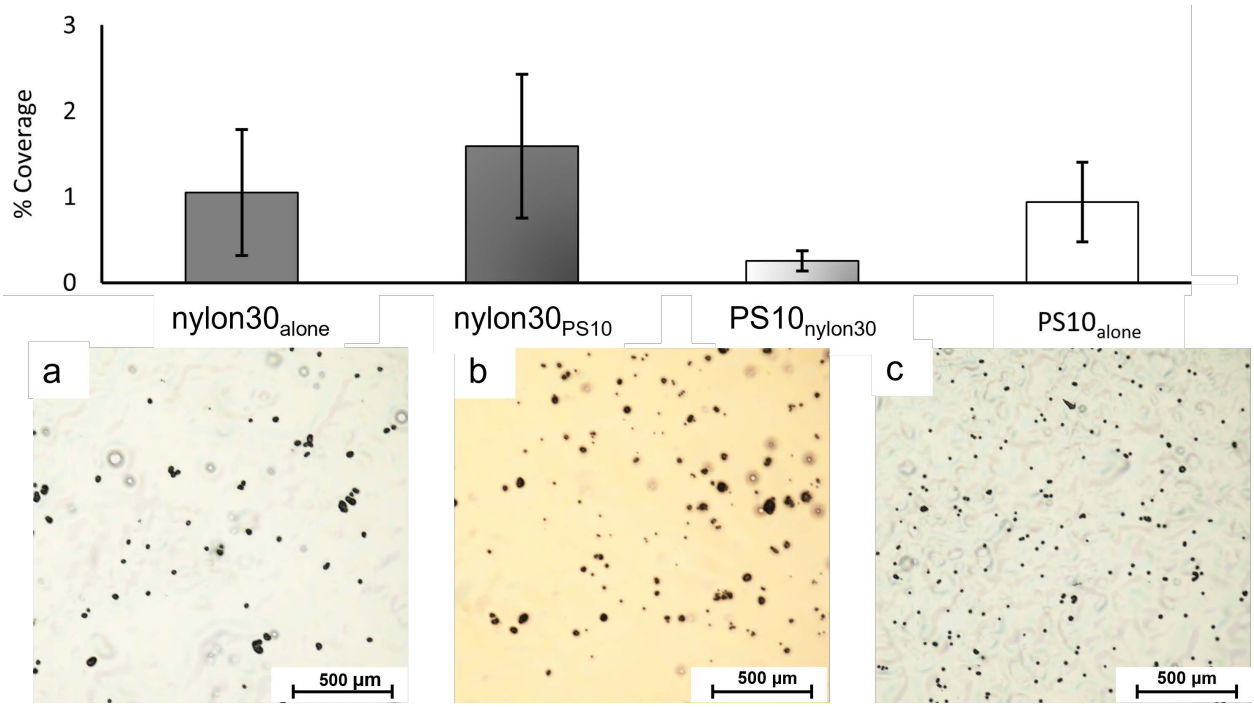

Figure 2.11: Comparison of %SAC for nylon30 and PS10 on 950k PEHA adhesive testing both parametrically and in mixed assay. A) 0.1 mg mL^{-1} nylon30 (nylon30 alone), b) mixed assay of 0.1 mg mL^{-1} of each nylon30/PS10 in DI water, c) 0.1 mg mL^{-1} PS10 (PS10 alone).

A second mixed assay was performed between polyolefin polymers PE50 and PE200 using the same 950K adhesive. These PE samples are much lower in density than nylon30 and are found near the meniscus of the aqueous fluid. The high buoyancy and hydrophobicity led to poor dispersion in water and relatively high levels of both homoge-

nous and heterogenous aggregation in water and on adhesive surfaces. Heterogenous clusters in the images could not be deconvoluted using ImageJ® software since ImageJ® relies on grayscale pixel intensity and cannot differentiate discrete particle boundaries. More heterogenous aggregation was observed with the PE50/PE200 compared to the PS10/nylon30 mixtures, probably due to the shared composition and hydrophobicity of the two particle types. A comparison mixture with nylon30/PE50 wasn't possible due to size overlap of the polydisperse white powders. Consideration of more advanced visualization software is underway and will be presented in future work.

Comparing across polymer samples based on particle size and composition, the most significant binding trend was with particle size, where the type of measurement is shown to directly bias the interpretation of the data (**Figure 2.12**). Regardless of the individual composition, the binding of smaller particles translated to more binding events per unit area and lower overall %SAC, whereas the binding of a few larger particles resulted in more coverage but fewer binding events. These results expose bias introduced into this work by our decision to spike the solutions with mass-based concentrations, where a specified mass of smaller MPs inherently contains more particles than an equivalent mass of larger particles. The %SAC and count data presented in **Figure 2.12** were acquired simultaneously through ImageJ interpretation of the image sets, which is a strength of the visual based assessment. Our findings could help bridge the literature gap between count based and mass based (comparable to %SAC) MP assessments.[58,59] Without knowing whether count or coverage is most telling, the reporting of only one mode of counting, especially in mixed particle systems can skew quantitative interpretations. To minimize bias and present the most accurate picture of MP presence, it seems best to present both values when sampling diverse MP distributions.

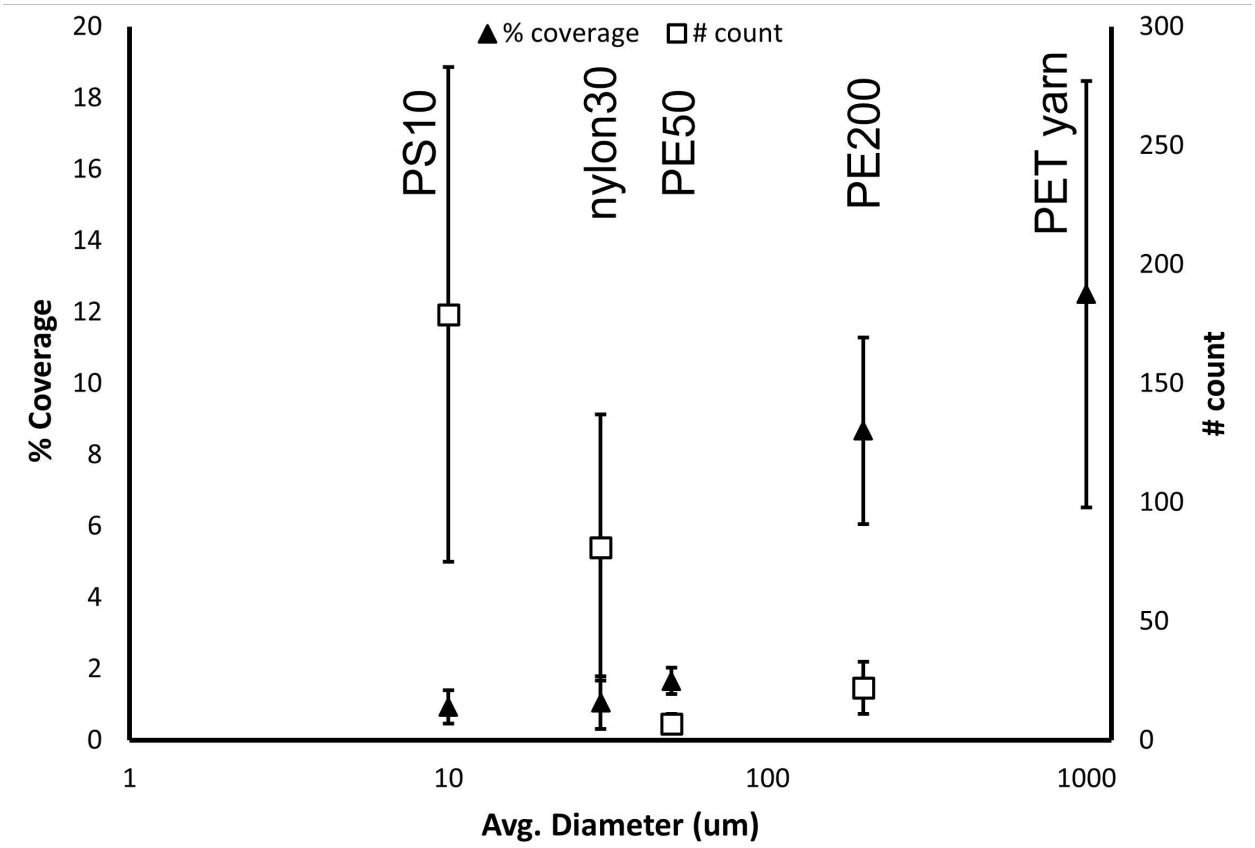

Figure 2.12: Plot of %SAC and particle count with respect to the particle average diameter for 0.1 mg mL^{-1} dispersions with 950k adhesive, 5 min shaking in DI water.

2.5 Conclusion

A simple, low-cost imaging-based assessment of MP capture was deployed using adhesive-coated glass slides to assess MP dispersions and to better understand adhesive-based capture. Three formulations of adhesives were tested with a selection of post-consumer and commercially available forms of MPs including nylon, PE, PET fibers, and PS. We developed an imaging protocol to analyze MP binding on adhesive-coated slides. Trends were established comparing capture efficiency with MP concentrations in aqueous solution altering particle types, particle concentration, adhesive exposure time, and including a variety of soluble and insoluble interferents.

As a comparative method, adhesive-mediated MP binding is a simple and inexpensive tool that allows one to parameterize assessments based on adhesive, MP species, and other environmental conditions. The slide-based binding assessment can accommodate a wide range of particle sizes, both for analysis and as impurities, and is more granular than gravimetric techniques due to a higher sensitivity to small particles. The technique also permits the simultaneous collection of count and surface area data, while allowing for subsequent testing such as flow cytometry and hemocytometry if amenable to analysis. The glass slide method is a simple and low-tech analysis, making it accessible to researchers without access to expensive infrastructure like FTIR spectrometers, flow cytometers, scanning electron microscopes (SEM), or even consistent access to the internet. ImageJ® is a self-contained image analysis tool that only has to be downloaded once, and then operates locally on the user's computer. Like other analysis tools, the slide observation technique has inherent limitations. The technique is affected by particle dispersion problems associated with polar interactions and density stratification, which contributes to heterogenous adhesive binding. The heterogeneous binding adds to complications with the image-based assessment by compromising the current software's ability to identify discrete particles and fibers.

We also identified an inherent bias in MP quantification based on the units reported. In mixed MP collections, as they commonly exist in the environment, weight-based assessments bias towards larger particles, and count-based assessments bias towards smaller particles, both complicating the harmonization of data and muddying our ability to convey information to health professionals, policy makers, and the general public. Therefore, we propose reporting both number count and size-related (i.e., weight or surface area) data where possible to interpret MP collections objectively.

2.6 References

[1] Yusheng Pan, Shu Hong Gao, Chang Ge, Qun Gao, Sijing Huang, Yuanyuan Kang, Gaoyang Luo, Ziqi Zhang, Lu Fan, Yongming Zhu, and Ai Jie Wang. Removing microplastics from aquatic environments: A critical review. *Environmental Science and Ecotechnology*, 13:100222, 2023. ISSN 26664984. doi:10.1016/j.ese.2022.100222. URL https://doi.org/10.1016/j.ese.2022.100222.

[2] Riaz Ahmed, Ansley K. Hamid, Samuel A. Krebsbach, Jianzhou He, and Dengjun Wang. Critical review of microplastics removal from the environment. *Chemosphere*, 293(January):133557, 2022. ISSN 18791298. doi:10.1016/j.chemosphere.2022.133557. URL https://doi.org/10.1016/j.chemosphere.2022.133557.

[3] Aravin Prince Periyasamy and Ali Tehrani-Bagha. A review on microplastic emission from textile materials and its reduction techniques. *Polymer Degradation and Stability*, 199:109901, 2022. ISSN 01413910. doi:10.1016/j.polymdegradstab.2022.109901. URL https://doi.org/10.1016/j.polymdegradstab.2022.109901.

[4] Radhakrishnan Yedhu Krishnan, Sivasubramanian Manikandan, Ramasamy Subbaiya, Natchimuthu Karmegam, Woong Kim, and Muthusamy Govarthanan. Recent approaches and advanced wastewater treatment technologies for mitigating emerging microplastics contamination – A critical review. *Science of the Total Environment*, 858(September 2022):159681, 2023. ISSN 18791026. doi:10.1016/j.scitotenv.2022.159681. URL https://doi.org/10.1016/j.scitotenv.2022.159681.

[5] Melania Fiore, Silvia F. Garofalo, Alessandro Migliavacca, Alessandro Mansutti, Debora Fino, and Tonia Tommasi. Tackling Marine Microplastics Pollution : an Overview of Existing Solutions. *Water, Air, and Soil Pollution*, 233:276, 2022. ISSN 1573-2932. doi:10.1007/s11270-022-05715-5. URL https://doi.org/10.1007/s11270-022-05715-5.

[6] P. S. Goh, H. S. Kang, A. F. Ismail, W. H. Khor, L. K. Quen, and D. Higgins. Nanomaterials for microplastic remediation from aquatic environment: Why nano matters? *Chemosphere*, 299(December 2021):134418, 2022. ISSN 18791298. doi:10.1016/j.chemosphere.2022.134418. URL https://doi.org/10.1016/j.chemosphere.2022.134418.

[7] Mario Urso and Martin Pumera. Nano/Microplastics Capture and Degradation by Autonomous Nano/Microrobots: A Perspective. *Advanced Functional Materials*, 32 (20), 2022. ISSN 16163028. doi:10.1002/adfm.202112120.

[8] Junliang Chen, Jing Wu, Peter C. Sherrell, Jun Chen, Huaping Wang, Wei xian Zhang, and Jianping Yang. How to Build a Microplastics-Free Environment: Strategies for Microplastics Degradation and Plastics Recycling. *Advanced Science*, 9(6): 1–36, 2022. ISSN 21983844. doi:10.1002/advs.202103764.

[9] Imran Ali, Xiao Tan, Juying Li, Changsheng Peng, Peng Wan, Iffat Naz, Zhipeng Duan, and Yinlan Ruan. Innovations in the Development of Promising Adsorbents for the Remediation of Microplastics and Nanoplastics – A Critical Review. *Water Research*, 230(September 2022):119526, 2023. ISSN 18792448. doi:10.1016/j.watres.2022.119526. URL https://doi.org/10.1016/j.watres.2022.119526.

[10] Cuizhu Sun, Zhenggang Wang, Lingyun Chen, and Fengmin Li. Fabrication of robust and compressive chitin and graphene oxide sponges for removal of microplastics with different functional groups. *Chemical Engineering Journal*, 393(March):124796, 2020. ISSN 13858947. doi:10.1016/j.cej.2020.124796. URL https://doi.org/10.1016/j.cej.2020.124796.

[11] Hongru Jiang, Yingshuang Zhang, Kai Bian, Chongqing Wang, Xu Xie, Hui Wang, and Hailong Zhao. Is it possible to efficiently and sustainably remove microplastics from sediments using froth flotation ? *Chemical Engineering Journal*, 448(June): 137692, 2022. ISSN 1385-8947. doi:10.1016/j.cej.2022.137692. URL https://doi.org/10.1016/j.cej.2022.137692.

[12] Ye Tang, Suhua Zhang, Yinglong Su, Dong Wu, Yaping Zhao, and Bing Xie. Removal of microplastics from aqueous solutions by magnetic carbon nanotubes. *Chemical Engineering Journal*, 406(August 2020):126804, 2021. ISSN 13858947. doi:10.1016/j.cej.2020.126804. URL https://doi.org/10.1016/j.cej.2020.126804.

[13] Jieun Lee, Jiae Wang, Yumin Oh, and Sanghyun Jeong. Highly efficient microplastics removal from water using in-situ ferrate coagulation : Performance evaluation by micro-Fourier-transformed infrared spectroscopy and coagulation mechanism. *Chemical Engineering Journal*, 451(P2):138556, 2023. ISSN 1385-8947. doi:10.1016/j.cej.2022.138556. URL https://doi.org/10.1016/j.cej.2022.138556.

[14] Huaijuan Zhou, Carmen C. Mayorga-Martinez, and Martin Pumera. Microplastic Removal and Degradation by Mussel-Inspired Adhesive Magnetic/Enzymatic Microrobots. *Small Methods*, 5(9):1–9, 2021. ISSN 23669608. doi:10.1002/smtd.202100230.

[15] P. Takunda Chazovachii, Julie M. Rieland, Violet V. Sheffey, Timothy M. E. Jugovic, Paul M. Zimmerman, Omolola Eniola-Adefeso, Brian J. Love, and Anne J. McNeil. Using Adhesives to Capture Microplastics from Water. *ACS ES&T Engineering*, 1 (12):1698–1704, 2021. ISSN 2690-0645. doi:10.1021/acsestengg.1c00272.

[16] Wei Huang, Ming Chen, Biao Song, Jiaqin Deng, Maocai Shen, Qiang Chen, Guangming Zeng, and Jie Liang. Microplastics in the coral reefs and their potential impacts on corals: A mini-review. *Science of the Total Environment*, 762: 143112, 2021. ISSN 18791026. doi:10.1016/j.scitotenv.2020.143112. URL https://doi.org/10.1016/j.scitotenv.2020.143112.

[17] Penghui Li, Xiaodan Wang, Min Su, Xiaoyan Zou, Linlin Duan, and Hongwu Zhang. Characteristics of Plastic Pollution in the Environment: A Review. *Bulletin of Environmental Contamination and Toxicology*, 107(4):577–584, 2021. ISSN 14320800. doi:10.1007/s00128-020-02820-1. URL https://doi.org/10.1007/s00128-020-02820-1.

[18] Julie M. Rieland, Zeyuan Hu, Julian S. Deese, and Brian J. Love. Pressure sensitive adhesives for quantifying microplastic isolation. *Separation and Purification Technology*, 307(November 2022):122819, 2023. ISSN 18733794. doi:10.1016/j.seppur.2022.122819. URL https://doi.org/10.1016/j.seppur.2022.122819.

[19] Ilona Leppänen, Timo Lappalainen, Tia Lohtander, Christopher Jonkergouw, Suvi Arola, and Tekla Tammelin. Capturing colloidal nano- and microplastics with plant-based nanocellulose networks. *Nature Communications*, 13(1):1–12, 2022. ISSN 20411723. doi:10.1038/s41467-022-29446-7.

[20] PlasticsEurope. Plastics – the Facts 2018: An analysis of European plastics production, demand and waste data. Technical report, 2018.

[21] Karen Duis and Anja Coors. Microplastics in the aquatic and terrestrial environment: sources (with a specific focus on personal care products), fate and effects. *Environmental Sciences Europe*, 28(1):1–25, 2016. ISSN 21904715. doi:10.1186/s12302-015-0069-y.

[22] MSFD Technical Subgroup on Marine Litter. Guidance on Monitoring Marine Litter. Technical report, 2013. URL http://europa.eu/.

[23] Behnam Pourdeyhimi. Surgical Mask Particle Filtration Efficiency (PFE): The Standard Needs to be Updated. *The Journal of Science and Medicine*, 2(3):1–11, 2020.

[24] Dafne Eerkes-Medrano, Richard C. Thompson, and David C. Aldridge. Microplastics in freshwater systems: A review of the emerging threats, identification of knowledge gaps and prioritisation of research needs. *Water Research*, 75:63–82, 2015. ISSN 18792448. doi:10.1016/j.watres.2015.02.012. URL http://dx.doi.org/10.1016/j.watres.2015.02.012.

[25] Yanina K. Müller, Theo Wernicke, Marco Pittroff, Cordula S. Witzig, Florian R. Storck, Josef Klinger, and Nicole Zumbülte. Microplastic analysis—are we measuring the same? Results on the first global comparative study for microplastic analysis in a water sample. *Analytical and Bioanalytical Chemistry*, 412(3):555–560, 2020. ISSN 16182650. doi:10.1007/s00216-019-02311-1.

[26] Atsuhiko Isobe, Kaori Uchiyama-Matsumoto, Keiichi Uchida, and Tadashi Tokai. Microplastics in the Southern Ocean. *Marine Pollution Bulletin*, 114(1):623–626, 2017. ISSN 18793363. doi:10.1016/j.marpolbul.2016.09.037. URL http://dx.doi.org/10.1016/j.marpolbul.2016.09.037.

[27] Defu He, Yongming Luo, Shibo Lu, Mengting Liu, Yang Song, and Lili Lei. Microplastics in soils: Analytical methods, pollution characteristics and ecological risks. *TrAC - Trends in Analytical Chemistry*, 109:163–172, 2018. ISSN 18793142. doi:10.1016/j.trac.2018.10.006. URL https://doi.org/10.1016/j.trac.2018.10.006.

[28] Silvia Morgana, Laura Ghigliotti, Noelia Estévez-Calvar, Roberto Stifanese, Alina Wieckzorek, Tom Doyle, Jørgen S. Christiansen, Marco Faimali, and Francesca Garaventa. Microplastics in the Arctic: A case study with sub-surface water and fish samples off Northeast Greenland. *Environmental Pollution*, 242:1078–1086, 2018. ISSN 18736424. doi:10.1016/j.envpol.2018.08.001.

[29] Fangni Du, Huiwen Cai, Qun Zhang, Qiqing Chen, and Huahong Shi. Microplastics in take-out food containers. *Journal of Hazardous Materials*, 399(February):122969, 2020. ISSN 18733336. doi:10.1016/j.jhazmat.2020.122969. URL https://doi.org/10.1016/j.jhazmat.2020.122969.

[30] Sebastian Primpke, Silke H. Christiansen, Win Cowger, Hannah De Frond, Ashok Deshpande, Marten Fischer, Erika B. Holland, Michaela Meyns, Bridget A. O'Donnell, Barbara E. Ossmann, Marco Pittroff, George Sarau, Barbara M. Scholz-Böttcher, and Kara J. Wiggin. *Critical Assessment of Analytical Methods for the Harmonized and Cost-Efficient Analysis of Microplastics*, volume 74. 2020. ISBN 0003702820921. doi:10.1177/0003702820921465.

[31] L. M. van Mourik, S. Crum, E. Martinez-Frances, B. van Bavel, H. A. Leslie, J. de Boer, and W. P. Cofino. Results of WEPAL-QUASIMEME/NORMANs first global interlaboratory study on microplastics reveal urgent need for harmonization. *Science of the Total Environment*, 772, 2021. ISSN 18791026. doi:10.1016/j.scitotenv.2021.145071.

[32] S. M. Mintenig, P. S. Bäuerlein, A. A. Koelmans, S. C. Dekker, and A. P. Van Wezel. Closing the gap between small and smaller: towards a framework to analyse nano- and microplastics in aqueous environmental samples. *Environmental Science: Nano*, 5(7):1640–1649, 2018. ISSN 20518161. doi:10.1039/c8en00186c.

[33] Plastic Pollution Measurement Science, 2023. URL https://www.nist.gov/programs-projects/plastic-pollution-measurement-science.

[34] Atsuhiko Isobe, Nina T. Buenaventura, Stephen Chastain, Suchana Chavanich, Andrés Cózar, Marie DeLorenzo, Pascal Hagmann, Hirofumi Hinata, Nikolai Kozlovskii, Amy L. Lusher, Elisa Martí, Yutaka Michida, Jingli Mu, Motomichi Ohno, Gael Potter, Peter S. Ross, Nao Sagawa, Won Joon Shim, Young Kyoung Song, Hideshige Takada, Tadashi Tokai, Takaaki Torii, Keiichi Uchida, Katerina Vassillenko, Voranop Viyakarn, and Weiwei Zhang. An interlaboratory comparison exercise for the determination of microplastics in standard sample bottles. *Marine Pollution Bulletin*, 146 (July):831–837, 2019. ISSN 18793363. doi:10.1016/j.marpolbul.2019.07.033. URL https://doi.org/10.1016/j.marpolbul.2019.07.033.

[35] Crislaine Bertoldi, Larissa Z. Lara, Adriano A. Gomes, and Andreia N. Fernandes. Microplastic abundance quantification via a computer-vision-based chemometrics-assisted approach. *Microchemical Journal*, 160:105690, 2021. ISSN 0026265X. doi:10.1016/j.microc.2020.105690. URL https://doi.org/10.1016/j.microc.2020.105690.

[36] Carmine Massarelli, Claudia Campanale, and Vito Felice Uricchio. A handy open-source application based on computer vision and machine learning algorithms to count and classify microplastics. *Water (Switzerland)*, 13(15), 2021. ISSN 20734441. doi:10.3390/w13152104.

[37] Fang Cheng, Yunlong Luo, and Ravi Naidu. Raman imaging combined with an improved PCA/algebra-based algorithm to capture microplastics and nanoplastics. *Analyst*, 147(19):4301–4311, 2022. ISSN 13645528. doi:10.1039/d2an00761d.

[38] Sabastian Simbarashe Mukonza and Jie-Lun Chiang. Satellite sensors as an emerging technique for monitoring macro- and microplastics in aquatic ecosystems. *Water Emerging Contaminants and Nanoplastics*, 1(4):17, 2022. doi:10.20517/wecn.2022.12.

[39] Jingxi Li, Fenglei Gao, Di Zhang, Wei Cao, and Chang Zhao. Zonal Distribution Characteristics of Microplastics in the Southern Indian Ocean and the Influence of Ocean Current. *Journal of Marine Science and Engineering*, 10(2), 2022. ISSN 20771312. doi:10.3390/jmse10020290.

[40] Costantino Creton. Pressure-Sensitive Adhesives An Introductory Course. *MRS Bulletin*, (June):434–439, 2003.

[41] Lihua Li, Matthew Tirrell, Gary A Korba, and Alphonsus V Pocius. Surface Energy and Adhesion Studies on Acrylic Pressure Sensitive Adhesives. *The Journal of Adhesion*, 76:307–334, 2001. doi:10.1080/00218460108030724.

[42] S Chu. Dynamic mechanical properties of pressure-sensitive adhesives. In L Lee, editor, *Dynamic mechanical properties of pressure-sensitive adhesives.*, chapter Adhesive B, pages 97–137. Plenum Press, New York, 1991.

[43] C.A Dahlquist. Creep. In D Satas, editor, *Creep. Handbook of pressure sensitive adhesive technology*, pages 121–138. Satas and Associates, Warwick, 3 edition, 1999.

[44] Kwong Yat Ho and Kalliopi Dodou. Rheological studies on pressure-sensitive silicone adhesives and drug-in-adhesive layers as a means to characterise adhesive performance. *International Journal of Pharmaceutics*, 333(1-2):24–33, 2007. ISSN 03785173. doi:10.1016/j.ijpharm.2006.09.043.

[45] Timothy M. E. Jugovic, Michael T. Robo, Woojung Ji, Madeline Clough, Anne McNeil, and Paul M. Zimmerman. Predicting Adhesive Behavior in Polyacrylates with Atomistic Simulation. *PCCP (Under Review)*, 2023.

[46] Identifying Polymers By Density, 2023. URL https://edu.rsc.org/experiments/identifying-polymers-by-density/385.article.

[47] Alba Maceira, Francesc Borrull, and Rosa Maria Marcé. Occurrence of plastic additives in outdoor air particulate matters from two industrial parks of Tarragona, Spain: Human inhalation intake risk assessment. *Journal of Hazardous Materials*, 373 (March):649–659, 2019. ISSN 18733336. doi:10.1016/j.jhazmat.2019.04.014. URL https://doi.org/10.1016/j.jhazmat.2019.04.014.

[48] Alistair Thorpe and Roy M. Harrison. Sources and properties of non-exhaust particulate matter from road traffic: A review. *Science of the Total Environment*, 400 (1-3):270–282, 2008. ISSN 00489697. doi:10.1016/j.scitotenv.2008.06.007. URL http://dx.doi.org/10.1016/j.scitotenv.2008.06.007.

[49] H. A. Nel and P. W. Froneman. A quantitative analysis of microplastic pollution along the south-eastern coastline of South Africa. *Marine Pollution Bulletin*, 101(1):274–279, 2015. ISSN 18793363. doi:10.1016/j.marpolbul.2015.09.043. URL http://dx.doi.org/10.1016/j.marpolbul.2015.09.043.

[50] Rebeca De La Fuente, Gábor Drótos, Emilio Hernández-García, Cristóbal López, and Erik Van Sebille. Sinking microplastics in the water column: Simulations in the Mediterranean Sea. *Ocean Science*, 17(2):431–453, 2021. ISSN 18120792. doi:10.5194/os-17-431-2021.

[51] Yulan Zhang, Shichang Kang, Steve Allen, Deonie Allen, Tanguang Gao, and Mika Sillanpää. Atmospheric microplastics: A review on current status and perspectives. *Earth-Science Reviews*, 203(December 2019):103118, 2020. ISSN 00128252. doi:10.1016/j.earscirev.2020.103118. URL https://doi.org/10.1016/j.earscirev.2020.103118.

[52] Hanping Chen, Zihao Liu, Xu Chen, Yingquan Chen, Zhiguo Dong, Xianhua Wang, and Haiping Yang. Comparative pyrolysis behaviors of stalk, wood and shell biomass: Correlation of cellulose crystallinity and reaction kinetics. *Bioresource Technology*, 310:123498, 2020.

[53] Keon Beigzadeh, Julie M Rieland, Catherine B Eastman, David J Duffy, and Brian J. Love. Characterization of Ingested Plastic Microparticles Extracted from Sea Turtle Post-Hatchlings at Necropsy. *Microplastics*, 1:254–262, 2022. doi:10.3390/ microplastics1020018.

[54] Weixiang Li, Xin Li, Jing Tong, Weiping Xiong, Ziqian Zhu, Xiang Gao, Shuai Li, Meiying Jia, Zhaohui Yang, and Jie Liang. Effects of environmental and anthropogenic factors on the distribution and abundance of microplastics in freshwater ecosystems. *Science of the Total Environment*, 856(August 2022):159030, 2023. ISSN 0048-9697. doi:10.1016/j.scitotenv.2022.159030. URL https://doi.org/10.1016/j.scitotenv.2022.159030.

[55] Yana Peykova, Olga V Lebedeva, Alexander Diethert, M Peter, and Norbert Willenbacher. Adhesive properties of acrylate copolymers : Effect of the nature of the substrate and copolymer functionality. *International Journal of Adhesion and Adhesives*, 34:107–116, 2012. doi:10.1016/j.ijadhadh.2011.12.001.

[56] Gabriela E. Fonseca, Timothy F.L. McKenna, and Marc A. Dubé. Effect of bimodality on the adhesive properties of pressure sensitive adhesives: Role of bimodal particle size and molecular weight distributions. *Industrial and Engineering Chemistry Research*, 49(16):7303–7312, 2010. ISSN 08885885. doi:10.1021/ie100204x.

[57] James E. Mark. Elastomeric Networks with Bimodal Chain-Length Distributions. *Accounts of Chemical Research*, 27(9):271–278, 1994. ISSN 15204898. doi:10.1021/ar00045a003.

[58] Qiongxuan Qiu, Zhi Tan, Jundong Wang, Jinping Peng, Meimin Li, and Zhiwei Zhan. Extraction, enumeration and identification methods for monitoring microplastics in the environment. *Estuarine, Coastal and Shelf Science*, 176:102–109, 2016. ISSN 02727714. doi:10.1016/j.ecss.2016.04.012. URL http://dx.doi.org/10.1016/j.ecss.2016.04.012.

[59] Lei Mai, L-J Bao, Lei Shi, C. S. Wong, and E. Y. Zeng. A review of methods for measuring microplastics in aquatic environments. *Environmental Science and Pollution Research*, 25(1):11319–11332, 2018. ISSN 18791026. URL https://doi.org/10.1016/j.scitotenv.2019.02.028%0Ahttps://doi.org/10.1016/j.scitotenv.2019.01.319%0Ahttp://dx.doi.org/10.1016/j.scitotenv.2018.12.313%0Ahttps://doi.org/10.1016/j.scitotenv.2018.12.047%0Ahttps://doi.org/10.1016/j.scitotenv.2018.12.273%0Ahtt.

CHAPTER 3

Ionic Liquid Processing of Untreated Coffee Fruit Residues

3.1 Introduction

The selection of biomass as a resource for dissolution-based processing has remained generally conservative, focusing primarily on forestry waste, plant stalks, and leafy components like corn stover and bagasse that have low innate moisture content and often compete as feedstocks for use in biofuel production and compost.[1,2] We propose to consider a wider range of industrial agriculture wastes that may have less intrinsic value and a larger waste footprint.[3,4,5] For example, leveraging the waste streams of industrial food production, such as coffee fruit waste, pineapple leaf and skin, and banana peel, could annually divert millions of tons of biomass[6,7] from landfill or agricultural runoff and reincorporate it into a circular economy. Most bench-scale ionic liquid (IL) solvation work to date has been done with highly purified cellulose from cotton discards,[8] microcrystalline cellulose,[9,10] and kraft pulp.[11,12] There is also a growing body of research on the dissolution of less pure biomass sources like untreated woody and herbaceous biomasses[13] as well as reclaimed materials.[14,15] As a biomass resource, coffee fruit has previously been investi-

gated for lignin extraction,[16] anthocyanin extraction,[17] direct extraction of short cellulosic fibers,[4] and bioethanol production.[18] Two previous publications have looked at coffee fruit for structural applications, using pretreatments and bleaching to break the fruit into its structural fibers.[4,19]

3.1.1 Impact of residual lignin and hemicellulose on ionic liquid processing of biomass

Residual non-cellulosic components of plant material have been observed to influence several steps in the process of IL-processed biomass. There is often a reduction in dissolution attributed to lignin binding to cellulose, which reduces the cellulose yield. Native cellulose also may have a higher molecular weight than desired for IL processing and is sometimes reduced simultaneously with the harsh pretreatments used to remove lignin and hemicellulose.[8] After the coagulation phase, inclusion of lignin and hemicellulose components has been associated with reduced cellulose crystallization and poorer mechanical properties.[20] However, in other instances, the presence of hemicellulose and lignin has been shown to improve the mechanical properties of coprecipitated cellulose fibers over those derived from pure cellulose.[21,22,23] We found the IL, 1,8-Diazabicyclo[5.4.0]undec-7-inium acetate ([DBUH][OAc]) to be non-specific towards the dissolution of lignin, cellulose, and hemicellulose, and therefore all three are conveyed in our dissolved coffee fruit.[24]

Lignin and hemicellulose have been shown to act as plasticizers to the dissolved cellulose, reducing the measured viscosity compared to equal concentrations of neat cellulose in ionic liquid.[25] Some reduction in solution viscosity is desirable for common fiber spinning processes like dry-jet wet spinning, especially for at-scale production. With pure cellulose solutions, the cellulose is often degraded to yield the target viscosity,[8] or supplementary molecular solvents, like dimethyl sulfoxide (DMSO), are added.[26] The challenge

with adding or retaining non-cellulose components is balancing viscosity and cohesion. To successfully extrude, stretch, electrospray, or dry-jet wet-spin IL-cellulose fibers, the cellulose solution must have a sufficiently low viscosity to flow, and a high enough cohesion to yield fibers instead of droplets.[26,27,28] In this work, parallel plate rheology was used to better understand the influence of retained lignocellulosic biomass residue, and to assess its capacity for direct fiber spinning given established observational benchmarks.[29] By investigating the solvation and reshaping of untreated coffee fruit (cascara), we seek to avoid the impacts of conventional biomass pretreatments such as the Kraft process, and other harsh chemical treatments which will be discussed in more detail in chapter 4.[30,31]

3.1.2 Utilization of untreated biomass residues in engineering applications

Untreated biomass is widely used in modern industrial society. Wood and natural fibers are among the earliest materials used by humans and remain important in modern architecture and textiles. Due to recent pressures on companies to reduce greenhouse gas emissions and make greener designs, there has been a resurgence in interest regarding natural and plant-derived materials.[32,33] There are numerous benefits associated with cellulosic materials, including low cost, high strength to weight ratio, and natural uniaxial reinforcement.[34] Biomass is also of interest for chemical feedstocks and biofuels.[35,36,37] Of particular interest are natural cellulosic fibers for composite reinforcement, such as for fiber reinforced polymer,[38] impregnated wood,[39] or all-cellulose composites.[27,39] The work presented in this chapter represents the first steps towards accessing the lignocellulosic content of coffee fruit for various structural applications.

3.2 Materials and Methods

3.2.1 Materials

1,8-Diazabicyclo[5.4.0]undec-7-ene, 99.5% glacial acetic acid, methanol, and dimethyl sulfoxide (DMSO) were acquired from Fisher Scientific and used as received. Cascara was acquired from De la Gente Coffee Cooperative (DGC) and coffee variety was not specified. Medical grade cotton balls were acquired from McMaster Carr as a source of nearly pure cellulose as a control.

3.2.2 Synthesis of ionic liquid [DBUH][OAc]

The IL 1,8-Diazabicyclo[5.4.0]undec-7-inium acetate [DBUH][OAc] was synthesized in a solvent free, 1-pot reaction at atmospheric conditions following the method in Parviainen et al.[40]. Briefly, under ice bath conditions and magnetic stirring, acetic acid was gradually added to 1,8-Diazabicyclo[5.4.0]undec-7-ene through a sheet of parafilm in a 1:1 mole ratio. On completion of the acid addition, the mixture was capped and left to stir until the solution viscosity rose to a point that hindered magnetic stirring, usually in about 3 hours. [DBUH][OAc] can freeze when acetic acid is added, which can prematurely inhibit mixing. When freezing occurred within the first hour of mixing, the reaction vial was removed from the ice bath and left to mix at room temperature. [DBUH][OAc] was subsequently characterized by nuclear magnetic resonance (NMR) spectroscopy and differential scanning calorimetry (DSC) (**Appendix A**).

3.2.3 Cascara preparation

Cascara, as acquired from DGC Coffee Coop, was initially fractionated in a coffee grinder before it was dried in an oven at 50° C overnight. Gravimetric determinations resolved that the equilibrium moisture level of cascara was $\sim$5% w/w. Cascara was pre-

pared at two size ranges for the dissolution efficiency and fiber drawing experiments respectively. For dissolution efficiency, cascara was coarsely ground and particles < 300 µm were excluded by sieving (McMaster Carr) to simplify particle removal after IL exposure. For fiber and film making, cascara particles were ground more finely to produce smaller particles (~ 100 µm) to aid in dissolution.

3.2.4 Biomass Solubility

The solubility of biomass in [DBUH][OAc] was assessed as a fraction of input biomass dissolved after 4h of heating at 80°C. 10 mL aliquots of [DBUH][OAc] were measured out into a 20 mL vial and heated to 80°C in an oil bath under magnetic stirring before adding dry, coarsely ground cascara (300–2000 µm). After 4 hours of heating, vials were removed from the oil bath, and 2 mL of DMSO was added as a cosolvent and shaken in to reduce the viscosity of the solution before pouring the solution over a 100 µm sieve (McMaster Carr) placed over a beaker. Additional DMSO was added in 2 mL increments, followed by washing with 3×2 mL of de-ionized (DI) water to wash the viscous IL from the undissolved material (UDM), with the dissolved fraction accumulating in the beaker under the sieve. After the initial rinse steps, UDM was retrieved from the sieve for subsequent washes, and the dissolved fraction was collected in the beaker and discarded. UDM was added to 30 mL of fresh DI water and sonicated for 30 min to ensure complete removal of IL and DMSO. The UDM was then vacuum filtered and dried overnight in the oven at 50°C before reweighing. Measurements were taken at 3, 5, 10, and 15% w/w loadings of dried cascara in quadruplicate. Solubility (S) was calculated using equation 3.1.

$$S = \left(1 - \frac{M_{undissolved}}{M_{initial}}\right) \times 100 \tag{3.1}$$

3.2.5 Biomass solutions

Cascara solutions were prepared by first drying finely ground cascara (100 µm) in an oven overnight at 50°C. Vials of [DBUH][OAc] were prepared by heating IL to 60°C to permit pipetting of 10 mL into 20 mL glass vials. Cascara was added to the vials at 3, 5, 10, and 15% w/w loadings in pure IL and heated for 4 hours at 80°C in an oil bath with magnetic stirring. After heating, vials were removed from the heat and cooled to ambient conditions before evaluation. Cotton solutions were also prepared as controls using medical grade cotton balls dissolved in [DBUH][OAc] at 3, 5, 10, and 15% w/w loadings with a similar heating profile. Biomass solutions were used to make fibers and films through coagulation in an anti-solvent. Initially, we used DI water as an anti-solvent until we acquired the ability to reprocess the solvents for recycling, at which point we transitioned to methanol. Methanol was found to be a better antisolvent, as it both improved biomass coagulation and evaporated more readily during rotary evaporation.

3.2.6 Cascara characterization

Cascara and cotton were analyzed following a National Renewable Energy Laboratory (NREL) two-stage acid hydrolysis protocol.[41] In brief, the biomass samples were screened using a 20-mesh screen and dried at 105 $\pm$ 2°C for 6 h. After that, 0.1 g of the oven-dried biomass was added to a 40 mL beaker in a water bath (30°C $\pm$ 3) and 1 mL of 72% sulfuric acid was added. During incubation, each sample was mixed every 10 minutes for 1 h. The acid concentration was then diluted by 28 mL DI water. Then, samples were autoclaved at 121°C for 1 h. Cellulose and hemicellulose were quantified post hydrolysis using high-performance liquid chromatography (HPLC) to measure glucan and xylan presence.

Lignin content was assessed using a Klason analysis. First, filter crucibles were washed, dried at 105°C for at least 4 hours, and cooled in a desiccator. The mixture from the beaker was filtered. In order to measure acid-soluble lignin, 2 mL of filtrate was col-

lected. To completely remove residual acid, the filtrated lignin was washed several times with DI water. The filter crucibles were dried in the oven at 105°C for a minimum 4 hours. The samples were then cooled and weighed to the nearest 0.1 mg. The percentage of acid-insoluble lignin (AIL) was then calculated using equation 3.2.

$$\%\text{AIL} = \frac{\text{mass of insoluble lignin (mg)}}{\text{mass of initial oven-dried lignin (mg)}} \times 100 \tag{3.2}$$

A UV-visible spectrophotometer (8453 UV-visible Spectrophotometer, Shimadzu) was used to determine acid-soluble lignin (ASL). The adsorption at 205 nm was used for calculations in Equation 3.3, where ϵ is the absorbtivity (L/g cm) at λ_{max} and the dilution (D) is expressed by Equation 3.4.

$$\%\text{ASL} = \frac{\text{UV absorption} \times 29.00\ \text{mL} \times D}{\epsilon \times \text{dry lignin (mg)} \times \text{path length}} \times 100 \tag{3.3}$$

$$D = \frac{\text{Volume (sample)} \times \text{Volume diluting solvent}}{\text{Volume (sample)}} \tag{3.4}$$

3.2.7 Rheology

Rheology was performed ($n > 4$) on cotton and cascara solutions in [DBUH][OAc] at 60°C on a TA Ares-M rheometer. Dynamic frequency sweeps were performed from 0.1–100 rad s^{-1} with a gap distance of 0.6 mm. Strain sweeps were performed first on each biomass solution to find the viscosity in the zero-shear regime and to select adequate strain values for frequency sweeps.

The viscosity data from the rheometer was fitted using both the Cross (Equation 3.5) and Carreau (Equation 3.6) models[42,43] to determine the zero-shear viscosity at 60° C. In this expression, $\dot{\gamma}$ is the shear rate, η_0 is the zero-shear viscosity, p is a time constant, and n is the power-law exponent. For cotton and cascara solutions of 5% and higher using the Matlab R2021a Curve Fitting Toolbox (**Appendix A**). Determination of the Newtonian

plateau was used for pure [DBUH][OAc] and 1% solutions of cotton and cascara. The Carreau model fits the data more consistently than the Cross model, so the Carreau values are presented for both cotton and cascara values.

$$\eta(\dot{\gamma}) = \frac{\eta_0}{(1 + p\dot{\gamma})^{(1-n)}} \tag{3.5}$$

$$\eta(\dot{\gamma}) = \eta_0(1 + (p\dot{\gamma})^2)^{\frac{(n-1)}{2}} \tag{3.6}$$

3.2.8 Fiber formation and drawing studies

Fibes

Fibers were prepared by hand extension and subsequent coagulation of the fiber/IL mixtures in an anti-solvent bath. A coagulation bath (6"$\times$9" Pyrex) was prepared with 500 mL of DI water as an anti-solvent for the IL at ambient temperature. Biomass solutions were heated to 70°C in an oven for 1 hour and processed while hot. Two stainless steel spatulas were used to extract a sample of the hot biomass solution that was stretched between the two spatulas to make threads that traversed the length of the coagulation bath. The fibrils were then lowered into the bath and anchored to the sides of the coagulation bath. Fibers were pulled in this way until the spinning solution cooled too much for the warm fibers to be stretched satisfactorily. At that point, the vial was reheated before pulling more fibers. Fibers were equilibrated in the coagulation bath for 30 minutes before transferring them to shaped aluminum foil to dry under tension. An instructional video is available online.[44]

Films

A coagulation bath with 500 mL of methanol was used as an anti-solvent. A solution of 10% w/w cascara solution was heated to 70°C for 1 hour. Using a stainless-steel spatula,

hot biomass solution was spread on a clean borosilicate microscope slide (25 mm x 75 mm) to deposit an even 1 mm-thick coating, then the slide was immersed in the coagulation bath and left for 1 hour. Before removal, films were checked for sufficient IL removal, marked by an even color across the whole film. When necessary, the bath was refreshed with clean methanol, and another 30 min of soaking was used. Finished films delaminated from the glass substrates, demonstrating anti-solvent penetration through the film thickness. Finished films were carefully retrieved from the bath and laid flat on parchment paper. A second layer of parchment paper was added on top, and the swelled films were sandwiched under a force of $\sim$ 1 N of evenly dispersed weight across the top to prevent the drying films from curling. The compressed films were left to dry between the sheets of parchment paper for at least 48 h. The coagulation bath solution including methanol, IL, and solubilized biomass, were retained for recycling using a rotary evaporator to distill off clean methanol for reuse. The biomass and IL residues from the evaporator were retained for future study.

3.2.9 X-ray diffraction and Fourier Transform Infrared analysis

The X-ray diffraction (XRD) patterns of biomass were obtained with a Rigaku Smartlab X-Ray Diffractometer using Cu $K\beta$ radiation at 40 kV and 44 mA. Scans were collected in the range of 2 *theta* $= 5 - 35^{\circ}$ at a scan rate of 2° min^{-1}. Fourier Transform Infrared (FTIR) spectrometry all samples was performed on a JASCO (FT/IR-4100) spectrometer operating in absorbance mode. We took 64 scans between 4000–600 cm^{-1} with a resolution of 4 cm^{-1}.

3.3 Limitations

There remain several unknowns regarding the complete composition of the coffee fruit. Notably, only the measured cellulose, hemicellulose, and lignin comprise only about 50%

of the cascara residue. I suspect that the mystery fraction consists largely of lipids, pectin, and non-structural sugars. The cascara has also yet to be characterized for molecular weight due to limited access to an appropriately equipped size exclusion chromatography (SEC) system. Finally, as we were attempting to make strain-strengthened fibers without access to an advanced spinning setup, we had to stretch the fibers by hand. As a result, they were somewhat thin and irregular, and possessed poor mechanical properties.

3.4 Results and Discussion

3.4.1 Biomass compositional assessments

Table 3.1: Compositional assessment of biomass

Sample	Cellulose (%)	Hemicellulose (%)	Acid Soluble Lignin (%)	Acid Insoluble Lignin (%)	Extracts[a] (%)
Untreated cascara	12.83 ± 0.01	7.10 ± 0.10	10.65 ± 0.40	21.9 ± 0.30	47.53 ± 0.80
Cascara film[b]	26.50	7.33	8.1	28.8	29.27
UDM	13.54 ± 0.10	5.60 ± 0.02	13.3 ± 0.01	20.05 ± 0.40	47.52 ± 0.52
Cotton	100 ± 3.92	-	2.61 ± 0.29	-	-

[a] Including lipids, proteins, non-structural sugars, and small molecule compounds.
[b] An individual sample was characterized for film, all others were performed in duplicate

We assessed whether there were any differences between the untreated cascara, precipitated films, and UDM. Initially, it was thought that the dissolved fraction was composed largely of cellulose, because the measured 65% dissolution rate corresponds well with Murthy and Naidu's measurement of 63% cellulose content in cascara.[45] However, measurement using the NREL protocols for cellulose, hemicellulose, acid-soluble lignin, and acid-insoluble lignin suggests that [DBUH][OAc] solvation is not selective for cellulose alone (**Table 3.1**). The cascara purchased from the De La Gente Cooperative in Guatemala contains substantially less cellulose by mass percent than measured by Murthy and Naidu[45] although they may have assessed a different coffee cultivar. When

normalized to consider exclusively the structural lignocellulosic biomass components, the untreated cascara is 24% cellulose and 62% total lignin compared to 38% and 52% respectively in the precipitated cascara films. The hemicellulose content remains relatively unchanged between the untreated cascara, precipitated film, and the undissolved material. Comparison of the UDM to the untreated coffee fruit shows limited difference beyond a slight increase in acid soluble lignin which appears to be minimally soluble in [DBUH][OAc]. The high cellulose content in the UDM suggests that further dissolution optimization could be achieved under different conditions. A large mass of extracts was also conveyed in the [DBUH][OAc], which along with the lignin and hemicellulose content interrupted cellulose crystallization on re-coagulation (**Figure 3.1**). In future work, we will assess the impacts of pretreatments that reduce how much lignin, lipids, proteins, and non-structural sugars are available when separations are performed using ionic liquids.

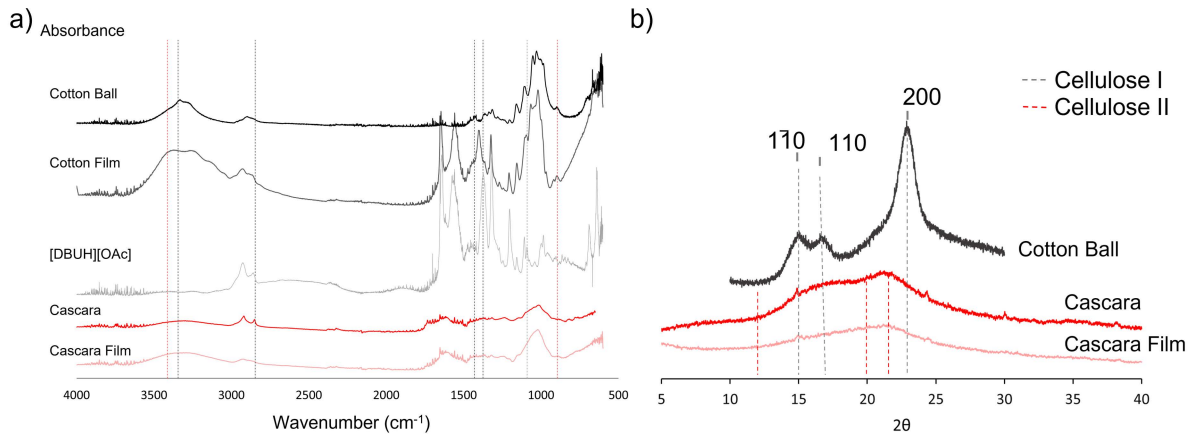

Figure 3.1: Analysis of native biomass and precipitated biomass films using a) FTIR and b) XRD. Dashed lines indicate expected peak positions of Cellulose I (black) and Cellulose II (red).

Comparisons were also performed using XRD and FTIR to assess the crystallinity of native biomass and precipitated films (**Figure 3.1**). Cotton extracted from cotton balls is highly pure cellulose I as demonstrated by characteristic XRD diffraction peaks at 15.1°, 16.6°, ad 22.8° corresponding to the [1-10], [110], and [200] diffraction lines of Cellulose

I.[46] The determination of cellulose crystals in cascara was more ambiguous. The native cascara FTIR scan confirms the characteristic bond absorptions in cellulose,[47,48] but there was extensive peak broadening in the XRD, and peaks were shifted from the usual cellulose I or II peaks.[46] The native cascara is more crystalline than the precipitated cascara film, which shows a larger amorphous halo in the XRD diffraction[47,49] and the absence of a shoulder at 1090 cm^{-1} (and 1111 cm^{-1} in Cellulose I) in the FTIR scan (**Figure 3.1a**) which is linked with both the cellulose I and cellulose II crystal structures.[48,50] A cotton film precipitated into antisolvent from [DBUH][OAc] was also assessed and identified as cellulose II based on FTIR peaks at 893 cm^{-1} and 3414 cm^{-1}, and the loss of peaks at 1375 cm^{-1}, 1430 cm^{-1}, and 3345 cm^{-1}.[51,52] The cotton film also retained some IL content, indicated by shared peaks between the cotton film and the spectra for [DBUH][OAc], which was not present in cascara films.

3.4.2 Biomass solubility assessments

Solubility testing of unprocessed cascara demonstrated partial solubility of cascara in [DBUH][OAc] at 3–15% w/w biomass loadings compared to the complete dissolution of cotton under the same conditions. After 4 hours of dissolution at 80° C, a consistent trend of 65 $\pm$ 1% of initial dry biomass was dissolved. We plot this trend in **Figure 3.2**, which shows a correlation between the amount of biomass added and how much biomass is ultimately dissolved. There is a strong linear relationship showing a consistent solubility of cascara in [DBUH][OAc], with some deviation starting at 15% cascara loading, which suggests the nearing of a saturation limit. A substantial mass of insoluble, undissolved material (UDM) remained even at low concentrations of cascara, suggesting strong intramolecular bonding within the lignocellulosic matrix[53] even after 4 hours of heating.

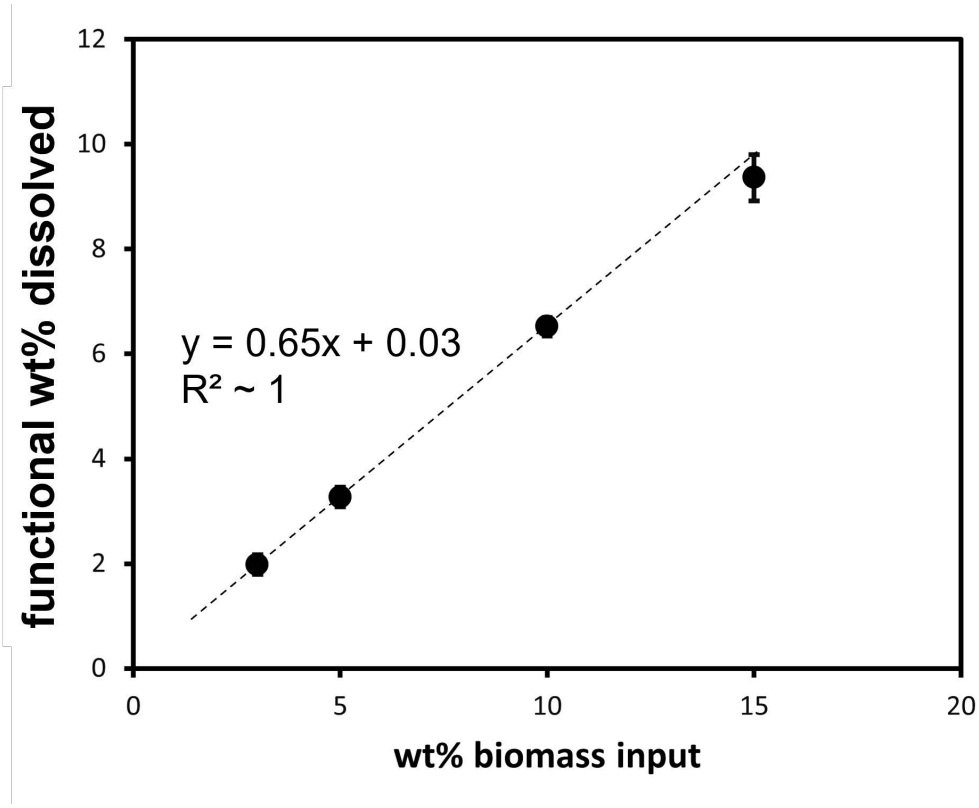

Figure 3.2: Solubility of dry cascara biomass in [DBUH][OAc] IL (% w/w) after 4h of heating at 80° C.

3.4.3 Rheological analysis

Rheological analysis was performed to assess how increased amounts of biomass loading affected the IL solution behavior, comparing cascara with a cotton control. Comparison of complex melt viscosity at elevated temperature for a range of biomass concentrations is presented in **Figure 3.3a,b**. Both cascara and the cotton/IL solutions experience a rise in viscosity with increasing biomass loading and show characteristic shear thinning at higher shear rates, as expected. The solutions were assumed to fit the Cox-Merz rule,[54,55] and zero shear values were calculated using both Newtonian plateau determination and the Carreau model fitting (**Table 3.2**).

Rheological analysis was performed to assess how increased amounts of biomass loading affected the IL solution behavior, comparing cascara with a cotton control. Com-

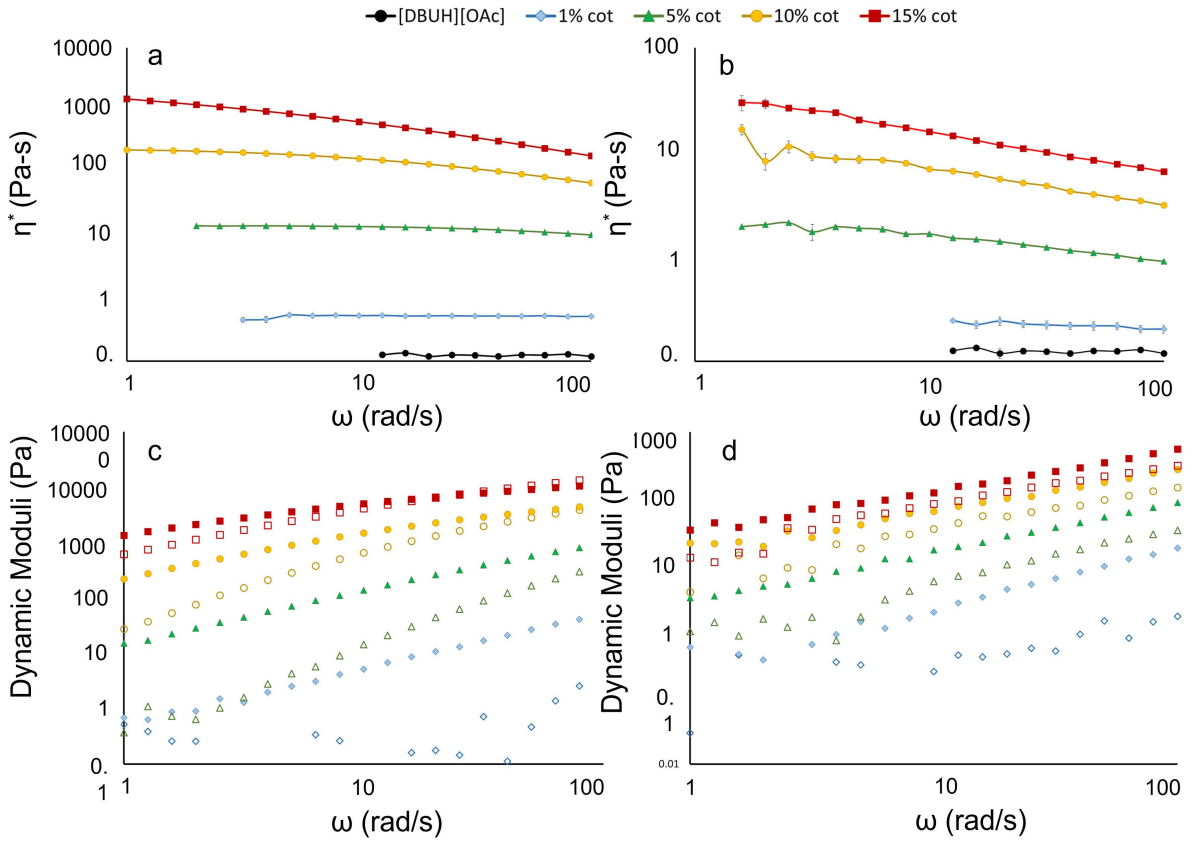

Figure 3.3: Concentration dependent rheology data, complex viscosities of cotton (a) and cascara (b), and storage (G') and loss moduli (G'') for cotton (c) and cascara (d) where closed symbols are G'' and open symbols are G'.

parison of complex melt viscosity at elevated temperature for a range of biomass concentrations is presented in **Figure 3.3a,b**. Both cascara and the cotton/IL solutions experience a rise in viscosity with increasing biomass loading and show characteristic shear thinning at higher shear rates, as expected. The solutions were assumed to fit the Cox-Merz rule,[54,55] and zero shear values were calculated using both Newtonian plateau determination and the Carreau model fitting (**Table 3.2**).

The cotton/IL solutions are much more viscous compared to equivalent concentrations of the cascara biomass evaluated under the same conditions. The lower viscosity of cascara solutions is likely a result of the presence of small molecule impurities like sugars and pigments that are naturally present in cascara, which also dissolve in the IL, as well

Table 3.2: Zero shear values (μ_0) and Carreau parameters for cotton and cascara at 60°C determined by Carreau model and Newtonian plateau calculations

Cotton							
Conc.	**η_0 (Pa.s)**	**STD**	**t**	**STD**	**n**	**STD**	**R^2**
0*	0.127	0.004	-	-	-	-	-
1*	0.529	0.007	-	-	-	-	-
5	14.4	0.05	0.045	0.00	0.79	0.00	0.999
10	232	1.8	0.21	0.01	0.63	0.01	0.997
15	1510	39	0.55	0.04	0.50	0.01	0.999
Cascara							
Conc.	**η_0 (Pa.s)**	**STD**	**t**	**STD**	**n**	**STD**	**R^2**
0*	0.127	0.004	-	-	-	-	-
1*	0.220	0.011	-	-	-	-	-
5	2.29	0.15	0.43	0.15	0.76	0.01	0.999
10	9.97	0.30	0.22	0.02	0.62	0.01	0.999
15	43.0	6.3	1.27	0.43	0.60	0.001	0.997

*Determined from Newtonian plateau

as the presence of small UDM particulate matter. De Silva and Byrne[56] observed a similar gap in Newtonian plateau magnitude between cotton with degree of polymerization (DP) 2680 and 495 dissolved in [AMIM][Cl]. The trend in zero shear viscosity of the cascara solutions also tracked similarly with zero shear curves of 265 DP microcrystalline cellulose in [DBUH][Prop][54] and poplar woody biomass in [Emim][OAc][57] (**Figure 3.4**).

The storage (G'') and loss (G') moduli of the cotton and cascara were also measured at 60° C (**Figure 3.3c,d**). As seen in **Figure 3.3c,d**, G'' is greater than G' in the measured range for all observed concentrations of cascara, although G' converges towards G'' with increasing cascara concentration. The cotton solutions demonstrate similar behavior, with solutions below 10% having a more fluid-like behavior up to 100 rad s^{-1}. At 10% cotton loading, the crossover point (COP) is approached, and at 15% the COP occurs at 6900 $\pm$ 60 Pa and 20 $\pm$ 1 rad s^{-1}. We interpret the COP as being due to molecular entanglements and the cohesiveness of polymer solutions which influence fiber drawing[59]. Lower temperatures would induce the COP at lower angular frequency in both the higher concentration cotton and cascara solutions. Sixta and coworkers[8] identified a narrow window of COPs that promoted high draw ratios during fiber spinning with ranges between 0.6–1.2 s-1 and around 3.7–5.8 kPa. Although high draw ratios, defined as the ratio of the rate

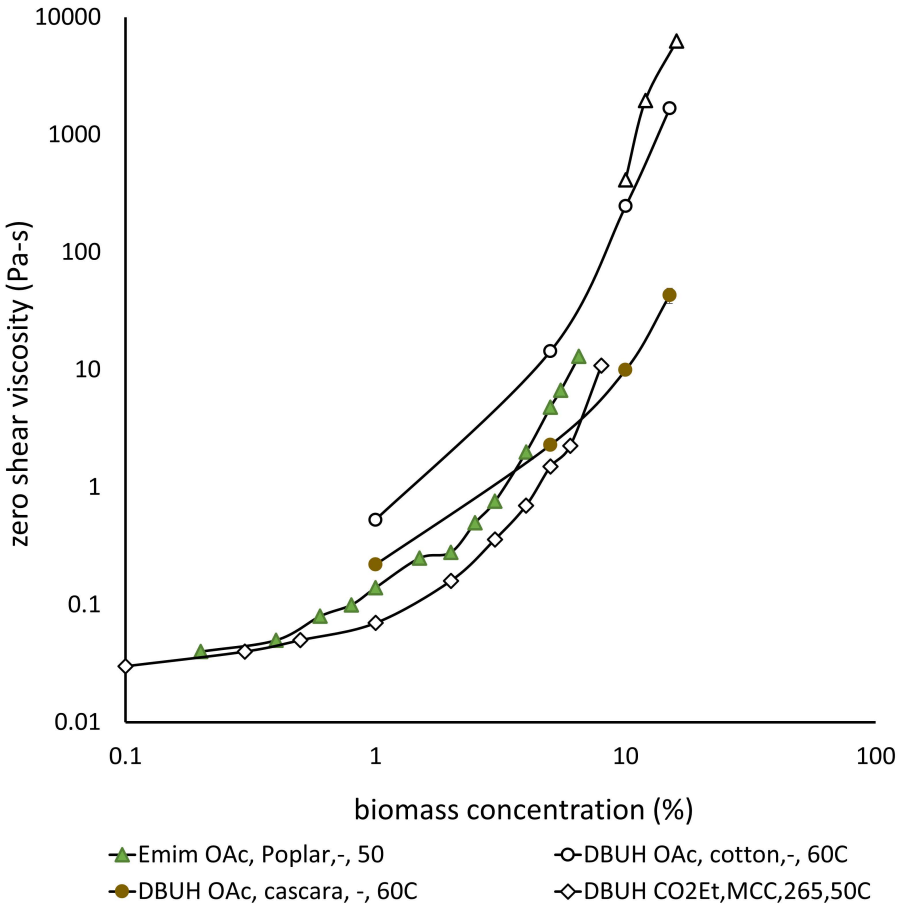

Figure 3.4: Comparison of concentration dependent η_0 values for a range of biomasses, ionic liquids, and temperatures including our data on cascara and cotton. Data IDs are presented as IL, biomass, molecular weight, temperature.[54,57,58]

of fiber extension to extrusion in industrial fiber spinning have been correlated with better fiber properties,[8,60] low draw ratios can still generate fibers when solutions are sufficiently cohesive.[61]

3.4.4 Coagulated product formation

Fibers

Fibers were pulled by hand in the biomass/IL gel state and coagulated in a room temperature water bath. Fiber dimensions were controlled by the amount of biomass solution

used and the degree to which it was drawn. Using the present method, fibers as long as 5 cm could consistently be produced. The ability to draw cohesive fibers was strongly impacted by the concentration of biomass in solution. Viable, precipitated fibers were drawn from cotton/IL solutions at 70°C with loadings as low as 3% w/w whereas cascara solutions required loadings of 8% and higher to yield cohesive fibers. The biomass loading and the quality of the biomass influence both the viscosity and the cohesiveness of the solution.[29] At 5% cascara in IL solutions, adding biomass solution to the coagulation bath resulted in nearly complete cohesive failure of fibers as IL was removed likely due to insufficient cellulose-cellulose bonds resulting from elevated levels of lignin and extractives presence. We also postulate that the cellulose in cascara is of lower molecular weight than that of the cotton, which would also add to the lower cohesive strength of dilute cascara solutions. A minimum number of polymer chain-chain interactions is required for the biomass solution to condense into a solid when the IL is washed away, with longer cellulose chains requiring fewer strands to achieve that threshold.[54]

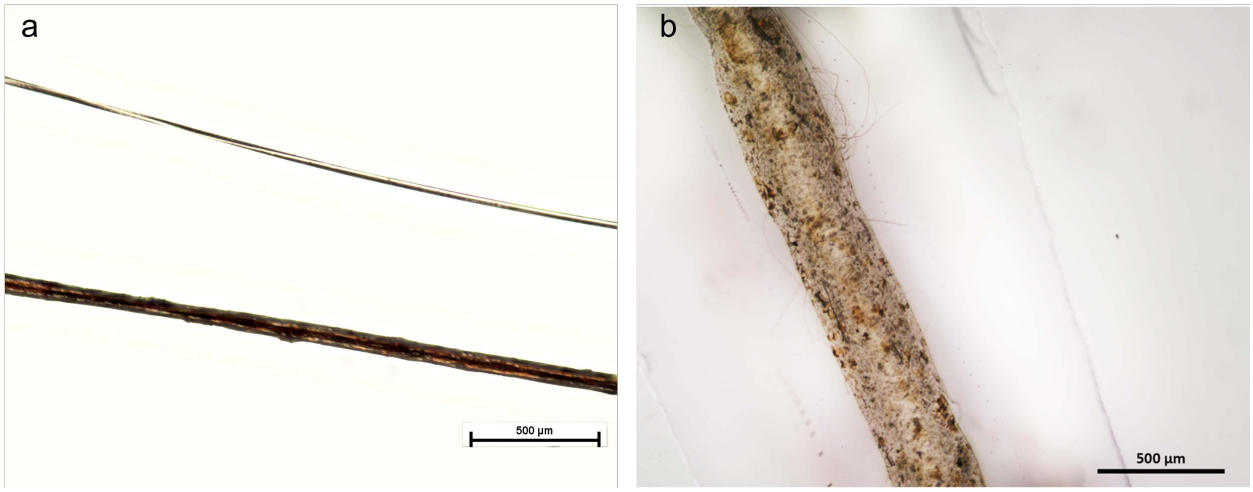

Figure 3.5: Optical image depicting hand drawn fibers. A) cotton derived fiber (top) and a cascara fiber (bottom) both from 10% w/w solutions. B) a cascara fiber swelled with water. Speckles are indicative of undissolved material.

As the hand drawing technique was being optimized, fibers of varying thickness were made from both cotton/IL and cascara/IL solutions, which were then measured using

optical microscopy (**Figure 3.5**). Fibers ranging in diameter from several hundred microns down to below 30 µm could be produced. The finest fibers had diameters of 26 $\pm$ 4 µm and 18 $\pm$ 1 µm respectively for cotton and cascara. Fiber diameters varied between 5 and 15% over their length. It is likely that thinner and more consistent fibers could be produced through automation,[11] as the current manual process is limited by technician skill. The ability to manually produce fibers on the diameter scale of commercially relevant fibers[62] suggests promise for the valorization of cascara biomass despite the high concentration of non-cellulose compounds.

Cascara derived fibers had a brown pigmentation due to the high lignin concentration and retention of natural pigments. Small fractions of undissolved material (UDM) were also retained in the cascara derived fibers and films (**Figure 3.5b,3.6b**). Fibril and film mechanical behavior were not assessed here, and offers area for future work, along with purifying cascara residues.

Films

Films were also made from 10% cascara/IL solution by coagulation of the cellulose rich regions in the antisolvent methanol. The low vapor pressure of methanol allowed for easier solvent recovery through rotary evaporation and subsequent recycling in film coagulation baths. Films of varying sizes were made by applying uniform layers of cascara/IL solution to glass substrates for subsequent coagulation in an antisolvent bath. Small films were made using borosilicate microscope slides, and larger films were made by applying solution to the external surface of 250 mL glass beakers. **Figure 3.6a** shows examples of films produced on microscope slides. Unlike with biomass fibers, coagulated films were dried on a flat surface under compression. Films left to dry uncompressed warped due to uneven lateral shrinkage. The films were assessed with an optical microscope and SEM. Analysis of the topography of the films with SEM showed that the surface structure of the films (**Figure 3.6c** is very similar to the surface of the dehydrated coffee fruit

(**Figure 3.6d**).

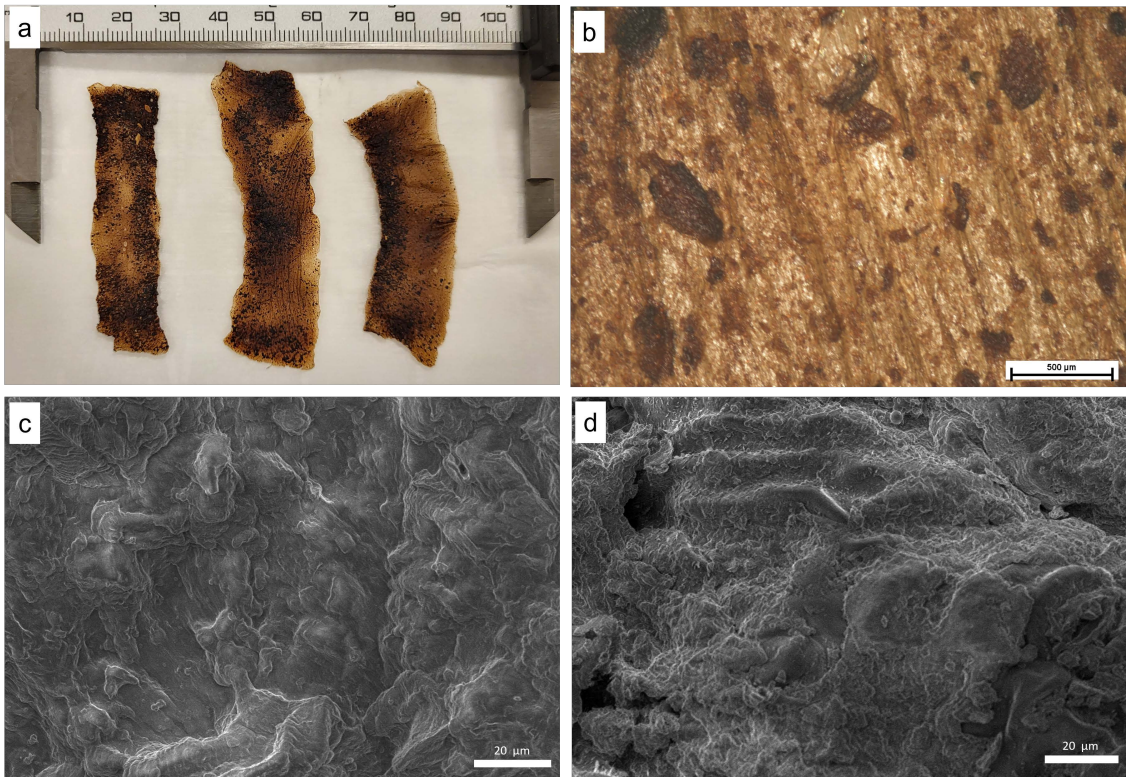

Figure 3.6: Images of films produced from 10% cascara solutions. A) full sized films, b) optical microscope image of a film showing embedded particulates, c) SEM image of a film, d) SEM image of an unprocessed cascara fruit

We continue to optimize film making conditions to make more robust samples to quantify the strength and stiffness of precipitated cascara and cotton. We are also devising ways to manipulate the solvation capacity of the IL for better separations of lignin and cellulose fractions to yield purer starting material. The current efforts demonstrate the viability of cascara as a value-added feedstock for man-made fibers as well as a possible source of lignin. Future work will look at pretreatments to isolate the cellulosic fraction of cascara as well as the recovery of the ionic liquid fraction from the coagulation bath. Although these preliminary fibers derived from hand-drawn cascara are inferior to native cotton, there might be many other uses for these derivative forms as-is beyond structural applications.

3.5 Conclusion

Native coffee fruit (cascara) and cotton were dissolved in [DBUH][OAc] ionic liquid at elevated temperatures and probed as sources of lignocellulosic feedstocks for producing fibers and films. Material balances¬ of the IL solutions and the precipitates produced by exposure to both methanol and DI water antisolvents were characterized and analyzed for cellulose crystallinity and lignin (acid soluble and insoluble). Coffee fruit was found to be 65% soluble in [DBUH][OAc] at 80° C. The coffee was less soluble than the cotton, which was completely soluble through 15% w/w. Comparing the measured zero shear viscosity trends with those in the literature shows that the cascara solutions perform similarly to low molecular weight microcrystalline cellulose and poplar woody biomasses.

Procedures were developed in which the soluble fraction could be spread or stretched and deposited into a coagulation bath, allowing for the precipitation of films and fibers as fine as 30 µm in diameter. Fibers were produced from both coffee fruit and cotton although they are both inferior to native cotton. The capacity to produce fibers and films from IL solutions offers a promising proof of concept, but there is a lot of work that is still needed to pretreat the biomass to isolate sugars and other non-structural elements before exposing the biomass to ionic liquids for biopolymer isolation. And finally, rheological analysis of the cascara solutions suggests that the unpurified solutions are not optimized for higher throughput fiber spinning. Further work will assess whether dilute ionic liquid and acid chlorite pretreatments aid in purifying cascara biomass to improve solvation and solution qualities. Altogether, preliminary assessment of coffee fruit as a value-added feedstock for cellulose and lignin seems promising. Efforts to develop schemes to fractionate cellulose and lignin rich residues in a more contained system open the possibility to leverage complex biomasses like cascara.

3.6 References

[1] S J Gerssen-gondelach, D Saygin, B Wicke, M K Patel, and A P C Faaij. Competing uses of biomass : Assessment and comparison of the performance of bio-based heat , power , fuels and materials. *Renewable and Sustainable Energy Reviews*, 40(April):964–998, 2014. ISSN 1364-0321. doi:10.1016/j.rser.2014.07.197. URL http://dx.doi.org/10.1016/j.rser.2014.07.197.

[2] Humberto Blanco-canqui and R. Lal. Corn Stover Removal for Expanded Uses Reduces Soil Fertility and Structural Stability. *SSSAJ*, 73(2), 2009. doi:10.2136/sssaj2008.0141.

[3] Diego B Menezes, Fernando M Diz, Luiz F Romanholo, R V Baudrit Luiz, P Costa Maria, Yendry Corrales Jose, Costa Rica, and San Jose. Starch-based biocomposite membrane reinforced by orange bagasse cellulose nanofibers extracted from ionic liquid treatment. *Cellulose*, 28:4137–4149, 2021. doi:10.1007/s10570-021-03814-w.

[4] Mounir El Achaby, Mariana Uesgas-Ramon, Nour-E Houda Fayoud, Maria Cruz Figueroa-Espinoza, Vera Trabadelo, Khalid Draoui, and Hicham Ben Youcef. Bio-sourced porous cellulose microfibrils from coffee pulp for wastewater treatment. *Cellulose*, 26:3873–3889, 2019. doi:10.1007/s10570-019-02344-w.

[5] Siti Nikmatin, Irmansyah Irmansyah, Bambang Hermawan, Teddy Kardiansyah, Frederikus Tunjung Seta, Irma Nur Afiah, and Rofiqul Umam. Oil Palm Empty Fruit Bunches as Raw Material of Dissolving Pulp for Viscose Rayon Fiber in Making Textile Products. *polymers*, 14, 2022.

[6] Lucie A. Pfaltzgraff, Mario De Bruyn, Emma C. Cooper, Vitaly Budarin, and James H. Clark. Food waste biomass: A resource for high-value chemicals. *Green Chemistry*, 15(2):307–314, 2013. ISSN 14639270. doi:10.1039/c2gc36978h.

[7] Zahid Anwar, Muhammad Gulfraz, and Muhammad Irshad. Agro-industrial lignocellulosic biomass a key to unlock the future bio-energy: A brief review. *Journal of Radiation Research and Applied Sciences*, 7(2):163–173, 2014. ISSN 1687-8507. doi:10.1016/j.jrras.2014.02.003. URL http://dx.doi.org/10.1016/j.jrras.2014.02.003.

[8] Shirin Asaadi, Michael Hummel, Sanna Hellsten, Tiina Härkäsalmi, Yibo Ma, Anne Michud, and Herbert Sixta. Renewable High-Performance Fibers from the Chemical Recycling of Cotton Waste Utilizing an Ionic Liquid. *ChemSusChem*, 9(22):3250–3258, 2016. ISSN 1864564X. doi:10.1002/cssc.201600680.

[9] Hao Zhang, Jin Wu, Jun Zhang, and Jiasong He. 1-allyl-3-methylimidazolium chloride room temperature ionic liquid: A new and powerful nonderivatizing solvent for cellulose. *Macromolecules*, 38(20):8272–8277, 2005. ISSN 00249297. doi:10.1021/ma0505676.

[10] Farouk Ibrahim, Muhammad Moniruzzaman, Suzana Yusup, and Yoshimitsu Uemura. Dissolution of cellulose with ionic liquid in pressurized cell. *Journal of Molecular Liquids*, 211:370–372, 2015. ISSN 01677322. doi:10.1016/j.molliq.2015.07.041. URL http://dx.doi.org/10.1016/j.molliq.2015.07.041.

[11] Anne Michud, Marjaana Tanttu, Shirin Asaadi, Yibo Ma, Eveliina Netti, Pirjo Kääriainen, Anders Persson, Anders Berntsson, Michael Hummel, and Herbert Sixta. Ioncell-F: ionic liquid-based cellulosic textile fibers as an alternative to viscose and Lyocell. *Textile Research Journal*, 86(5):543–552, 2016. ISSN 00405175. doi:10.1177/0040517515591774.

[12] Pobitra Halder, Sazal Kundu, Savankumar Patel, Adi Setiawan, Rob Atkin, Rajarathinam Parthasarthy, Jorge Paz-Ferreiro, Aravind Surapaneni, and Kalpit Shah. Progress on the pre-treatment of lignocellulosic biomass employing ionic liquids. *Renewable and Sustainable Energy Reviews*, 105(September 2018):268–292, 2019. ISSN 18790690. doi:10.1016/j.rser.2019.01.052. URL https://doi.org/10.1016/j.rser.2019.01.052.

[13] Yanhua Chen, Na Teng, Haizhen Chen, Jing Chen, Fei Liu, Haining Na, and Jin Zhu. Evaluation of Electrospinnability of Celluloses Derived from Different Biomass Resources. *Fibers and Polymers*, 19(5):1128–1134, 2018. ISSN 12299197. doi:10.1007/s12221-018-8016-3.

[14] Y. Ma, M. Hummel, M. Määttänen, A. Särkilahti, A. Harlin, and H. Sixta. Upcycling of waste paper and cardboard to textiles. *Green Chemistry*, 18(3):858–866, 2016. ISSN 14639270. doi:10.1039/c5gc01679g.

[15] Cynthia Adu, Chenchen Zhu, Mark Jolly, Robert M Richardson, and Stephen J Eichhorn. Continuous and sustainable cellulose filaments from ionic liquid dissolved paper sludge nano fi bres. *Journal of Cleaner Production*, 280:124503, 2021. ISSN 0959-6526. doi:10.1016/j.jclepro.2020.124503. URL https://doi.org/10.1016/j.jclepro.2020.124503.

[16] Leta Deressa Tolesa, Bhupender S. Gupta, and Ming Jer Lee. Treatment of Coffee Husk with Ammonium-Based Ionic Liquids: Lignin Extraction, Degradation, and Characterization. *ACS Omega*, 3(9):10866–10876, 2018. ISSN 24701343. doi:10.1021/acsomega.8b01447.

[17] Emille R B A Prata and S. Leandro Oliveira. Fresh coffee husks as potential sources of anthocyanins. *LWT*, 40:1555–1560, 2007. doi:10.1016/j.lwt.2006.10.003.

[18] Verónica Alejandra Bonilla-hermosa, Whasley Ferreira Duarte, and Rosane Freitas Schwan. Utilization of coffee by-products obtained from semi-washed process for production of value-added compounds. *Bioresource Technology*, 166:142–150, 2014. doi:10.1016/j.biortech.2014.05.031.

[19] Sofía Collazo-Bigliardi, Rodrigo Ortega-Toro, and Amparo Chiralt Boix. Isolation and characterisation of microcrystalline cellulose and cellulose nanocrystals from coffee

husk and comparative study with rice husk. *Carbohydrate Polymers*, 191(October 2017):205–215, 2018. ISSN 01448617. doi:10.1016/j.carbpol.2018.03.022. URL https://doi.org/10.1016/j.carbpol.2018.03.022.

[20] Ning Sun, Weiying Li, Breena Stoner, Xinyu Jiang, Xingmei Lu, and Robin D Rogers. Composite fibers spun directly from solutions of raw lignocellulosic biomass dissolved in ionic liquids †. *Green Chemistry*, 13:1158–1161, 2011. doi:10.1039/c1gc15033b.

[21] Tiina Nypelö, Shirin Asaadi, Günther Kneidinger, Herbert Sixta, and Johannes Konnerth. Conversion of wood-biopolymers into macrofibers with tunable surface energy via dry-jet wet-spinning. *Cellulose*, 25(9):5297–5307, 2018. ISSN 1572882X. doi:10.1007/s10570-018-1902-4.

[22] Gabriele Schild and Eva Liftinger. Xylan enriched viscose fibers. *Cellulose*, 21: 3031–3039, 2014. doi:10.1007/s10570-014-0302-7.

[23] Saurabh Singh and Z.V.P. Murthy. Study of cellulosic fibres morphological features and their modifications using hemicelluloses. *Cellulose*, 24(8):3119–3130, 2017. ISSN 1572-882X. doi:10.1007/s10570-017-1353-3.

[24] Julie M. Rieland, Saeid Nikafshar, Zeyuan Hu, Mojgan Nejad, and Brian J. Love. Ionic liquid-mediated biopolymer extraction from coffee fruit. 2023.

[25] Yibo Ma, Shirin Asaadi, Leena Sisko Johansson, Patrik Ahvenainen, Mehedi Reza, Marina Alekhina, Lauri Rautkari, Anne Michud, Lauri Hauru, Michael Hummel, and Herbert Sixta. High-Strength Composite Fibers from Cellulose-Lignin Blends Regenerated from Ionic Liquid Solution. *ChemSusChem*, 8(23):4030–4039, 2015. ISSN 1864564X. doi:10.1002/cssc.201501094.

[26] Julie M. Rieland and Brian J. Love. Ionic liquids: A milestone on the pathway to greener recycling of cellulose from biomass. *Resources, Conservation and Recycling*, 155(September 2019):104678, 2020. ISSN 18790658. doi:10.1016/j.resconrec.2019.104678. URL https://doi.org/10.1016/j.resconrec.2019.104678.

[27] Johanna M. Spörl, Fabio Batti, Marc Phillip Vocht, Raphael Raab, Alexandra Müller, Frank Hermanutz, and Michael R. Buchmeiser. Ionic Liquid Approach Toward Manufacture and Full Recycling of All-Cellulose Composites. *Macromolecular Materials and Engineering*, 303(1):1–8, 2018. ISSN 14392054. doi:10.1002/mame.201700335.

[28] Xin Zhang, Yimin Mao, Madhusudan Tyagi, Feng Jiang, Doug Henderson, Bo Jiang, Zhiwei Lin, Ronald L. Jones, Liangbing Hu, Robert M. Briber, and Howard Wang. Molecular partitioning in ternary solutions of cellulose. *Carbohydrate Polymers*, 220 (February):157–162, 2019. ISSN 01448617. doi:10.1016/j.carbpol.2019.05.054. URL https://doi.org/10.1016/j.carbpol.2019.05.054.

[29] Shirin Asaadi. *Dry-Jet Wet Spinning of Technical and Textile Filament Fibers from a Solution of Wood Pulp and Waste Cotton in an Ionic Liquid*. PhD thesis, Aalto University, 2019. URL https://aaltodoc.aalto.fi/handle/123456789/40199.

[30] Rickard Arvidsson, Duong Nguyen, and Magdalena Svanström. Life cycle assessment of cellulose nanofibrils production by mechanical treatment and two different pretreatment processes. *Environmental Science and Technology*, 49(11):6881–6890, 2015. ISSN 15205851. doi:10.1021/acs.est.5b00888.

[31] Aashish Prasad, Maria Sotenko, Thomas Blenkinsopp, and Stuart R. Coles. Life cycle assessment of lignocellulosic biomass pretreatment methods in biofuel production. *International Journal of Life Cycle Assessment*, 21(1):44–50, 2016. ISSN 16147502. doi:10.1007/s11367-015-0985-5. URL http://dx.doi.org/10.1007/s11367-015-0985-5.

[32] Finding Sustainability In Surprising Places, 2020. URL https://corporate.ford.com/articles/sustainability/agave.html.

[33] Global natural fiber composites market forecast expected to reach $6.9 billion by 2028 at a CAGR of 7.7%, 2023. URL https://finance.yahoo.com/news/global-natural-fiber-composites-market-155300236.html?guccounter=1&guce_referrer=aHR0cHM6Ly93d3cuZWNvc2lhLm9yZy8&guce_referrer_sig=AQAAAAZ1l_F7SYttaAh_us7-0hpakrzQbOkvXfGMFspOJIywEeJcxA7fULV017wTOLe38ukF-TefSbSsTh18NwnonDAP0.

[34] Aliakbar Gholampour and Togay Ozbakkaloglu. *A review of natural fiber composites: properties, modification and processing techniques, characterization, applications*, volume 55. Springer US, 2020. ISBN 1085301903990. doi:10.1007/s10853-019-03990-y. URL https://doi.org/10.1007/s10853-019-03990-y.

[35] Nur Aainaa Syahirah Ramli and Nor Aishah Saidina Amin. Catalytic hydrolysis of cellulose and oil palm biomass in ionic liquid to reducing sugar for levulinic acid production. *Fuel Processing Technology*, 128:490–498, 2014. ISSN 03783820. doi:10.1016/j.fuproc.2014.08.011. URL http://dx.doi.org/10.1016/j.fuproc.2014.08.011.

[36] Álvaro Silva Lima, Bruno Sales de Oliveira, Selesa Vanessa Shabudin, Mafalda Almeida, Mara Guadalupe Freire, and Katharina Bica. Purification of anthocyanins from grape pomace by centrifugal partition chromatography. *Journal of Molecular Liquids*, 326:115324, 2021. ISSN 01677322. doi:10.1016/j.molliq.2021.115324. URL https://doi.org/10.1016/j.molliq.2021.115324.

[37] Brittany J. Allison, Juan Canales Cádiz, Nardrapee Karuna, Tina Jeoh, and Christopher W. Simmons. The Effect of Ionic Liquid Pretreatment on the Bioconversion of Tomato Processing Waste to Fermentable Sugars and Biogas. *Applied Biochemistry and Biotechnology*, 179(7):1227–1247, 2016. ISSN 15590291. doi:10.1007/s12010-016-2061-4. URL http://dx.doi.org/10.1007/s12010-016-2061-4.

[38] Chuanwei Miao and Wadood Y. Hamad. Cellulose reinforced polymer composites and nanocomposites: A critical review. *Cellulose*, 20(5):2221–2262, 2013. ISSN 09690239. doi:10.1007/s10570-013-0007-3.

[39] Mitsuhiro Shibata, Naozumi Teramoto, Taro Nakamura, and Yoshinobu Saitoh. All-cellulose and all-wood composites by partial dissolution of cotton fabric and wood in ionic liquid. *Carbohydrate Polymers*, 98(2):1532–1539, 2013. ISSN 01448617. doi:10.1016/j.carbpol.2013.07.062. URL http://dx.doi.org/10.1016/j.carbpol.2013.07.062.

[40] Arno Parviainen, Alistair W.T. King, Ilpo Mutikainen, Michael Hummel, Christoph Selg, Lauri K.J. Hauru, Herbert Sixta, and Ilkka Kilpeläinen. Predicting cellulose solvating capabilities of acid-base conjugate ionic liquids. *ChemSusChem*, 6(11): 2161–2169, 2013. ISSN 18645631. doi:10.1002/cssc.201300143.

[41] A Sluiter, B Hames, R Ruiz, C Scarlata, J Sluiter, D Templeton, and D Crocker Nrel. Determination of Structural Carbohydrates and Lignin in Biomass. Technical Report July, National Renewable Energy Laboratory, 2011.

[42] P. J. Carreau, D. C. R. De Kee, and R. P. Chabra. Principles and Applications. In *Rheology of Polymeric Systems*. Hanser, New York, 1997.

[43] R J Sammons, J R Collier, T G Rials, and S Petrovan. Rheology of 1-Butyl-3-Methylimidazolium Chloride Cellulose Solutions . I . Shear Rheology. *Journal of Applied Polymer Science*, 110:1175–1181, 2008. doi:10.1002/app.

[44] Julie Rieland, Zeyuan Hu, and B J Love. Making hand pulled fibers from ionic liquid–biomass, 2022. URL https://www.youtube.com/watch?v=Aqtdy8E4q0Y.

[45] Pushpa S Murthy and M Madhava Naidu. Resources , Conservation and Recycling Sustainable management of coffee industry by-products and value addition — A review. *"Resources, Conservation and Recycling"*, 66:45–58, 2012. ISSN 0921-3449. doi:10.1016/j.resconrec.2012.06.005. URL http://dx.doi.org/10.1016/j.resconrec.2012.06.005.

[46] Jie Gong, Jun Li, Jun Xu, Zhouyang Xiang, and Lihuan Mo. Research on cellulose nanocrystals produced from cellulose sources with various polymorphs. *RSC Advances*, 7:33486–33493, 2017. doi:10.1039/C7RA06222B. URL http://dx.doi.org/10.1039/C7RA06222B.

[47] Mary L Nelson and Robert T O'Connor. Relation of Certain Infrared Bands to Cellulose Crystallinity and Crystal Lattice Type . Part II . A New Infrared Ratio for Estimation of Crystallinity in Celluloses I and II *. *Journal of Applied Polymer Science*, 8: 1325–1341, 1964.

[48] Mary L Nelson and Robert T O'Connor. Relation of Certain Infrared Bands to Cellulose Crystallinity and Crystal Lattice Type . Part I . Spectra of Lattice Types I , 11 , I11 and of Amorphous Cellulose *. *Journal of Applied Polymer Science*, 8:1311–1324, 1964.

[49] Simon Bates, George Zografi, David Engers, Kenneth Morris, Kieran Crowley, and Ann Newman. Analysis of Amorphous and Nanocrystalline Solids from Their X-Ray Diffraction Patterns. *Pharmaceutical Research*, 23(10), 2006. doi:10.1007/s11095-006-9086-2.

[50] Elizabeth Dinand, Michel Vignon, Henri Chanzy, and Laurent Heux. Mercerization of primary wall cellulose and its implication for the conversion of cellulose I $\rightarrow$ cellulose II. *Cellulose*, 9:7–18, 2002.

[51] Dietrich Fengel, Hannes Jakob, and Claudia Strobel. Influence of the Alkali Concentration on the Formation of Cellulose II Study by X-Ray Diffraction and FTIR Spectroscopy. *Holzforschung*, 49(6):505–511, 1995.

[52] F Carrillo, X Colom, J J Sunol, and J Saurina. Structural FTIR analysis and thermal characterisation of lyocell and viscose-type fibres. *European Polymer Journal*, 40: 2229–2234, 2004. doi:10.1016/j.eurpolymj.2004.05.003.

[53] Chang Geun Yoo, Xianzhi Meng, Yunqiao Pu, and Arthur J Ragauskas. The critical role of lignin in lignocellulosic biomass conversion and recent pretreatment strategies : A comprehensive review. *Bioresource Technology*, 301(November 2019):122784, 2020. ISSN 0960-8524. doi:10.1016/j.biortech.2020.122784. URL https://doi.org/10.1016/j.biortech.2020.122784.

[54] Lucile Druel, Philipp Niemeyer, Barbara Milow, and Tatiana Budtova. Rheology of cellulose-[DBNH][CO2Et] solutions and shaping into aerogel beads. *Green Chemistry*, 20(17):3993–4002, 2018. ISSN 14639270. doi:10.1039/c8gc01189c.

[55] Anne Michud, Michael Hummel, and Herbert Sixta. Influence of molar mass distribution on the final properties of fibers regenerated from cellulose dissolved in ionic liquid by dry-jet wet spinning. *Polymer*, 75:1–9, 2015. ISSN 00323861. doi:10.1016/j.polymer.2015.08.017.

[56] Rasike De Silva and Nolene Byrne. Utilization of cotton waste for regenerated cellulose fibres: Influence of degree of polymerization on mechanical properties. *Carbohydrate Polymers*, 174:89–94, 2017. ISSN 01448617. doi:10.1016/j.carbpol.2017.06.042. URL http://dx.doi.org/10.1016/j.carbpol.2017.06.042.

[57] Ngoc A. Nguyen, Keonhee Kim, Christopher C. Bowland, Jong K. Keum, Logan T. Kearney, Nicolas André, Nicole Labbé, and Amit K. Naskar. A fundamental understanding of whole biomass dissolution in ionic liquid for regeneration of fiber by solution-spinning. *Green Chemistry*, 21(16):4354–4367, 2019. ISSN 1463-9262. doi:10.1039/c9gc00774a.

[58] Frank Hermanutz, Frank Gähr, Eric Uerdingen, Frank Meister, and Birgit Kosan. New developments in dissolving and processing of cellulose in ionic liquids. *Macromolecular Symposia*, 262(1):23–27, 2008. ISSN 10221360. doi:10.1002/masy.200850203.

[59] Lauri K.J. Hauru, Michael Hummel, Kaarlo Nieminen, Anne Michud, and Herbert Sixta. Cellulose regeneration and spinnability from ionic liquids. *Soft Matter*, 12(5): 1487–1495, 2016. ISSN 17446848. doi:10.1039/c5sm02618k.

[60] Aakash Sharma, Shailesh Nagarkar, Shirish Thakre, and Guruswamy Kumaraswamy. Structure–property relations in regenerated cellulose fibers: comparison of fibers manufactured using viscose and lyocell processes. *Cellulose*, 26 (6):3655–3669, 2019. ISSN 1572882X. doi:10.1007/s10570-019-02352-w. URL https://doi.org/10.1007/s10570-019-02352-w.

[61] Kenny Kong, Michael A Wilding, N Ibbett, and Stephen J Eichhorn. Molecular and crystal deformation of cellulose : uniform strain or uniform stress ? *Faraday Discussions*, 139:283–298, 2008. doi:10.1039/b715488g.

[62] R Sinclair. Understanding textile fibres and their properties:what is a textile fibre? In *Textiles and Fashion*, pages 1–27. Elsevier Ltd, 2015. ISBN 9781845699314. doi:10.1016/B978-1-84569-931-4.00001-5. URL http://dx.doi.org/10.1016/B978-1-84569-931-4.00001-5.

CHAPTER 4

Influence of Pretreatments on the Ionic Liquid Processing of Coffee Fruit Residues

4.1 Introduction

4.1.1 Biomass pretreatments and impacts

Biomass pretreatments are performed for a variety of reasons, including cellulose isolation, delignification, and cosmetic bleaching. While cellulose isolation is particularly desirable for digesting biomass to biofuel,[1] in other applications, such as paper-making, there is more compositional tolerance for hemicellulose content, and only lignin is specifically targeted for extraction.[2] Physical, chemical, and enzymatic pretreatments have been used although chemical methods are the most common in industrial use. Physical pretreatments such as milling and steam explosion require less hazardous inputs but tend to have high energy requirements making them prohibitively expensive at scale.[3] In contrast, the chemical treatment methods often require harsh conditions (i.e., acidic, basic, or

oxidative) that are both dangerous for workers and have negative environmental consequences.[4] Due to the recalcitrance of native lignocellulosic biomass, concentrated acids (e.g. H_2SO_4, glacial Acetic acid etc.), bases (e.g. sodium hydroxide (NaOH), calcium hydroxide (CaOH), potassium hydroxide (KOH), etc.), and bleaching agents (e.g. chlorite, hypochlorite, peroxide etc.) are often required to hydrolyze the bonds binding lignin and hemicellulose to cellulose.[5] Chemical pretreatments can be tailored for specific extraction, with acid-based treatments primarily targeting hemicellulose hydrolysis and alkali- and oxidative methods aimed at the removal of lignin and hemicellulose.[6]

In the last decade, greener pretreatment options have been investigated including IL, organosolv, and various physico-chemical treatments like supercritical fluids and microwave treatments.[6] These treatments present various tradeoffs between greenhouse gas emissions, energy consumption, treatment effectiveness, cost, and scalability.[7,8] Other work has looked into the tolerance of systems to lignin and hemicellulose content that have historically required isolated cellulose.[9,10,11] Given the non-selectivity of some ILs, we hoped to understand how a combination of pretreatments might influence the ability to extract more refined products from complex biomasses via IL processing.

4.1.2 Utilization of the whole biomass

Current trends in industry towards circular economy practices and the identification of lucrative by-product value streams is contributing to a densification of extraction. With the advent of new applications and more economically feasible extraction technologies, material streams which have previously been discarded as waste are now being reconsidered.[12,13,14] This is particularly relevant in agribusiness, where disposal of biomass can be costly and environmentally damaging.[15,16] For example, earlier research has assessed coffee discards (i.e. both spent grounds and fruit) for a variety of value-added uses including extraction of anthocyanins and caffeine, fermentation, mushroom substrate, and animal feed.[17] Coffee fruit (cacara) poses a unique challenge to direct utilization due to

its elevated concentrations of caffeine and tannins, which are toxic to many lifeforms and considered anti-nutrients.[17,18] Therefore, an in-line process that initially extracts caffeine and tannins for use in food and stock chemicals, extracts usable lignin, then finally yields a cellulose-rich material for further uses would maximize material utilization and minimize total waste.[19] Moreover, process and technology development for biomass fractionation and extraction would be easily transferable between similar crops.

4.1.3 Behavior of cellulosic materials precipitated from ionic liquids

Ionic liquids (ILs) dissolve lignocellulosic material by interrupting the strong hydrogen bonded matrix that cellulose forms. Various ILs non-innocently bond to the cellulose backbone,[20,21] hydrolyze the glycosidic bonds of the cellulose backbone,[21,22] and swell the biomass permitting partial solubility of the hemicellulose-lignin complex.[23,24] When cellulose is dissolved, its native crystal structure is lost, and it takes on the behavior of a characteristic polymer solution.[9,6] Native plant cellulose exists in a monoclinic crystal structure called Cellulose I,[25] which has excellent material properties and is the desired structure for applied cellulose materials.[26,27,28] However, Cellulose I is kinetically unfavorable and undergoes a rearrangement when cellulose is reprecipitated. Reprecipitated cellulose generally has a higher amorphous fraction, and any crystallites take on the Cellulose II unit cell, which is also monoclinic, but more thermodynamically stable.[25]

Common outputs of cellulose-IL research include cellulose-rich pulps,[29] extruded fibers,[30] semi-dissolved biomass composites,[31] and spun fiber.[32,33] The form of output is heavily influenced by cost constraints, for example, bench-scale fiber spinning set-ups are prohibitively expensive requiring a syringe pump and godet spinner. An intermediary to full dry-jet wet-spinning is the direct extrusion of thick fibers from a syringe pump system into a coagulation bath. These 2 forms are the most commonly characterized for tensile properties, although there is a substantial difference between the yielded fibers. The vast majority of mechanical testing has been performed on samples derived from purified cellu-

lose, although there is increasing interest in the impacts of lignin and hemicellulose.[9,10,11] While there are many structural applications for cellulose-derived products, there are also numerous uses for less robust materials such as fillers and insulation, that can benefit from the unique properties of biomass such as the hydrophobicity of lignin,[34] low cost, and renewability.

4.2 Materials and Methods

4.2.1 Materials

1,8-Diazabicyclo [5.4.0] undec-7-ene, 99.5% glacial acetic acid, methanol, ethanol, sodium chlorite, sulfuric acid, and dimethyl sulfoxide (DMSO) were acquired from Fisher Scientific and used as received. Cascara was acquired from De la Gente Coffee Cooperative (DGC) and coffee variety was not specified.

4.2.2 Ethanol pretreatment

Cascara as received from DGC, without size reduction, was dried in an oven at 50°C overnight. Dried cascara (100g) was then introduced to 60°C ethanol (500 mL, 95% purity) and heated at 60°C for 6 hr in an oven.[35] After heating, cascara was drained over a sieve, rinsed with more ethanol, and dried overnight in a 50°C oven.

4.2.3 Dilute ionic liquid pretreatment

The IL [DBUH][OAc] was prepared as outlined in 3.2.2. IL was dispensed into a 500 mL glass jar, and the mass of IL was determined. DI water was weighed to add 10 wt% using a tared syringe. Oven-dried, whole, ethanol treated cascara was dispensed to 10 wt% with respect to the total fluid mass (10 wt% DI water in [DBUH][OAc]). The IL-water solution was preheated to 80°C in an oil bath under magnetic stirring before introducing

the dried cascara. The mixture was allowed to cook for 4 hr before removing from heat and straining over a 500 mL sieve. The cascara was rinsed with DMSO 3 times (5 mL) then 3 rinses with DI water before returning the rinsed jar with fresh DI water. The dilute IL-treated (DILT) cascara in DI water was sonicated in a bath sonicater for 1 hr, then the water was decanted, and fresh water added for another round of sonication (1 hr). After sonication, the DILT cascara was strained and left overnight to dry at ambient conditions.

4.2.4 Acid chlorite pretreatment

Acid chlorite bleaching of cascara was conducted following the methods used by Hallac & Sannigrahi and Zhang et al..[36,37] First, 10g of oven dried, ethanol treated (ET) cascara was measured out into 375 mL of DI water. The water/cascara mixture was transferred to an oven to heat water to 75°C and allow cascara to become saturated with water $\sim$ 1 hr. The mixture was then transferred to a 75°C oil bath under magnetic stirring and 2.5 mL of acetic acid and 3g of $NaClO_2$ were added. The mixture was mixed for 2 hrs before adding a second addition of acetic acid (2.5 mL) and $NaClO_2$ (3g) and was allowed to heat for 2 more hours (4 hrs total). By hour 2, the dark brown cascara is bleached to a blotchy pale yellow color, and all solids should be pale by the end of the 4 hours. Strong mixing is required as the fruit is prone to floating and fruit not in contact with the bleaching solution will not be effectively treated. The mixture was then removed from heat and allowed to cool before opening. All steps involving $NaClO_2$ were conducted in a well-functioning fume hood.

Hazard warning: $NaClO_2$ is a strong oxidizer with acute oral toxicity (cat. 3), acute dermal toxicity (cat. 2), causes severe skin burns and eye damage, and may have negative health effects associated with prolonged/repeat exposure.[38] It is moderately stable and not hygroscopic although interaction with strong acids can form ClO_2 gas which is incredibly hazardous.[39] Under bleaching conditions using $NaClO_2$ and dilute acids in the presence of organic matter, the generation of ClO_2 is minimized.[40] Usage of $NaClO_2$

should be conducted with proper protection gear and adequate ventilation.

4.2.5 Cascara characterization

Biomass was analyzed as outlined in section 3.2.6. Briefly, a National Renewable Energy Laboratory (NREL) two-stage acid hydrolysis protocol[41] was followed. The biomass samples were screened and dried. Then 0.1 g of the oven-dried biomass was incubated in sulfuric acid before dilution with water and autoclaving. Cellulose and hemicellulose were quantified post hydrolysis using high-performance liquid chromatography (HPLC) to measure glucan and xylan presence. Next, lignin content was assessed using a Klason analysis. Acid-soluble lignin was determined using UV-visible spectrometry, and acid-insoluble lignin was determined gravimetrically.

4.2.6 Solubility assessment

Treated biomass was coarsely ground (300-2000 µm) in a coffee grinder before dissolution in 10 mL of [DBUH][OAc] at 100°C for 4 hours. Cascara samples were assessed in triplicate for rates of dissolution at 1, 5, and 10% w/w. After heating, 2mL of DMSO was added as a co-solvent to reduce the viscosity of the solvated fraction and assist in washing away the solvated cellulose. Undissolved material was strained over a 100 µm sieve (McMaster Carr) placed over a beaker, and additional DMSO washes were used to wash away IL. Subsequently undissolved material was sonicated in excess water until [DBUH][OAc] and DMSO were removed. Finally, the undissolved material was strained and left overnight to dry. The material was oven dried before mass measurement. Solubility (S) was calculated using **equation 4.1**.

$$S = \left(1 - \frac{M_{undissolved}}{M_{initial}}\right) \times 100 \tag{4.1}$$

4.2.7 Preparation of ionic liquid solutions

First treated cascara was dried in an oven at 80°C for 2hr before grinding fine in a coffee grinder ($\sim$ 100 µm). Molten [DBUH][OAc] was dispensed into a tared glass jar and 10% w/w finely ground, treated cascara was added to the IL. Samples were heated at 100°C for 48 hr under magnetic stirring. After removal from heat, samples were stored at ambient conditions until used for rheological assessment and fiber making.

4.2.8 Rheological assessment

Rheology was performed on 10% w/w loaded treated cascara solutions (n > 3) at elevated temperatures (55°C, 60°C, 70°C, and 80°C) on a TA Ares-M rheometer. Dynamic frequency sweeps were performed from 0.1–100 rad/sec with a gap distance of 0.6 mm. Strain sweeps were performed first on each biomass solution to find the viscosity in the zero-shear regime and to select adequate strain values for frequency sweeps.

Viscosity data was fitted to determine the zero-shear viscosities using both the Cross and Carreau models[42,43] as outlined in section 3.2.7. It was assumed that cascara-[DBUH][OAc] solutions fit the Cox-Merz rule.[43,44] The Cox-Merz rule determines if zero-shear viscosities can be calculated from complex viscosity as determined from shear-controlled rheological data as opposed to steady shear viscosity obtained from strain-controlled rheological data.[45] The Cross and Carreau models were fit using curve fitting packages in Matlab R2021a. The Carreau model fit the data more consistently than the Cross model, so the Carreau values are used in subsequent calculations.

4.2.9 Arrhenius calculations

Arrhenius calculations ($\eta \sim A\exp(E_\alpha/RT)$) were performed using zero-shear values (η_0) calculated using the Carreau Model to determine the activation energy (E_α) of shear

flow.[46] Activation energies for the three pretreatments was calculated for 10% w/w solutions using the following expression:

$$L_n(\eta_0) = E_\alpha / RT + \ln(A), \tag{4.2}$$

where A is the pre-exponential factor, T is temperature in Kelvins, and R is the ideal gas law (R = 8.31 J $K^{-1}mol^{-1}$). E_α was determined by linear fitting of the zero-shear data against $1/T$ where the slope is equal to E_α/R.

4.2.10 Extruded fibers

Extruded fibers for making composites were prepared by adding 10 wt% dimethyl sulfoxide (DMSO) to 48-hour dissolution samples of 10 wt% treate cascara in [DBUH][OAc] (prepared as described in chapter 3). DMSO addition volume was determined by calculating the added mass of DMSO and dividing by the density of DMSO (1.1004 g mL^{-1}). Samples were heated to 80°C and a vortex mixer was used to thoroughly mix the DMSO into the viscous IL/Biomass solution. While hot, the ternary solution was poured into a 10 mL syringe, and the syringe plunger was used to extrude the viscous mixture into a bath of room temperature methanol. Extruded fibers were left to soak in the methanol bath for 1 hr before removal to a sheet of aluminum foil to dry overnight. The next day, the fibers were returned to fresh methanol for 2 hrs to remove residual IL and DMSO. Dried fibers were stored under ambient conditions until used for tensile testing and x-ray diffractometry (XRD). The solvent baths were subsequently collected for methanol recovery using a rotary evaporator.

4.3 Limitations

The research presented in this chapter have a number of limitations. First, the treated cascara samples have yet to be thoroughly characterized resulting in a large unknown fraction ($\sim$ 50%) in the current presentation. Some fraction of this unknown portion is expected to be pectins and ash, which will be explored more thoroughly before final submission of this work as a journal article. The cellulose fraction of the cascara has also not yet been calculated for molecular weight.

4.4 Results and Discussion

4.4.1 Assessment of pretreated biomasses

Table 4.1: Characterization of treated and untreated cascara

Sample	Cellulose (%)	Hemicellulose (%)	Acid Soluble Lignin (%)	Acid Insoluble Lignin (%)	Other[a] (%)
Untreated cascara[b]	12.83 ± 0.01	7.10 ± 0.10	10.65 ± 0.40	21.90 ± 0.30	47.53 ± 0.80
Ethanol Treated	11.25 ± 0.49	7.35 ± 0.35	10.14 ± 0.30	20.43 ± 0.73	50.83 ± 1.33
IL Treated	13.35 ± 0.64	5.20 ± 0.71	9.78 ± 0.02	20.27 ± 0.49	51.40 ± 0.31
Acid Chlorite Treated	21.65 ± 0.35	9.75 ± 0.21	9.35 ± 0.81	6.83 ± 0.64	52.43 ± 0.52

[a]Here, other includes pectic substances, and ash that were not accounted for
[b]Reference - **Chapter 3**

Pretreatments of the cascara were assessed to understand their impacts on biomass composition and their subsequent impact on extruded fibers. The 3 treatments included ET (60°C, 6hr), DILT using [DBUH][OAc] (10% DI water, 80°C, 4hr), and an acid chlorite bleaching treatment (ACT). The ET was also used as a precursor to the other 2 pretreatments. The ET extracted pigment and waxy compounds that retard the dissolution and subsequent coagulation of cascara isolates in our previous work with untreated cascara. The ET and the DILT extractions are identified as greener and less dangerous pretreatments to be assessed against the more conventional ACT, which is known to generate

ClO_2 gas as a byproduct.[40] All 3 treatments showed measurable extraction, with recovery yields of 95%, 41%, 24% for ET, DILT, and ACT respectively.

The 3 treated cascara samples were chemically assessed to compare the impacts of the respective treatments. As with the untreated samples assessed in chapter 3, the cascara samples treated with ET, DILT, and ACT were not subjected to other pretreatments or extractions (i.e. water[47]) prior to chemical analysis. The lack of water extraction may account for the elevated volume of non-structural material labeled extracts in **Table 4.1**, however the continued measurement of high levels of unidentified content even after chemical treatment is considered strange. Both the DILT and ACT demonstrated measurable increases in relative cellulose content and reductions elsewhere in the lignin and hemicellulose fractions. The DILT yielded a mild increase in cellulose (4%) and moderate reductions in hemicellulose (27%) and acid-soluble lignin (1%). The ACT yielded a 69% increase in cellulose as a result of the comparable 69% decrease in acid-insoluble lignin and 12% reduction in acid-soluble lignin (12%).

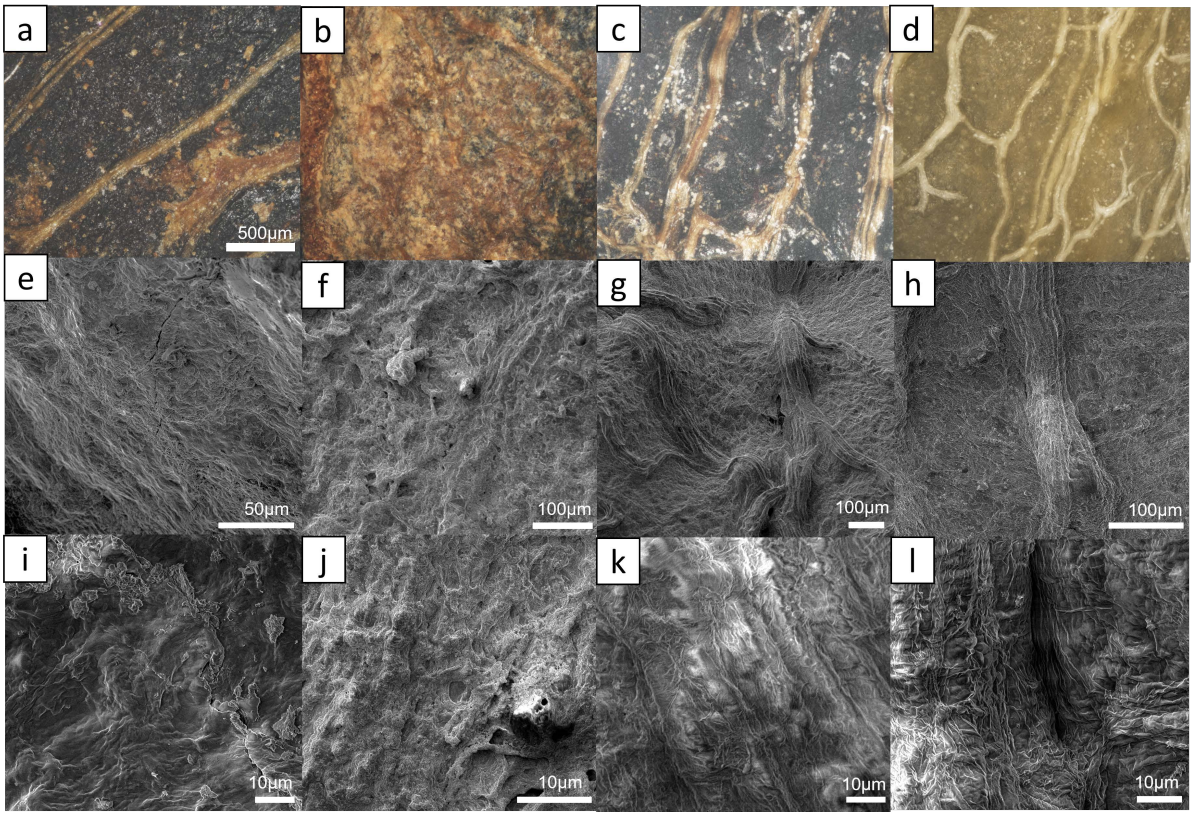

Figure 4.1: Optical and SEM images of the inner wall of cascara fruits before and after treatments. In order, the images show untreated cascara (a,e,i), ethanol treated cascara (b,f,j), dilute IL treated cascara (c,g,k), and acid chlorite treated cascara (d,h,l). Images a, b, c, and d are optical microscope images and have the same scaling. Images e-l are SEM micrographs of the cascara.

To better understand the resulting structures of the treated cascara, optical and SEM microscopy were performed (**Figure 4.1**). Preliminary observation of the inner wall of an untreated cascara shows that the fruit has structural fibers running longitudinally through the fruit (**4.1a**). The untreated fruit also has a smoother surface under high magnification, with numerous small particulates (**4.1i**). After ET there appears to be minimal visible change. However, after both the DILT and ACT, the structural fibers of the fruits become more visible to the optical microscope and are observed to be closer together than in the untreated cascara (**4.1c,d**), suggesting that fibers from deeper in the fruit have become exposed after the treatments. SEM micrographs of the structural fibers in the DILT and ACT cascara show early signs of fibrillation (**4.1g,h**), with more defined striation of the fibers in the DILT cascara, which may be linked to its higher solubility rate in [DBUH][OAc] (**Figure 4.2**).

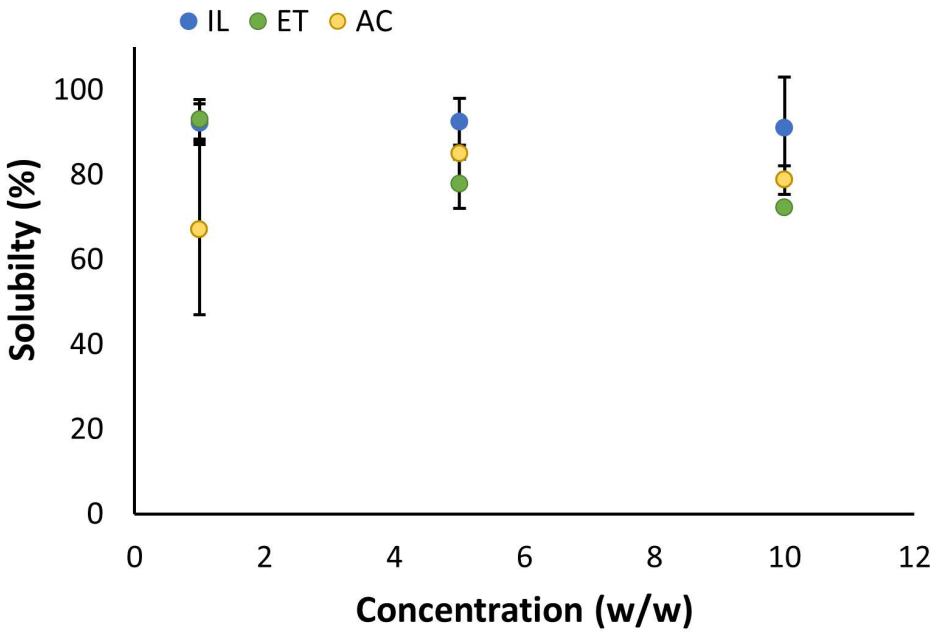

Figure 4.2: Solubility of treated cascara samples in the ionic liquid, Diazabicyclo[5.4.0]undec-7-inium acetate ([DBUH][OAc]) heated for 4 hr at 100°C.

The solubility of treated cascara increased substantially for all pretreatments compared to untreated cascara, and the solubility rate was fairly consistent across the different con-

centrations of biomass loading (**Figure 4.2**). All the treated cascara samples averaged a solubility greater than 75%, with ET 81% soluble, DILT 92%, and ACT 77% soluble in [DBUH][OAc] compared to the 65% solubility of untreated cascara.

4.4.2 Rheological assessment

Rheology measures the melt-flow properties of complex fluids which determine the behavior of materials during melt processing. In the literature, cellulose-IL systems are shown to have behavior characteristic to polymer melts and solutions, demonstrating temperature and concentration dependent viscosity, and shear thinning behavior.[43,48] Previously we investigated the rheological behavior of untreated cascara solvated in [DBUH][OAc] (in chapter 3). The untreated cascara demonstrated concentration dependent viscosity and shear thinning, however the viscosity was severely reduced compared to equal loadings of pure cotton in [DBUH][OAc] suggesting that the elevated levels of lignin, hemicellulose, extracts, and pectic substances plasticized the system, and interrupted the short-range cellulose interactions. Reduction in select components of the cascara composition through the different pretreatments (**Table 4.2**) resulted in substantial increases in viscosity.

Cellulose-IL solutions are often defined by their zero shear viscosities (η_0), which is the projected viscosity of the solution at rest or extrapolated to very low shear rates.[49] The zero shear values for the treated samples were determined using both the Cross and Carreau models (**Table 4.2**) (Chapter 3). As with the untreated cascara, the Carreau model was found to give more consistent values for the zero shear values and was therefore used for the subsequent Arrhenius calculations (**Figure 4.4**) although, the Cross values are in-line with other data presented elsewhere in the literature.[50,51]

Temperature dependent complex viscosity curves at 10% biomass loading are presented in **Figure 4.3**. Temperatures were selected from the melting point of [DBUH][OAc] (55°C) through 80°C to assess the behavior of the molten solutions across a broad por-

Table 4.2: Cross and Carreau Model values for hot ethanol, ionic liquid, and acid chlorite pretreated cascara

Ethanol Treated						
	Cross Model			Carreau Model		
Temp (°C)	η_0 (Pa.s)	p	n	η_0 (Pa.s)	p	n
55	$13.7*10^4 \pm 9.4*10^4$	$11.9*10^5 \pm 2.3*10^5$	0.436 ± 0.05	2197 ± 864	1155 ± 142	0.437 ± 0.05
60	$10.6*10^4 \pm 6.7*10^4$	1251 ± 1047	0.165 ± 0.01	6673 ± 1046	41.1 ± 10.3	0.166 ± 0.01
70	22 ± 0.65	0.72 ± 0.04	0.404 ± 0.00	16.9 ± 0.42	1.88 ± 0.06	0.59 ± 0.00
80	8.1 ± 1.0	0.41 ± 0.13	0.446 ± 0.02	6.5 ± 0.35	1.78 ± 0.35	0.66 ± 0.00
Ionic Liquid Treated						
Temp (°C)	η_0 (Pa.s)	p	n	η_0 (Pa.s)	t	n
55	124 ± 26.7	2.29 ± 1.65	0.38 ± 0.07	78.7 ± 18.9	2.60 ± 1.37	0.52 ± 0.03
60	87.9 ± 26.1	4.29 ± 3.49	0.47 ± 0.07	55.5 ± 8.52	4.84 ± 2.42	0.62 ± 0.02
70	20.6 ± 0.70	0.37 ± 0.02	0.37 ± 0.00	17.0 ± 0.54	1.33 ± 0.03	0.60 ± 0.00
80	10.8 ± 0.61	0.20 ± 0.03	0.33 ± 0.01	9.40 ± 0.44	0.90 ± 0.09	0.61 ± 0.00
Acid Chlorite Treated						
Temp (°C)	η_0 (Pa.s)	p	n	η_0 (Pa.s)	t	n
55	4720 ± 2549	53.2 ± 47.5	0.29 ± 0.04	7364 ± 2286	116 ± 44.3	0.34 ± 0.01
60	$27.0*10^4 \pm 29.5*10^4$	$2.48*10^4 \pm 2.85*10^4$	0.29 ± 0.02	5905 ± 3674	145 ± 92.2	0.33 ± 0.04
70	1293 ± 386	41.3 ± 19.9	0.33 ± 0.02	430 ± 61.7	9.85 ± 2.09	0.38 ± 0.01
80	232 ± 5.01	4.47 ± 0.14	0.31 ± 0.00	141 ± 2.08	4.36 ± 0.06	0.43 ± 0.00

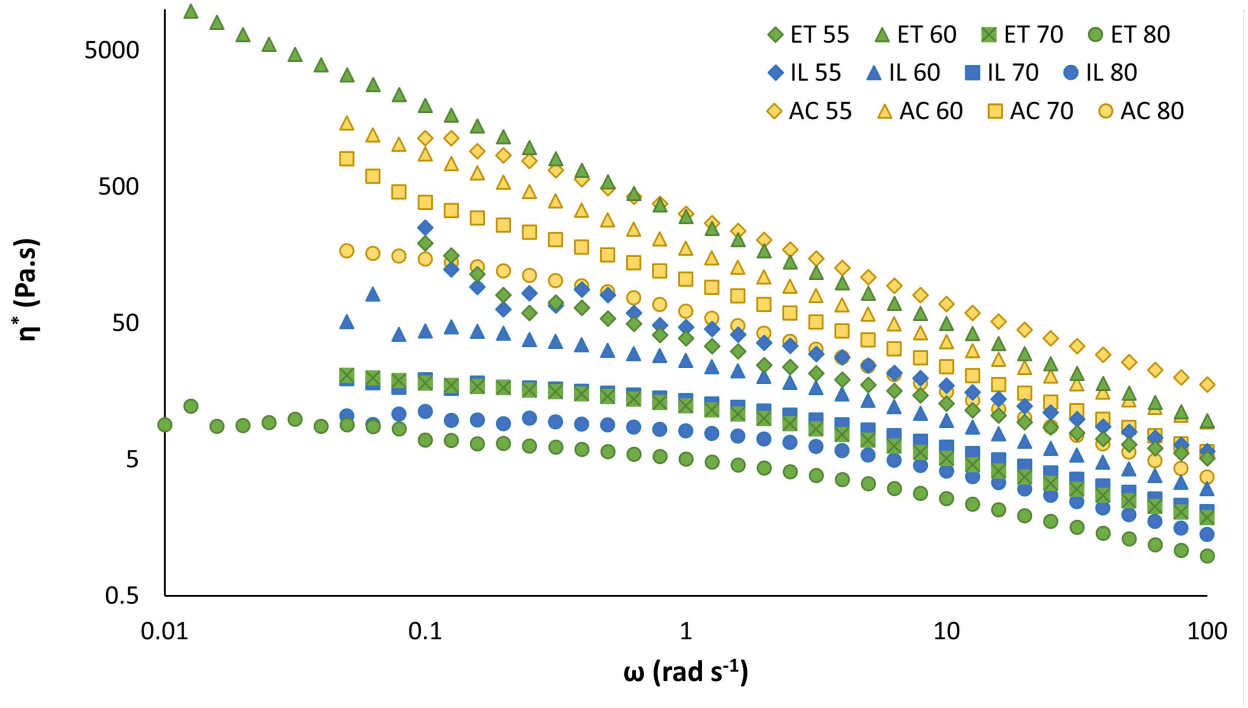

Figure 4.3: Temperature dependent complex viscosities of hot ethanol, dilute IL, and acid chlorite treated cascara. Data is presented as an average of 3 replicates, and error bars indicate 1 standard deviation

tion of the IL functional temperature range. Generally, the solutions demonstrated expected trends, with the solutions relaxing more with increasing temperature. However, the ET group displays unique features, having both the widest spread in complex viscosities as well as breaking the trend of increasing viscosity with reduced temperature (**Figure 4.3**). The ET pretreatment was also implemented before both the DILT and ACT pretreatments on all treated samples, so it is interesting that its complex viscosity range overlaps both the DILT and ACT samples. While the ET samples present the least change from untreated cascara in relative lignocellulosic composition, the treatment extracted a substantial volume (5%) of waxy substance. The ethanol extracts are expected to consist of non-structural sugars, chlorophyll, waxes, and other minor components.[47] The removal of these compounds yields an impressive jump in complex viscosity compared to the untreated cascara and cotton (**Figure 4.5**) previously tested (Chapter 3).

Arrhenius calculations were performed to better understand the thermal flow relation-

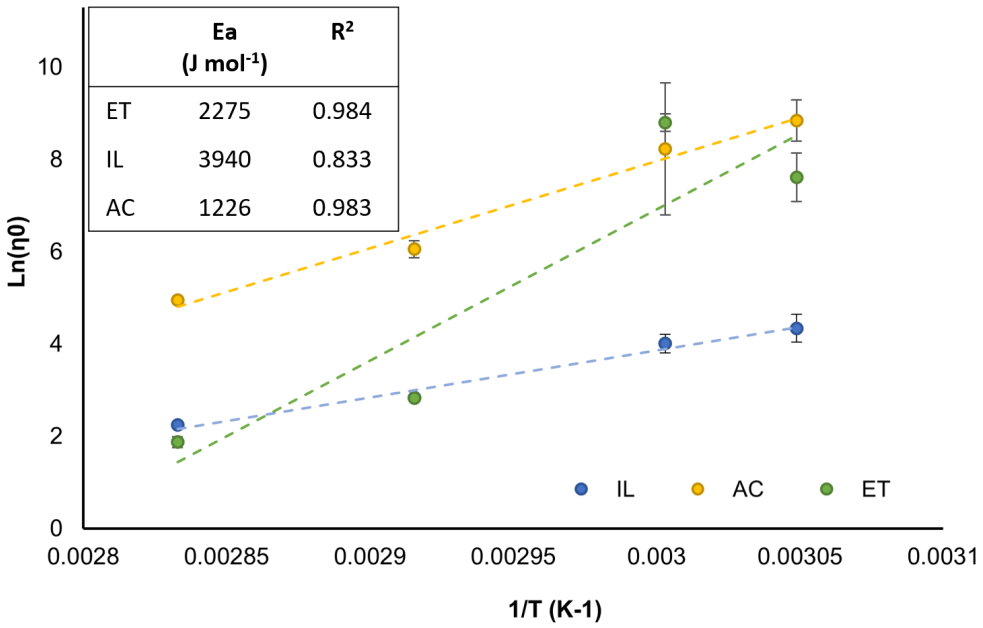

Figure 4.4: Arrhenius plot comparing hot ethanol, dilute IL, and acid chlorite pretreatments of cascara including activation energy calculations

ship between the three pretreatments (**Figure 4.4**). The Arrhenius equation is used to determine the activation energy (E_α) to induce flow[46,52] in the IL solutions. The Arrhenius activation energy offers a metric of comparison to other common engineering fluids to benchmark the capacity for viscous IL-cellulose solutions to be processed at industrial scale.[21] Herein, the activation energies of the cascara-IL solutions are calculated from the slope of the linear relationship between $\ln(\eta_0)$ and the inverse of temperature in Kelvins (**Figure 4.4**). Previously, the Vogel-Tammann-Fulcher (VTF) equation has been found to be more appropriate for analyzing the viscosity-temperature relationship of cellulose-IL solutions,[21,46] although the linear approximation of the Arrhenius model was found to be sufficient for the treated cascara.

Complex viscosity data for 10% biomass loadings at 60°C are presented in **Figure 4.5** to more clearly visualize the impacts of the three pretreatments on the dissolved cascara compared to untreated cascara and cotton. All 3 pretreatments demonstrated improved solution consistency at low frequencies compared to untreated cascara, which is pre-

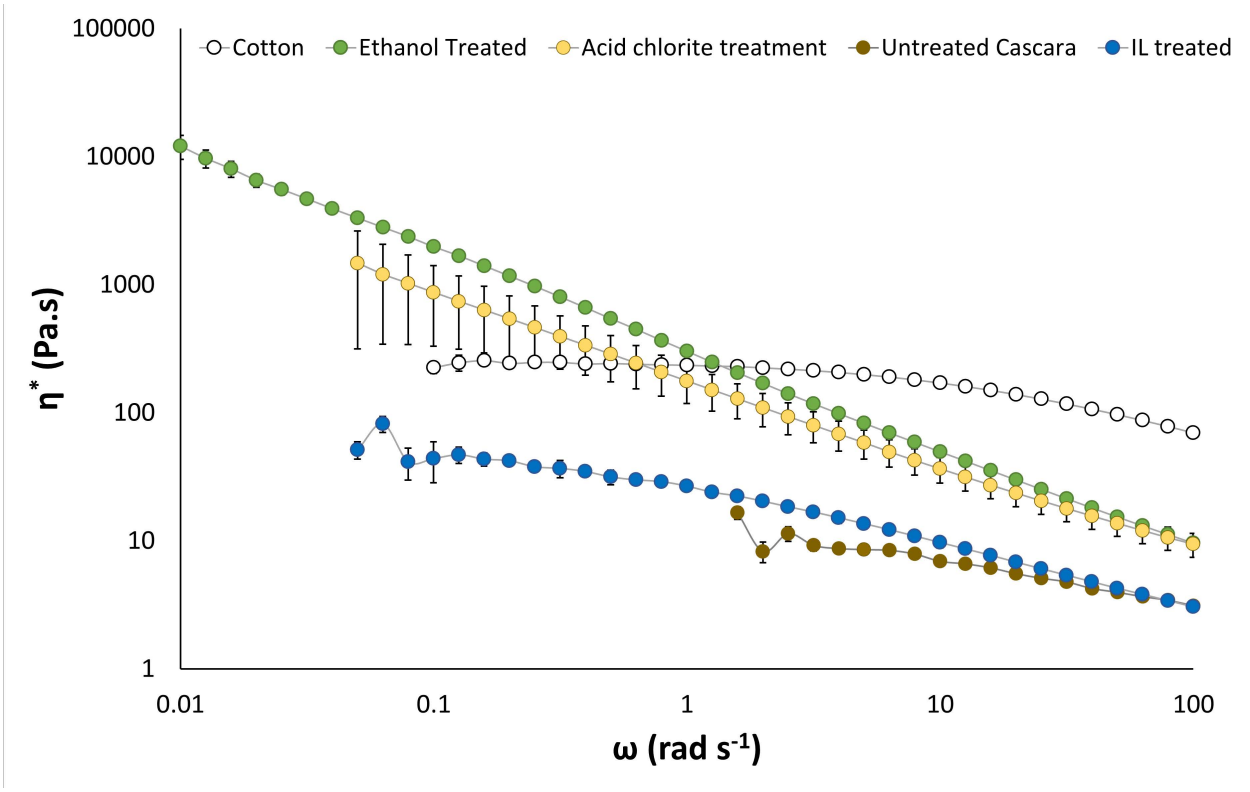

Figure 4.5: Plot of 10% loaded biomass at 60°C. Data is presented as an average of 3 replicates, and error bars indicate 1 standard deviation.

sented at a truncated frequency due to unstable measurements below 1 rad s^{-1}. The DILT pretreatment is notably very similar to the untreated cascara despite having been subjected to the ET pretreatment prior to DILT. The overall low viscosity of the DILT cascara (Figure 4.5) may be a result of incomplete removal of IL after the pretreatment, resulting in a lower real fraction of biomass in the analyzed samples. The viscous quality of IL treated cascara will be investigated further prior to the preparation of this chapter's contents for journal publication. Both the ET (6700 Pa.s) and ACT (5900 Pa.s) treated cascara at 60°C yield higher zero shear viscosities than cotton (230 Pa.s) (**Table 4.2**). This suggests that the native cellulose may have a higher molecular weight than the cellulose in the assessed, which can range between 800-10,000 DP.[27] The ET and ACT samples also show a precipitous drop off at higher frequencies compared to the cotton likely as a result of the retained hemicellulose and lignin.

4.4.3 Fibers

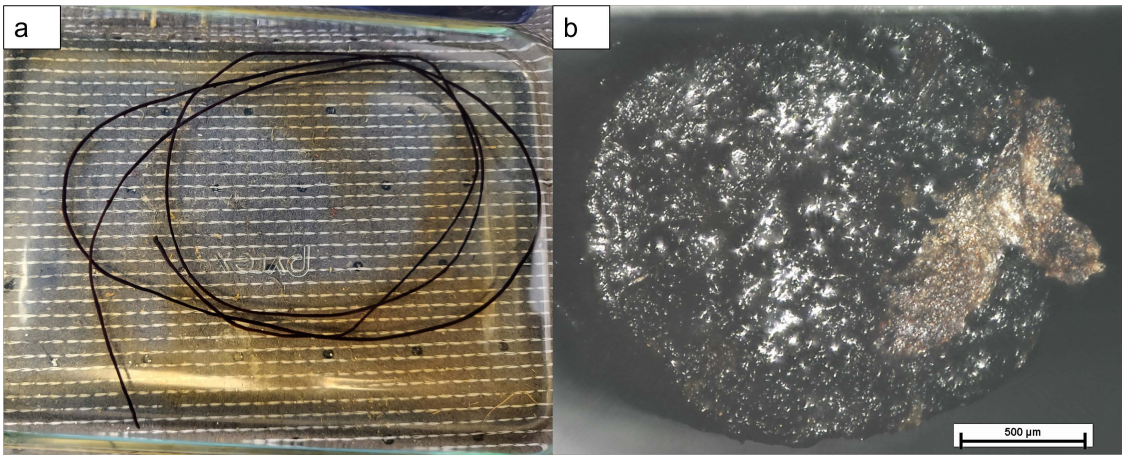

Figure 4.6: Optical microscope images of ethanol treated fibers as extruded. A) long fiber in methanol during second washing soak, b) cross section of swelled fiber after first washing soak in methanol

Long fibers (>40 cm) made from treated cascara-IL-DMSO solutions were extruded from a needle-less Luer Lock syringe and coagulated in a methanol anti-solvent bath. Fibers were extruded directly into the anti-solvent bath without any drawing tension, likely limiting their crystalline order and tensile properties.[53] Although there was some variation in the extruded fiber dimension, all fibers were initially extruded at a similar diameter to the Luer Lock orifice (1600 $\pm$ 200 µm diameter). On introduction to the anti-solvent, the surface of the fiber rapidly coagulates,[54,55] resulting in a circular cross-section with the dimension of the initially extruded fiber (**Figure 4.6**). Since the solvated biomass (10 w/w biomass in IL) is swelled substantially by the IL and DMSO solution, the coagulated dimension of the fiber collapses substantially (500 $\pm$ 200 µm diameter) when the solvents are removed resulting in the irregular cross-sections of the dried fibers (**Figure 4.7d,e,f**) and the visible wrinkles on their surfaces (**Figure 4.7a,b,c**). While swollen with anti-solvent and IL, the fibers were fragile, and prone to failure when the outer coagulated skin was punctured. However, once washed of IL, the fibers showed minimal rates of mass uptake in methanol; 0%, 3%, and 5%, respectively, for ET, DILT, and ACT fibers

respectively.

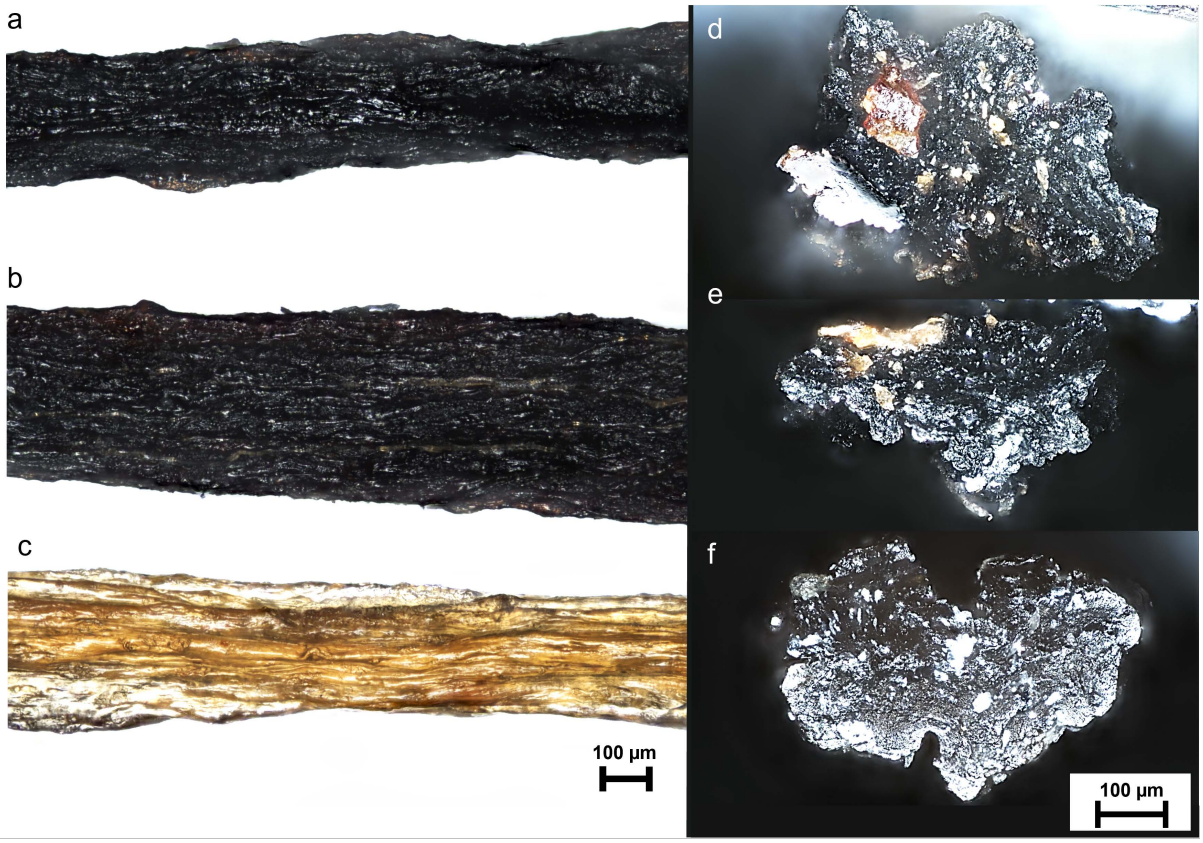

Figure 4.7: Optical microscope images of fibers (a,b,c) and fiber cross-sections (d,e,f) for ethanol treated (a,d), dilute IL treatment (b,e), and acid chlorite treatment (c,f).

Fibers made from pretreated cascara were more robust than fibers made from untreated cascara across the board. During the fiber drying process, all treated fibers held their shape when dried directly on an aluminum foil surface, while fibers made from untreated cascara collapsed and fused to the aluminum foil unless dried under tension.[56] Treated fibers were also much more robust to handling. As seen in **Figure 4.7**, the high-surface area fibers introduce unique tradeoffs. The high surface area of the extruded fibers could be leveraged in resin composites to yield good load transfer and better cohesion; however, the textured surface area simultaneously functions as stress-risers that contribute to their extreme brittleness. As noted above, the coagulation behavior of solution-based biomass fibers- wherein an external skin of biomass preliminarily coagu-

lates at the fiber surface- introduces limitations where the initial diameter of the fiber is "locked in". IL-extruded fibers elsewhere in the literature tend to have smoother rounder surfaces, likely due to their much smaller diameters ($\ll$ 100 µm).[57,58,59] Two aspects of thin fibers may contribute to these improved properties including 1) more rapid IL diffusion and coagulation of fibers across smaller radii (i.e., Ficks law), and 2) the surface area to volume ratio of cylindrical fibers ($2\pi rh/\pi r^2 h$) before solvent extraction induced volume reduction is magnified at large radii. As a continuing effort, physical properties of the fibers will be investigated in the form of continuous fiber composites, which will be included in published form of this chapter's contents.

4.5 Conclusion

Common biomass pretreatments including hot ethanol treatment (ET), dilute ionic liquid treatment (DILT), and acid chlorite treatment (ACT), were applied to coffee fruit (cascara) to understand how they influence the chemical composition and processing in [DBUH][OAc] IL. Treated cascara was assessed as a cellulose rich source for making IL extruded fibers. All three treatments yielded improved solubility of cascara in [DBUH][OAc] compared to untreated cascara, with 81%, 92%, and 77% for ET, DILT, and ACT samples respectively. Solvated samples were assessed rheologically and found to behave characteristically as polymer solutions. Overall the ACT cascara was the most viscous of the treatments, and was on-par with or higher than the viscosity of cotton. The comparatively low solubility of the ACT cascara suggests that the cascara may have a high cellulose molecular weight. ET cascara was the next most viscous followed by DILT solutions. The ACT was the most effective at removing lignin (50% removal) although the hemicellulose was untouched. In comparison, the DILT yielded modest reductions in both hemicellulose and lignin content. The ET had negligible impact on the lignocellulosic content, however, it did effectively remove extractives. The treated cascara was dissolved

in [DBUH][OAc] for 48 hr at 100°C before extrusion into long fibers ($>$ 40 cm) with a dry diameters of 500 $\pm$ 200 µm. The fibers with circular cross-sections were initially coagulated in methanol. After solvent exchange and drying, the fiber cross-sections collapsed into irregular lobbed shapes. The fibers were robust to handling and were much less fragile than fibers made from untreated cascara. Even with just the ET, the cascara-derived fibers were greatly improved while maintaining its original lignin and hemicellulose content. These results suggest that value-added fibers could be made from unconventional biomass like cascara, using less harsh treatments than are currently used in industry. Future work will dig deeper into characterizing the cascara biomass and assessing the physical properties of cascara fibers.

4.6 References

[1] Ying Ying Tye, Keat Teong Lee, Wan Nadiah Wan Abdullah, and Cheu Peng Leh. The world availability of non-wood lignocellulosic biomass for the production of cellulosic ethanol and potential pretreatments for the enhancement of enzymatic saccharification. *Renewable and Sustainable Energy Reviews*, 60:155–172, 2016. ISSN 18790690. doi:10.1016/j.rser.2016.01.072. URL http://dx.doi.org/10.1016/j.rser.2016.01.072.

[2] Olumoye Ajao, Mariya Marinova, Oumarou Savadogo, and Jean Paris. Hemicellulose based integrated forest biorefineries: Implementation strategies. *Industrial Crops and Products*, 126(October):250–260, 2018. ISSN 09266690. doi:10.1016/j.indcrop.2018.10.025. URL https://doi.org/10.1016/j.indcrop.2018.10.025.

[3] P Senthil Kumar and P R Yaashikaa. *Organic Cotton | Trigema*. Springer Singapore, 2018. ISBN 9789811087820. doi:10.1007/978-981-10-8782-0. URL https://www.trigema.de/en/sustainability/organic-cotton/.

[4] Shady S. Hassan, Gwilym A. Williams, and Amit K. Jaiswal. Emerging technologies for the pretreatment of lignocellulosic biomass. *Bioresource Technology*, 262 (March):310–318, 2018. ISSN 18732976. doi:10.1016/j.biortech.2018.04.099. URL https://doi.org/10.1016/j.biortech.2018.04.099.

[5] Parveen Kumar, Diane M. Barrett, Michael J. Delwiche, and Pieter Stroeve. Methods for pretreatment of lignocellulosic biomass for efficient hydrolysis and biofuel production. *Industrial and Engineering Chemistry Research*, 48(8):3713–3729, 2009. ISSN 08885885. doi:10.1021/ie801542g.

[6] Yanrong Liu, Yi Nie, Xingmei Lu, Xiangping Zhang, Hongyan He, Fengjiao Pan, Le Zhou, Xue Liu, Xiaoyan Ji, and Suojiang Zhang. Cascade utilization of lignocellulosic biomass to high-value products. *Green Chemistry*, 21(13):3499–3535, 2019. ISSN 14639270. doi:10.1039/c9gc00473d.

[7] Rickard Arvidsson, Duong Nguyen, and Magdalena Svanström. Life cycle assessment of cellulose nanofibrils production by mechanical treatment and two different pretreatment processes. *Environmental Science and Technology*, 49(11):6881–6890, 2015. ISSN 15205851. doi:10.1021/acs.est.5b00888.

[8] Aashish Prasad, Maria Sotenko, Thomas Blenkinsopp, and Stuart R. Coles. Life cycle assessment of lignocellulosic biomass pretreatment methods in biofuel production. *International Journal of Life Cycle Assessment*, 21(1):44–50, 2016. ISSN 16147502. doi:10.1007/s11367-015-0985-5. URL http://dx.doi.org/10.1007/s11367-015-0985-5.

[9] Yibo Ma, Shirin Asaadi, Leena Sisko Johansson, Patrik Ahvenainen, Mehedi Reza, Marina Alekhina, Lauri Rautkari, Anne Michud, Lauri Hauru, Michael Hummel, and

Herbert Sixta. High-Strength Composite Fibers from Cellulose-Lignin Blends Regenerated from Ionic Liquid Solution. *ChemSusChem*, 8(23):4030–4039, 2015. ISSN 1864564X. doi:10.1002/cssc.201501094.

[10] Ngoc A. Nguyen, Keonhee Kim, Christopher C. Bowland, Jong K. Keum, Logan T. Kearney, Nicolas André, Nicole Labbé, and Amit K. Naskar. A fundamental understanding of whole biomass dissolution in ionic liquid for regeneration of fiber by solution-spinning. *Green Chemistry*, 21(16):4354–4367, 2019. ISSN 1463-9262. doi:10.1039/c9gc00774a.

[11] Gabriele Schild and Eva Liftinger. Xylan enriched viscose fibers. *Cellulose*, 21: 3031–3039, 2014. doi:10.1007/s10570-014-0302-7.

[12] Elena Husanu, Angelica Mero, Jose Gonzalez Rivera, Andrea Mezzetta, Julian Cabrera Ruiz, Felicia D'andrea, Christian Silvio Pomelli, and Lorenzo Guazzelli. Exploiting Deep Eutectic Solvents and Ionic Liquids for the Valorization of Chestnut Shell Waste. *ACS Sustainable Chemistry and Engineering*, 8(50):18386–18399, 2020. ISSN 21680485. doi:10.1021/acssuschemeng.0c04945.

[13] Emille R B A Prata and S. Leandro Oliveira. Fresh coffee husks as potential sources of anthocyanins. *LWT*, 40:1555–1560, 2007. doi:10.1016/j.lwt.2006.10.003.

[14] Álvaro Silva Lima, Bruno Sales de Oliveira, Selesa Vanessa Shabudin, Mafalda Almeida, Mara Guadalupe Freire, and Katharina Bica. Purification of anthocyanins from grape pomace by centrifugal partition chromatography. *Journal of Molecular Liquids*, 326:115324, 2021. ISSN 01677322. doi:10.1016/j.molliq.2021.115324. URL https://doi.org/10.1016/j.molliq.2021.115324.

[15] Lucie A. Pfaltzgraff, Mario De Bruyn, Emma C. Cooper, Vitaly Budarin, and James H. Clark. Food waste biomass: A resource for high-value chemicals. *Green Chemistry*, 15(2):307–314, 2013. ISSN 14639270. doi:10.1039/c2gc36978h.

[16] M. Wadhwa and S. P. M. Bakshi. *Utilization of fruit and vegetable wastes as livestock feed and as substrates for generation of other value-added products*. 2013. ISBN 978-92-5-107631-6. doi:13578251. URL http://www.fao.org.webtranslate-widget.systransoft.com/docrep/018/i3273e/i3273e.pdf.

[17] Pushpa S Murthy and M Madhava Naidu. Resources , Conservation and Recycling Sustainable management of coffee industry by-products and value addition — A review. *"Resources, Conservation and Recycling"*, 66:45–58, 2012. ISSN 0921-3449. doi:10.1016/j.resconrec.2012.06.005. URL http://dx.doi.org/10.1016/j.resconrec.2012.06.005.

[18] L Fan, A. T Soccol, A Pandey, and C. R Soccol. Cultivation of Pleurotus Mushrooms on Brazilian Coffee Husk and Effects of Caffeine and Tannic Acid. *Micologia Aplicada International*, 15(1):15–21, 2003.

[19] Satoshi Akao, Koutaro Maeda, Yoshihiko Hosoi, Hideaki Nagare, Morihiro Maeda, and Taku Fujiwara. Cascade utilization of water chestnut: Recovery of phenolics, phosphorus, and sugars. *Environmental Science and Pollution Research*, 20(8): 5373–5378, 2013. ISSN 09441344. doi:10.1007/s11356-013-1547-7.

[20] Tom Welton, Matthew T. Clough, Uwe Vagt, Sunghee Son, Patricia A. Hunt, and Karolin Geyer. Ionic liquids: not always innocent solvents for cellulose. *Green Chemistry*, 17(1):231–243, 2014. ISSN 1463-9262. doi:10.1039/c4gc01955e.

[21] André Pinkert, Kenneth N. Marsh, Shusheng Pang, and Mark P. Staiger. Ionic liquids and their interaction with cellulose. *Chemical Reviews*, 109(12):6712–6728, 2009. ISSN 00092665. doi:10.1021/cr9001947.

[22] Thomas Heinze, Katrin Schwikal, and Susann Barthel. Ionic liquids as reaction medium in cellulose functionalization. *Macromolecular Bioscience*, 5(6):520–525, 2005. ISSN 16165187. doi:10.1002/mabi.200500039.

[23] Rita de C.M. Miranda, Jaci Vilanova Neta, Luiz Fernando Romanholo Ferreira, Walter Alves Gomes, Carina Soares do Nascimento, Edelvio de B. Gomes, Silvana Mattedi, Cleide M.F. Soares, and Álvaro S. Lima. Pineapple crown delignification using low-cost ionic liquid based on ethanolamine and organic acids. *Carbohydrate Polymers*, 206(June 2018):302–308, 2019. ISSN 01448617. doi:10.1016/j.carbpol.2018.10.112. URL https://doi.org/10.1016/j.carbpol.2018.10.112.

[24] Muhammad Moniruzzaman and Tsutomu Ono. Separation and characterization of cellulose fibers from cypress wood treated with ionic liquid prior to laccase treatment. *Bioresource Technology*, 127:132–137, 2013. ISSN 18732976. doi:10.1016/j.biortech.2012.09.113. URL http://dx.doi.org/10.1016/j.biortech.2012.09.113.

[25] Zugenmaier Peter. Order in cellulosics: Historical review of crystal structure research on cellulose. *Carbohydrate Polymers*, 254(August 2020):117417, 2021. ISSN 01448617. doi:10.1016/j.carbpol.2020.117417. URL https://doi.org/10.1016/j.carbpol.2020.117417.

[26] Zhenghui Liu, Xiaofu Sun, Mingyang Hao, Chengyi Huang, Zhimin Xue, and Tiancheng Mu. Preparation and characterization of regenerated cellulose from ionic liquid using different methods. *Carbohydrate Polymers*, 117:54–62, 2015. ISSN 01448617. doi:10.1016/j.carbpol.2014.09.053. URL http://dx.doi.org/10.1016/j.carbpol.2014.09.053.

[27] Dieter Klemm, Brigitte Heublein, Hans Peter Fink, and Andreas Bohn. Cellulose: Fascinating biopolymer and sustainable raw material. *Angewandte Chemie - International Edition*, 44(22):3358–3393, 2005. ISSN 14337851. doi:10.1002/anie.200460587.

[28] Takashi Nishino, Kiyofumi Takano, and Katsuhiko Nakamae. Elastic modulus of the crystalline regions of cellulose polymorphs. *Journal of Polymer Science Part B: Polymer Physics*, 33(11):1647–1651, 1995. ISSN 10990488. doi:10.1002/polb.1995.090331110.

[29] Agnieszka Brandt-Talbot, Florence J.V. Gschwend, Paul S. Fennell, Tijs M. Lammens, Bennett Tan, James Weale, and Jason P. Hallett. An economically viable ionic liquid for the fractionation of lignocellulosic biomass. *Green Chemistry*, 19(13): 3078–3102, 2017. ISSN 14639270. doi:10.1039/c7gc00705a.

[30] Jiming Yang, Xingmei Lu, Yanqiang Zhang, Junli Xu, Yongqing Yang, and Qing Zhou. A facile ionic liquid approach to prepare cellulose fiber with good mechanical properties directly from corn stalks. *Green Energy and Environment*, 5 (2):223–231, 2020. ISSN 24680257. doi:10.1016/j.gee.2019.12.004. URL https://doi.org/10.1016/j.gee.2019.12.004.

[31] Luke M. Haverhals, Matthew P. Foley, E. Kate Brown, Douglas M. Fox, Hugh C. De Long, and Paul C. Trulove. Natural fiber welding: Ionic liquid facilitated biopolymer mobilization and reorganization. In *ACS Symposium Series*, volume 1117, pages 145–166. 2012. ISBN 9780841227637. doi:10.1021/bk-2012-1117.ch006.

[32] Anne Michud, Marjaana Tanttu, Shirin Asaadi, Yibo Ma, Eveliina Netti, Pirjo Kääriainen, Anders Persson, Anders Berntsson, Michael Hummel, and Herbert Sixta. Ioncell-F: ionic liquid-based cellulosic textile fibers as an alternative to viscose and Lyocell. *Textile Research Journal*, 86(5):543–552, 2016. ISSN 00405175. doi:10.1177/0040517515591774.

[33] Wei Jiang, Liangfeng Sun, Ayou Hao, and Jonathan Chen. Regenerated cellulose fibers from waste bagasse using ionic liquid. *Textile Research Journal*, 81(18):1949–1958, 2011. ISSN 00405175. doi:10.1177/0040517511414974.

[34] Chang Geun Yoo, Xianzhi Meng, Yunqiao Pu, and Arthur J Ragauskas. The critical role of lignin in lignocellulosic biomass conversion and recent pretreatment strategies : A comprehensive review. *Bioresource Technology*, 301(November 2019):122784, 2020. ISSN 0960-8524. doi:10.1016/j.biortech.2020.122784. URL https://doi.org/10.1016/j.biortech.2020.122784.

[35] Kai Xuan Liu, Hong Qiang Li, Jie Zhang, Zhi Guo Zhang, and Jian Xu. The effect of non-structural components and lignin on hemicellulose extraction. *Bioresource Technology*, 214:755–760, 2016. ISSN 18732976. doi:10.1016/j.biortech.2016.05.036. URL http://dx.doi.org/10.1016/j.biortech.2016.05.036.

[36] Dongcheng Zhang, Yunqiao Pu, Ved Naithani, Hasan Jameel, and J Ragauskas. Elucidating carboxylic acid profiles for extended oxygen delignification of high-kappa softwood kraft pulps. *Holzforschung*, 60:123–129, 2006. doi:10.1515/HF.2006.020.

[37] Bassem B. Hallac, Poulomi Sannigrahi, Yunqiao Pu, Michael Ray, Richard J. Murphy, and Arthur J. Ragauskas. Biomass characterization of Buddleja davidii: A potential

feedstock for biofuel production. *Journal of Agricultural and Food Chemistry*, 57(4): 1275–1281, 2009. ISSN 00218561. doi:10.1021/jf8030277.

[38] Sodium Chlorite - Safety Data Sheet. Technical report, ThermoFisher Scientific, 2012. URL https://www.fishersci.com/store/msds?partNumber=AC223235000&productDescription=SODIUM+CHLORITE%2C+TECH.%2C+500GR&vendorId=VN00033901&countryCode=US&language=en.

[39] Chlorine Dioxide Gas - Safety Data Sheet. Technical report, ClorDiSys Solutions Inc., 2019. URL https://clordisys.com/pdfs/sds/SDS-ChlorineDioxideGas.pdf.

[40] M. C. Taylor, J. F. White, G. P. Vincent, and G. L. Cunningham. Sodium chlorite: Properties and reactions. *Industrial and Engineering Chemistry*, 32(7):899–903, 1940. ISSN 00197866. doi:10.1021/ie50367a007.

[41] A Sluiter, B Hames, R Ruiz, C Scarlata, J Sluiter, D Templeton, and D Crocker Nrel. Determination of Structural Carbohydrates and Lignin in Biomass. Technical Report July, National Renewable Energy Laboratory, 2011.

[42] P. J. Carreau, D. C. R. De Kee, and R. P. Chabra. Principles and Applications. In *Rheology of Polymeric Systems*. Hanser, New York, 1997.

[43] R J Sammons, J R Collier, T G Rials, and S Petrovan. Rheology of 1-Butyl-3-Methylimidazolium Chloride Cellulose Solutions . I . Shear Rheology. *Journal of Applied Polymer Science*, 110:1175–1181, 2008. doi:10.1002/app.

[44] Lucile Druel, Philipp Niemeyer, Barbara Milow, and Tatiana Budtova. Rheology of cellulose-[DBNH][CO2Et] solutions and shaping into aerogel beads. *Green Chemistry*, 20(17):3993–4002, 2018. ISSN 14639270. doi:10.1039/c8gc01189c.

[45] W. P. Cox and E. H. Merz. Correlation of Dynamic and Steady Flow Viscosities. *Journal of Polymer Science*, 28(118):619–622, 1958.

[46] Romain Sescousse, Kim Anh Le, Michael E. Ries, and Tatiana Budtova. Viscosity of cellulose-imidazolium-based ionic liquid solutions. *Journal of Physical Chemistry B*, 114(21):7222–7228, 2010. ISSN 15205207. doi:10.1021/jp1024203.

[47] A Sluiter, R Ruiz, C Scarlata, J Sluiter, and D Templeton. Determination of Extractives in Biomass: Laboratory Analytical Procedure (LAP), NREL/TP-510-42619. (January), 2008.

[48] Julie M. Rieland and Brian J. Love. Ionic liquids: A milestone on the pathway to greener recycling of cellulose from biomass. *Resources, Conservation and Recycling*, 155(September 2019):104678, 2020. ISSN 18790658. doi:10.1016/j.resconrec.2019.104678. URL https://doi.org/10.1016/j.resconrec.2019.104678.

[49] Linda Härdelin, Erik Perzon, Bengt Hagström, Pernilla Walkenström, and Paul Gatenholm. Influence of molecular weight and rheological behavior on electrospinning cellulose nanofibers from ionic liquids. *Journal of Applied Polymer Science*, 130 (4):2303–2310, 2013. ISSN 00218995. doi:10.1002/app.39449.

[50] Shirin Asaadi, Michael Hummel, Sanna Hellsten, Tiina Härkäsalmi, Yibo Ma, Anne Michud, and Herbert Sixta. Renewable High-Performance Fibers from the Chemical Recycling of Cotton Waste Utilizing an Ionic Liquid. *ChemSusChem*, 9(22):3250–3258, 2016. ISSN 1864564X. doi:10.1002/cssc.201600680.

[51] Simone Haslinger, Michael Hummel, Adina Anghelescu-Hakala, Marjo Määttänen, and Herbert Sixta. Upcycling of cotton polyester blended textile waste to new man-made cellulose fibers. *Waste Management*, 97:88–96, 2019. ISSN 18792456. doi:10.1016/j.wasman.2019.07.040. URL https://doi.org/10.1016/j.wasman.2019.07.040.

[52] E. Ike. Arrhenius-Type Relationship of Viscosity as a Function of Temperature for Mustard and Cotton Seed Oil. *International Research Journal of Pure and Applied Physics*, 9(1):44–55, 2021.

[53] Shirin Asaadi. *Dry-Jet Wet Spinning of Technical and Textile Filament Fibers from a Solution of Wood Pulp and Waste Cotton in an Ionic Liquid*. PhD thesis, Aalto University, 2019. URL https://aaltodoc.aalto.fi/handle/123456789/40199.

[54] Artur Hedlund, Tobias Köhnke, and Hans Theliander. Diffusion in Ionic Liquid-Cellulose Solutions during Coagulation in Water: Mass Transport and Coagulation Rate Measurements. *Macromolecules*, 50(21):8707–8719, 2017. ISSN 15205835. doi:10.1021/acs.macromol.7b01594.

[55] Lauri K.J. Hauru, Michael Hummel, Kaarlo Nieminen, Anne Michud, and Herbert Sixta. Cellulose regeneration and spinnability from ionic liquids. *Soft Matter*, 12(5):1487–1495, 2016. ISSN 17446848. doi:10.1039/c5sm02618k.

[56] Julie Rieland, Zeyuan Hu, and B J Love. Making hand pulled fibers from ionic liquid–biomass, 2022. URL https://www.youtube.com/watch?v=Aqtdy8E4q0Y.

[57] Frank Hermanutz, Marc Philip Vocht, Nicole Panzier, and Michael R. Buchmeiser. Processing of Cellulose Using Ionic Liquids. *Macromolecular Materials and Engineering*, 304(2):1–8, 2019. ISSN 14392054. doi:10.1002/mame.201800450.

[58] Tao Cai, Huihui Zhang, Qinghua Guo, Huili Shao, and Xuechao Hu. Structure and Properties of Cellulose Fibers from Ionic Liquids. *Journal of Applied Polymer Science*, 115:1047–1053, 2010. ISSN 00218995. doi:10.1002/app.

[59] Carina Olsson and Gunnar Westman. Wet spinning of cellulose from ionic liquid solutions-viscometry and mechanical performance. *Journal of Applied Polymer Science*, 127(6):4542–4548, 2013. ISSN 00218995. doi:10.1002/app.38064.

CHAPTER 5

Conclusion

5.1 Summary

This dissertation presented on two research projects linked with textile sustainability. First, the ability of pressure-sensitive adhesives (PSA) to capture microplastics was investigated. Second, untreated and treated coffee fruit (cascara) biomass was investigated for processing with ionic liquids. These research projects respectively consider the waste produced from textile use and disposal, and the sourcing of better textile fibers.

In chapter 2, I assessed PSA coated glass slides submerged in aqueous solutions containing microplastics with a range of sizes. Three formulations of PSAs were used and evaluated in binding several common microplastics, including nylon, polystyrene, polyethylene, and polyethylene terephthalate fibers. Using the open-source software ImageJ®, the number and size distribution of removed microplastics were quantified. Observation of the adhesives after aqueous capture showed that the molecular weight distribution of the adhesive played an important role in microplastic capture and film robustness. A 50:50 bimodal mixture of 92k and 950k PEHA was found to provide the most robust films and good particle capture. The PSA-based capture of particles was generally robust to physical and chemical interferents in the aqueous media, although surfactants

and fine particulate matter greatly reduced capture.

Throughout the work on this effort, I found that common methods of reporting microplastic quantities produce biases with respect to particle size. When there is a size distribution of microplastics, reporting a particle count biases the result toward smaller particles, but weighting the particles by size biases the result toward larger particles. In order to gain a more holistic understanding of the size distribution of environmental microplastics, we propose that microplastic quantities should be reported as both number counts and with units that incorporate particle size (e.g., mass, volume, or surface area). Regardless of the counting method, however, we found that pressure-sensitive adhesives provide a robust and effective means of microplastic capture and removal.

In the second section of this work I investigated ionic liquid processed coffee fruit (cascara). In chapter 3, the superbase-derived ionic liquid, 1,8-Diazabicyclo [5.4.0]undec-7-inium acetate ([DBUH][OAc]) was evaluated for its ability to dissolve and reshape dried cascara. I compared the solubility of untreated cascara to industrially-treated cotton. We found that the cascara was 65% soluble in the ionic liquid, while the cotton was 100% soluble. The inclusion of the cascara's lignin (32.55%), hemicellulose (7.10%), and extractives including lipids, proteins, and non-structural sugars likely contributed to its reduced solubility as well as its low complex viscosity. The cascara was coagulated into films and fine fibers, with diameters of less than 20 µm. The [DBUH][OAc] was non-selective for cellulose, conveying lignin and hemicellulose into the coagulated films, although the dissolution and shaping process did yield a notable reduction in acid-soluble lignin (24%). The ability of the untreated cascara to coagulate into these films and fibers is a promising sign for use of cascara as a biomass resource.

While untreated cascara was used in chapter 3, in conventional biomass applications, harsh chemical treatments are commonly used to isolate pure cellulose from biomass before material processing. Our work in chapter 3 provided a baseline for understanding the properties of cascara-derived fibers and films. In chapter 4, I expanded the work with

cascara to consider three pretreatments, including a simple ethanol extraction, a dilute ionic liquid (10% DI water) pretreatment using [DBUH][OAc], and a more conventional acid chlorite bleaching treatment. The ethanol extraction had no impact on the lignocellulosic content of the cascara while the dilute ionic liquid and the acid chlorite treatment increased the relative cellulose content 4% and 69%, respectively. The three pretreatments all increased the solubility of the cascara in [DBUH][OAc]. The pretreated samples also had increased viscosity compared to equivalent untreated cascara and cotton solutions, suggesting that the molecular weight of the cellulose in cascara may be higher than the molecular weight of the representative cellulose used in this study. Finally, we coagulated long fibers ($>$ 40 cm) of treated cascara coagulated from ionic liquid solution into methanol. The dried fibers had diameters of 500 $\pm$ 200 µm with lobed, irregular cross-sections.

Fibers made from treated cascara were much more robust than those made from untreated cascara. The fibers made from ethanol extracted cascara performed similarly to the conventional acid chlorite treatment in rheology despite not removing lignin or hemicellulose. Continuing work will assess the tensile properties of treated cascara fibers. Overall, this work demonstrates that more environmentally benign pretreatments like the ethanol extraction and dilute ionic liquid pretreatment may be able to substitute for more dangerous, conventional treatments.

5.2 Future Work – Microplastics

Both project areas discussed in this thesis represent rich problem spaces that pose many unanswered questions. While the microplastic work herein represents a small section of a larger multidisciplinary project, the engineering portion has many exciting avenues to grow. Future work should seek to address the problems encountered over the course of this dissertation work as well as explore device designs for PSA-based capture.

5.2.1 Improving image based analysis

In the current work, image analysis was performed using the NIH hosted, open-source software, ImageJ®. The software's built-in 'Analyze Particles' feature offered a quick and convenient way to count particles and particle clusters while simultaneously measuring the surface area of each particle. However, there were limitations to applying this software for microplastic analysis; 1) individual particles in clusters could not be differentiated and 2) large, dense aggregates of particles and fibers that formed a 'continuous phase' across the image area could not be handled by the software. Moving forward, new counting software should be considered, whether that includes pre-built software packages or bespoke code. The second limitation would be easier to tackle and could be easily programmed within the same framework as the existing 'analyze particle' function. The first limitation, however, would require more complex software, likely leveraging machine learning to enable a trainable program that can identify subtle features like individual particle boundaries, overlapping particles, and unique particle species.

5.2.2 Exploring substrate geometries

As a proof of concept, the flat glass slides investigated in this work, as well as previously investigated spherical bead substrates, represent a promising technology that should be explored further. Preliminary studies with beads and glass slides demonstrate that capture scales with substrate surface area. Moving forward, device construction should be investigated, considering appropriate substrate design for different microplastic-polluted environments. Possible environments of interest include in-drum or in-line washing machine effluent, wastewater treatment plant reservoirs, open water, and HVAC filtration. Each of these scenarios would require different geometries, adhesive preparations, and binding considerations that in turn would require new modes of assessment. As a starting point, geometries such as stacked meshes, roll-to-roll sheets, and active forms of

capture like coated turbines present interesting areas for consideration.

5.3 Future Work - Cascara

The current assessment of cascara dissolution and reshaping in ionic liquid represents a preliminary investigation into the viability of extracting lignocellulosic material from cascara. As a stepping stone into future work, many questions and unknowns were identified in the process. I identify three key areas for future work including expanding the assessment of green pretreatments, assessing the ability simultaneously extract value-added components of the biomass, and finally considerations towards recycling the [DBUH][OAc].

5.3.1 Expanding assessment of green pretreatments

In the presented work, three pretreatments were selected from the numerous biomass pretreatments that have been explored in the literature. Future work should dig deeper into the existing literature to identify environmentally sustainable treatment processes that are effective at isolating the desired components of the cascara biomass. For example, in standard lignocellulosic chemical analysis processes, water and ethanol treatments are both used to remove extractives.[1] The addition of a water treatment as outlined in Slutier et al.[2] on top of the presently investigated ethanol treatment may add further improvement.

The organosolv process also looks to be a promising process that relies on acidified, heated polar solvents like ethanol and methanol.[3] In the present work, the hot ethanol treatment was effective at improving the extruded fiber quality. In the organosolv process, the solvents are pressurized and heated above their boiling point and are expected to be even more effective. There are likely other green pretreatments that may be worth assessing as well.

5.3.2 Assessing intermediary extraction of value-added components

Building on the previous recommendation, pre-treatments should also be considered with respect to the form of the extracted content. Cascara is a complex biomass, with many nonstructural elements that could yield added value. As discussed in chapter 4, small molecule components like caffeine and anthocyanins could be extracted for alternative use. Subsequently, treatment to extract usable forms of lignin could be investigated. There is a rich literature around the use of lignin for stock chemicals and engineering materials. Direct next steps would involve characterizing the forms of lignin present in cascara, and then assessing the best ways to extract usable forms of the lignin.

5.3.3 Recycling of ionic liquid

Finally, ionic liquid recyclability is an important consideration for both the sustainability of the process and its economic feasibility. In the literature, other ionic liquids have been found to be recyclable for several iterations, often recovered from the anti-solvent bath via evaporation and distillation processes. However, the majority of these investigations have been done using pure cellulose, which leaves minimal residues upon fiber coagulation. In contrast, the coagulated cascara yields a dark residue that concentrates in the ionic liquid fraction after rotary evaporation of the anti-solvent. Preliminary assays were performed to attempt to remove the cascara residue from the recovered [DBUH][OAc] via liquid-liquid separation, however, an adequate solvent was not found. Moving forward, the recovered ionic liquid should be assessed for dissolution capacity to understand the impact of retained residues. Furthermore, residue removal should be assessed using an expanded solvent range for liquid-liquid separation and various column filtrations.

5.4 References

[1] a. Sluiter, B. Hames, R. Ruiz, C. Scarlata, J. Sluiter, D. Templeton, and D. Crocker. NREL/TP-510-42618 analytical procedure - Determination of structural carbohydrates and lignin in Biomass. *Laboratory Analytical Procedure (LAP)*, (April 2008):17, 2012. ISSN 9781234556709. doi:NREL/TP-510-42618. URL http://www.nrel.gov/docs/gen/fy13/42618.pdf.

[2] A Sluiter, R Ruiz, C Scarlata, J Sluiter, and D Templeton. Determination of Extractives in Biomass: Laboratory Analytical Procedure (LAP), NREL/TP-510-42619. (January), 2008.

[3] Sarita Cândida Rabelo, Pedro Yoritomo Souza Nakasu, Eupídio Scopel, Michelle Fernandes Araújo, Luiz Henrique Cardoso, and Aline Carvalho da Costa. Organosolv pretreatment for biorefineries: Current status, perspectives, and challenges. *Bioresource Technology*, 369(November 2022), 2023. ISSN 18732976. doi:10.1016/j.biortech.2022.128331.

APPENDIX A

A.1 Mixed assay and individual parametric study observations

The distribution of MPs in water dispersion greatly affects the ability for the glass slide technique to produce a representative visualization of MP capture at a given concentration of particles. For example, the large post-consumer PE200 is highly buoyant as demonstrated by the higher levels of adsorption towards the top of the glass slide.

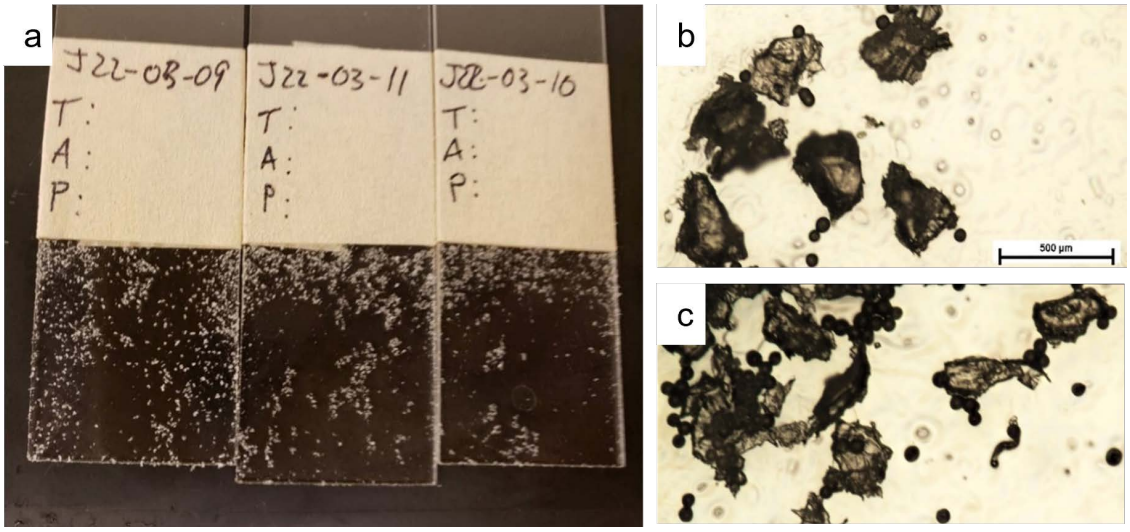

Figure A.1: Images from PE50/PE200 shake test. a) Images of glass slides including the full adhesive region. b and c) Show the high level of aggregation between the PE50 spheres and PE200 flakes which make it difficult for ImageJ® to identify counts for the respective particle types.

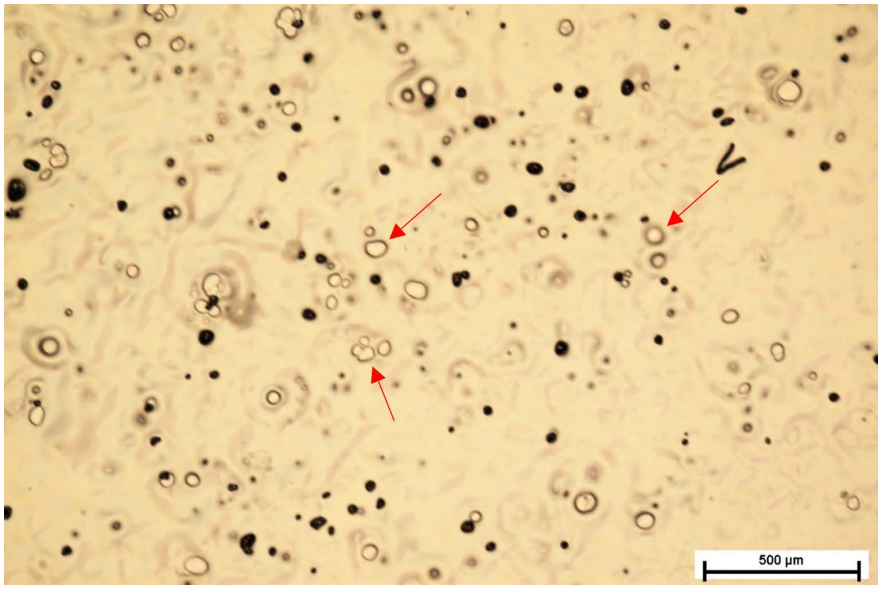

Figure A.2: Microscope image from PS10/nylon30 shake test showing moderate degradation of the 950k adhesive after 5 minutes. Red arrows indicate regions of adhesive migration where holes have opened up

Table A.1: %SAC and number count data for parametric and mixed assay experiments on 950k PEHA at 0.1 mg mL^{-1} under 5 min shaking

MP species	%SAC	STD	# Count[a]	STD
$PS10_{alone}$	0.9	0.5	179	104
$PS10_{nylon30}$	0.3	0.1	50	41
$Nylon30_{alone}$	1.1	0.7	81	56
$Nylon30_{PS10}$	1.6	0.8	101	71
$PE50_{PE200}$	1.7	0.4	22	11
$PE200_{PE50}$	8.7	2.3	7	4
PET $fibers_{alone}$[b]	12.5	6.0	-	-

[a]# Count is a representation of average number of particles per a 2.8 mm x 1.9 mm rectangle
[b]PET fibers could not be discretely counted see **Figure 2.4**

Table A.2: Gravimetric data for parametric and mixed assay experiments in percent total capture

MP species	capture (%)	STD (%)
PE50/PE200	22	4
PET fiber	95	13
PS10/nylon30*	-17	3
$Nylon30_{alone}$	14	10

*PS10 samples both with nylon30 and alone experienced negative capture. Observation of adhesive region showed abrading of the PSA **Figure A2**

A.2 [DBUH][OAc] Characterization

NMR

NMR spectra were recorded using a Bruker Avance Neo 500 (500 MHz ^{1}H Freq). 1,8-diazabicyclo[5.4.0]undec-7-enium acetate, [DBUH][OAc]: ^{1}HNMR (500 MHz, DMSO-d6) δH 3.45 (2H, m), 3.40 (2H, t), 3.18 (2H, t), 2.68 (2H, m), 1.87 (2H, m), 1.64-1.44 (9H, m); 1

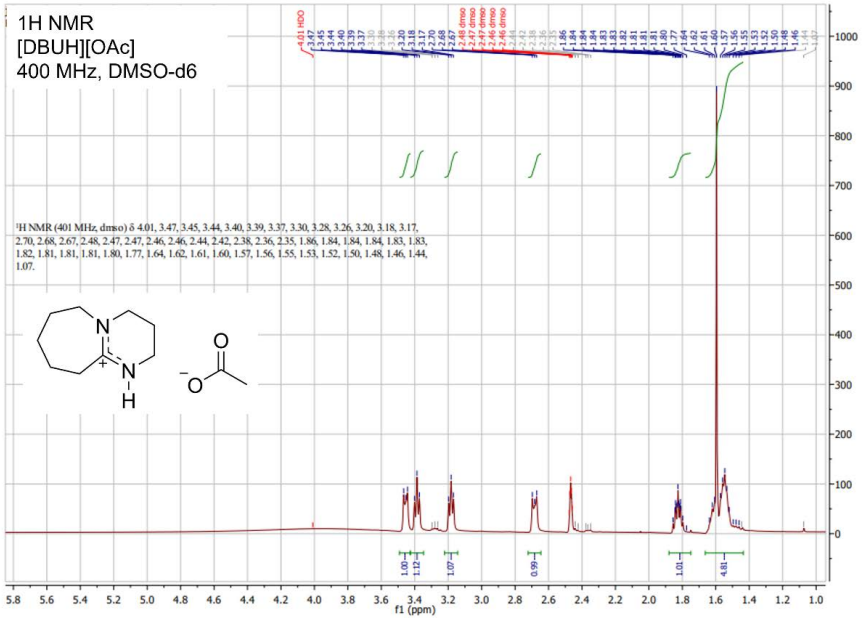

Figure A.3: ^{1}HNMR spectra of [DBUH][OAc]

DSC

Differential scanning calorimetry (DSC) was performed using a TA DSC Q2000.

Cold crystallization was initiated by holding sample at 20°C for 10 minutes before continuing to ramp at 2°C/min until 60°C. Onset melt temperature is in good agreement with Kuzmina et al.[1] We observed that [DBUH][OAc] tends to exist as a metastable fluid at room temperature, which seems to have been observed by Parviainen et al.[2], who re-

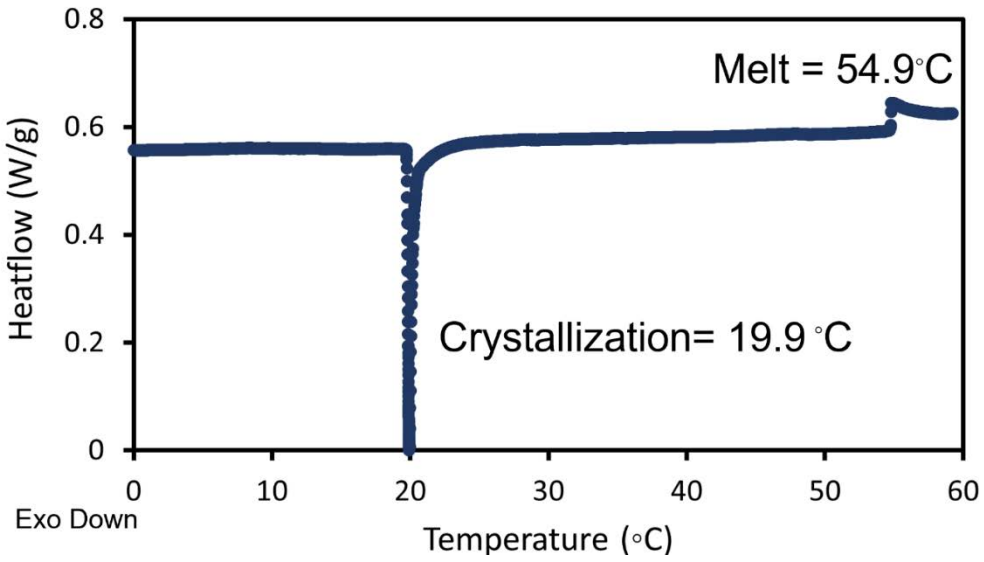

Figure A.4: DSC scan for [DBUH][OAc] demonstrating induced cold crystallization and onset melting.

Table A.3: Cross and Carreau model parameters for [DBUH][OAc]/cotton

	Cross Model			Carreau		
	η_0	τ ($\times 10^{-3}$)	n	η_0	τ ($\times 10^{-3}$)	n
5%	14.6 ± 0.17	4.1 ± 0.05	0.05 ± 0.01	14.4 ± 0.05	45 ± 0.5	0.8 ± 0.001
10%	250 ± 14	37.0 ± 3.5	0.20 ± 0.06	230 ± 2	210 ± 10	1.0 ± 0.0004
15%	2600 ± 93	580 ± 22	0.40 ± 0.001	1500 ± 39	550 ± 40	0.5 ± 0.005

ported [DBUH][OAc] as a room temperature ionic liquid (RTIL).

A.3 Cross and Carreau model fitting

Curve-dfitting was performed with the curve fitting package in Matlab R2021a using a leave-one-out cross validation (LOOCV) method.[3]

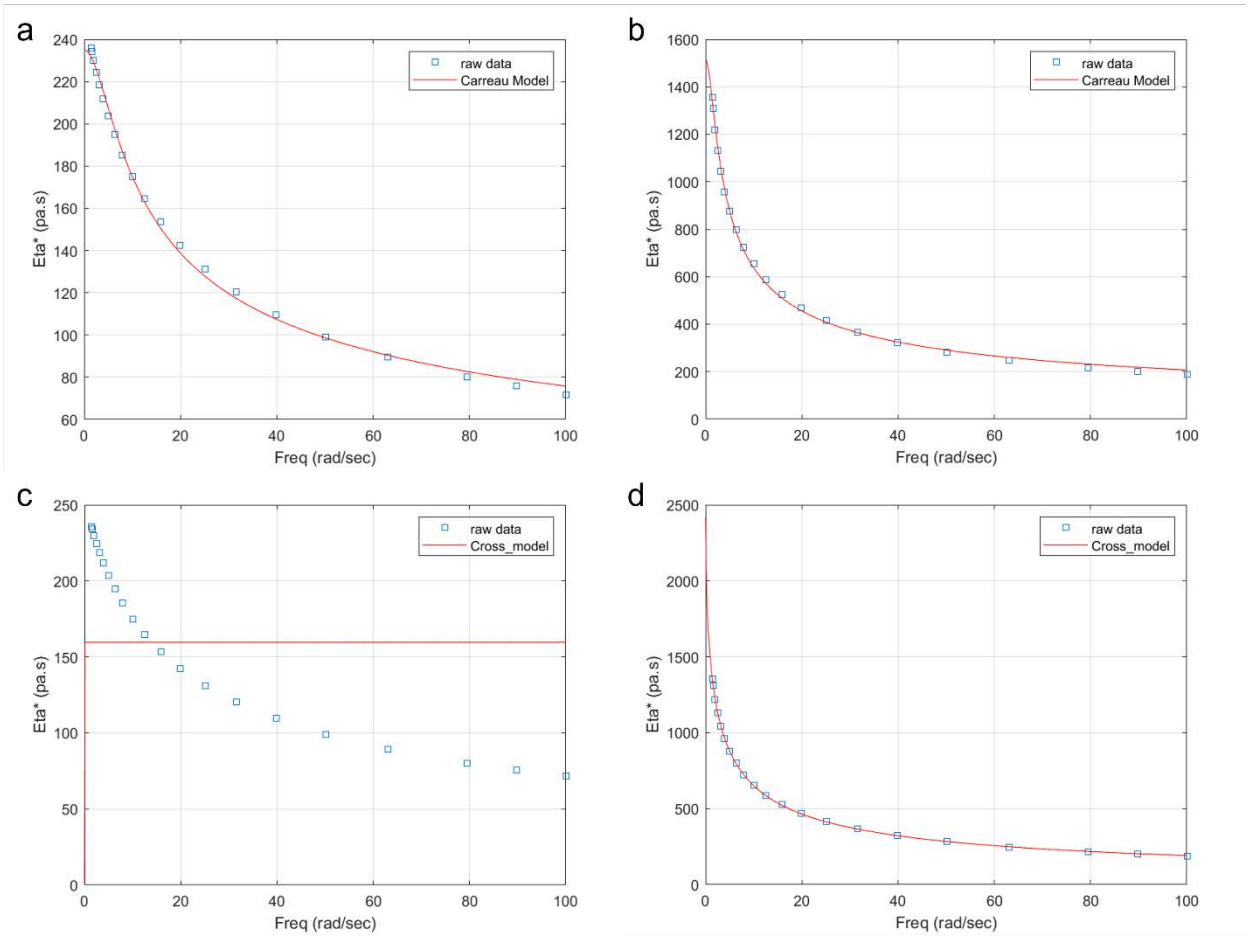

Figure A.5: Matlab curve fitting output for both Cross and Carreau models on cascara (a,c) and cotton (b,d)

A.4 References

[1] Olga Kuzmina, Jyoti Bhardwaj, Sheril Rizal Vincent, Nandula Dasitha Wanasekara, Livia Mariadaria Kalossaka, Jeraime Griffith, Antje Potthast, Sameer Rahatekar, Stephen James Eichhorn, and Tom Welton. Superbase ionic liquids for effective cellulose processing from dissolution to carbonisation. *Green Chemistry*, 19(24):5949–5957, 2017. ISSN 14639270. doi:10.1039/c7gc02671d.

[2] Arno Parviainen, Alistair W.T. King, Ilpo Mutikainen, Michael Hummel, Christoph Selg, Lauri K.J. Hauru, Herbert Sixta, and Ilkka Kilpeläinen. Predicting cellulose solvating capabilities of acid-base conjugate ionic liquids. *ChemSusChem*, 6(11):2161–2169, 2013. ISSN 18645631. doi:10.1002/cssc.201300143.

[3] Zach. A quick intro to leave-one-out cross validation (LOOCV), 2020. URL https://www.statology.org/leave-one-out-cross-validation-in-r/.